LA-12699

Mexico City Air Quality Research Initiative

Volume III
Modeling and Simulation

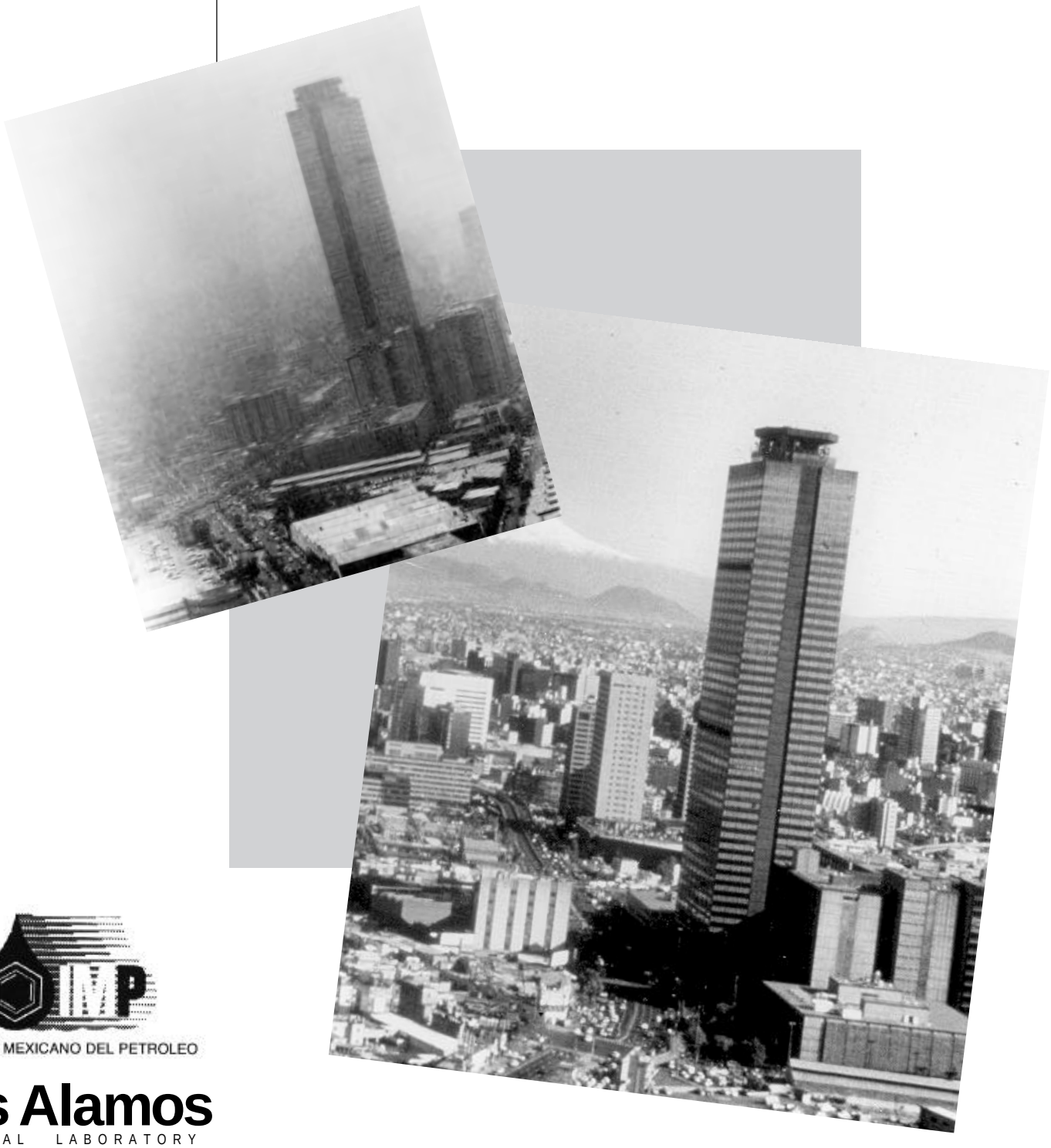

INSTITUTO MEXICANO DEL PETROLEO

Los Alamos
NATIONAL LABORATORY

Los Alamos National Laboratory is operated by the University of California for the United States Department of Energy under contract W-7405-ENG-36.

Edited by Ann Mauzy, Group IS-1
Photocomposition by Kathy Valdez, Group IS-1
Cover design by Gloria Sharp, Group IS-1

An Affirmative Action/Equal Opportunity Employer

LA-12699

UC-902
Issued: June 1994

Mexico City Air Quality Research Initiative

Volume III
Modeling and Simulation

Authors:
Instituto Mexicano del Petróleo
Los Alamos National Laboratory

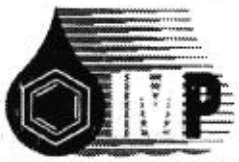

INSTITUTO MEXICANO DEL PETROLEO
Mexico City, MEXICO

Los Alamos
NATIONAL LABORATORY
Los Alamos, New Mexico 87545

Volume III
Table of Contents

ACRONYM LIST

AQMP	Air Quality Management Program
CINESTAV	Centro de Investigación y Estudios Avanzadados (Center for Investigation and Advanced Studies)
CIT	see footnote p. 45
CNG	compressed natural gas
DDF	Departmento Distrito Federal (Federal District Department
DF	Distrito Federal (Federal District)
DST	daylight savings time
EdoMex	Estado de México (State of Mexico)
EKMA	Empirical Kinetic Modeling Approach
EPA	Environmental Protection Agency
FEAT	fuel efficiency automotive test
GC	gas chromatography
HOTMAC	a three-dimensional, time-dependent mesoscale model
IMECA	Indice Metropolitano de Calidad del Aire (Metropolitan Air Quality Index)
JICA	Japan International Cooperation Agency
LCC	Lurmann, Carter, and Coyner
LPG	liquefied petroleum gas
MARI	Mexico City Air Quality Research Initiative
MCMA	Mexico City Metropolitan Area
MOBILE4	EPA automotive emissions model
MOBILE-MCMA	version of MOBILE4 model adapted for MCMA
NCAR	National Center for Atmospheric Research
NMOC	nomethane organic compounds
OZIPM	Ozone Isopleth Plotting with Optional Mechanisms
PEMEX	Petróleos Mexicanos (Mexican National Petroleum Co.)
PICCA	Programa Integral Contra la Contaminación Atmosférica (Integrated Program Against Atmospheric Contamination)
RAMS	Regional Atmospheric Modeling System
RAPTAD	a Monte Carlo dispersion and transport model
SEDESOL	Secretaría de Desarollo Social (Secretariat for Social Development)
SODAR	sound detection and ranging
STI	Secretariado Técnico Intergubernamental (Intergovernmental Technical Secretariat)
TÜV	TÜV-Reinland, a German consulting firm
UNAM	Mexican National University
UTM	universal Mercator transverse
UTMX	universal Mercator transverse on X axis
UTMY	universal Mercator transverse on Y axis
VOC	volatile organic compounds

A. OVERVIEW

1. Objectives

The objective of the modeling and simulation task was to develop, test, and apply an appropriate set of models that could translate emission changes into air quality changes. Specifically, we wanted to develop models that could describe how existing measurements of ozone (O_3), carbon monoxide (CO), and sulfur dioxide (SO_2) would be expected to change if their emissions were changed. The modeling must be able to address the effects of difference in weather conditions and changes in land use as well as the effects of changes in emission levels. It must also be able to address the effects of changes in the nature and distribution of the emissions as well as changes in the total emissions. A second objective was to provide an understanding of the conditions that lead to poor air quality in Mexico City. We know in a general sense that Mexico City's poor air quality is the result of large quantities of emissions in a confined area that is subject to light winds, but we did not know much about many aspects of the problem. For example, is the air quality on a given day primarily the result of emissions on that day...or is there an important carryover from previous nights and days? With a good understanding of the important meteorological circumstances that lead to poor air quality, we learn what it takes to produce an accurate forecast of impending poor air quality so that we can determine the advisability of emergency measures.

2. Background

The task of developing a comprehensive air quality modeling system for Mexico City was a challenging one. The development of a good air quality system for a major urban area is difficult under the best of circumstances, but Mexico City poses additional problems. Mexico City's topography, altitude, and latitude are significantly different than those cities where we have gained the most experience. While Mexico City has an extensive meteorological and air quality monitoring network, it provides comprehensive data from only a few locations and, of course, it is limited to surface measurements. In addition few cities have the complex terrain enjoyed by Mexico City. Because of the complex terrain, measurements tend to be representative of a much more limited area, so that many more measurements are needed to define the behavior of wind fields and pollution dispersion. In many other cities we can deduce a great deal of information from the measurements and thus we don't need to develop as comprehensive meteorological models as were needed for Mexico City.

There is less experience in Mexico City in the development and testing of emissions inventories. In other major cities the inventories have been under development for literally decades, while in Mexico City, the kind of inventory needed as input to photochemical models did not exist before this project.

There are three major components needed to help develop a good understanding of urban air quality in major cities. These components are

- measurements,
- emission inventories, and
- air quality models.

Despite many years of development around the world, none of the components, even in the most studied of the world's cities, can be considered perfect. Measurements may be accurate, but they are not representative of everything we would like to know. Emissions inventories typically embody major uncertainties. It appears that in cities where there has been considerable work over many years, the emissions inventories are inconsistent with ambient measurements. For example, in the Southern California Air Quality Study, (Gertler and Pierson, 1991) measurements of CO, hydrocarbons (HC) and nitrogen oxides (NO_X) were made in a traffic tunnel. The levels of NO_X found in the tunnel were consistent with those expected from the emission inventory. However, the HC levels were about three times greater than expected from the inventory, while CO levels were about twice as large as expected. There is a variety of other studies (Oliver, et al., 1993) that support the conclusion that there are significant uncertainties in the emissions inventories used throughout the world.

Air quality models have had both successes and failures. In some instances, the inputs to the models are of such poor quality that an apparent success must be viewed with skepticism. For example, in Los Angeles the models have been giving good results, but we now know that the input to the models was seriously in error. Not only were the bulk emissions wrong, but the critical ratio of HC to oxides of nitrogen was seriously in error. The models gave good answers, but only fortuitously; the simulations did not actually represent the true world. This poses a potentially serious problem. Air quality management strategies drawn from unrealistic simulations will not produce the expected results.

Many of these concerns are magnified when applied to Mexico City, where the measurements are more limited, and the emissions have not been studied as thoroughly as they have in some of the major cities in the U.S. The routine measurements in the Mexico City area, which are taken near the surface, are taken only in the city itself so that there is little information about what is crossing into and out of the city at the boundaries. The focus of the monitoring, carried out by the Secretaría de Desarollo Social (SEDESOL), has been on the pollutants of health-related concern, such as CO, O_3, and SO_2. This monitoring is quite appropriate if one wants to know what the current air quality is, but it does not provide a full understanding because it tells us little about the building blocks for O_3, such as HC and NO_X. Typically, there are only five stations monitoring NO_X and two monitoring nonmethane HC. There is no routine monitoring of HC speciation, which is very important to O_3 formation.

The routine measurements are nevertheless very important in helping us to understand the model performance and the air quality situation. However, the measurements are not sufficiently complete that they can be used in lieu of modeling. As with other cities, the measurements, models, and emission inventories must be used together to obtain a good tool for air quality planning.

The three major air quality concerns addressed in this study are CO, O_3, and SO_2. The O_3 ambient standards are exceeded approximately 350 days a year in Mexico City. Carbon monoxide ambient standards are also exceeded many times a year, while SO_2 standards are much less frequently exceeded. Both SO_2 and CO are monitored continuously around the city, and their behavior also provides important insights into the

dispersion of pollutants such as NO_X and HC, which react to form O_3. The CO is a problem associated with emissions at low level, primarily mobile sources. The SO_2 emissions have important low-level sources, but are also associated with major, industrial, tall-stack sources and are found in the hot gases that rise above the stacks. Pollutants that are emitted from tall stacks have a much different behavior from those emitted near the surface. At night, emissions from tall stacks may be prevented from mixing down to the ground, while emissions from low-level sources can produce high pollution concentrations because of limited mixing under an inversion cap. Nitrogen oxides are emitted from both surface and elevated sources. An understanding of the behavior of SO_2 helps to understand NO_X dispersion without the complications of NO_X chemistry. Neither SO_2 nor CO are very reactive, so they can be treated adequately without using chemistry models. In the case of CO, the local concentrations are very sensitive to local winds and local source distributions. Typically, CO is estimated with simple models and interpolated, or locally measured, winds. The SO_2 emissions can also be influenced by local winds and local sources, but there is an additional complication posed by sources that are intermittently mixed down to the surface monitors from tall stacks.

The O_3 is formed in the atmosphere by reactions involving HC, NO_X, and sunlight. Since O_3 takes time to form and is formed during the daytime when there is more mixing, it is not as sensitive to either small-scale sources or the details of the wind fields. Ozone can be sensitive to local high concentrations of nitric oxide (NO), which can locally reduce O_3 concentrations. Because O_3 is formed from both NO_X and reactive HC, it is possible to get the right answer for the wrong reasons.

There have been two strategies for O_3 modeling. The most common strategy involves the use of a variety of meteorological measurements interpolated in time and space to estimate the winds, stabilities, and mixing heights that are used to drive the photochemical models. The second approach is to use a limited set of measurements as input to a three-dimensional, time-dependent meteorological model. In the latter case, the physics are built into the model, while in the former case, the physics are inferred from measurements. In a trend that is indicative of the future, investigators are moving toward the second approach—using physics intensive models. For this work, the second approach was chosen because of the limitations of the existing measurements.

B. METEOROLOGICAL MODELING

1. Objectives

The objective of the meteorological modeling was to provide transport variables for the dispersion and air chemistry models and to help provide an understanding of the air quality situation.

2. Background

Frequently, air quality modeling relies on simplistic assumptions about winds and transport parameters. For example, in some simple situations a wind measured at a single site will be taken as representative of the winds throughout the region of interest. However, if the terrain is complex, such simple assumptions are of little use. In complex terrain measurements are frequently representative of only very small volumes of air surrounding the site of the measurement. For major urban areas there are two approaches to defining transport variables. One involves interpolating between measurements to provide winds at all points of interest. The other approach involves modeling winds with a meteorological model that can compute a full, three-dimensional, time-dependent wind field. The intent of the latter approach is to represent the important physics in detail rather than to rely on a dense system of wind measurements that implicitly contain the physics.

Mexico City lies at an elevation of approximately 2200 meters above sea level in a U-shaped basin that opens to the north. Mountains on the east and southeast sides of the basin form a barrier with a height of approximately 3500 meters while two isolated peaks reach elevations in excess of 5000 meters. The city occupies a major part of the southwest portion of the basin. Upper-level wind measurements are provided by rawinsondes at the airport; low-level winds are measured at several sites within the city. Many of the sites have obstructed upwind fetches in a variety of directions. During the wintertime when the worst air quality episodes occur, the winds are frequently light and out of the northeast. This means the winds are light within the city, but significant slope winds develop that influence the behavior of the pollutants. The result of this combination of circumstances is a relatively short-residence time for morning rush-hour emissions, but a long-residence time for afternoon and evening emissions.

3. Description of the Model

HOTMAC is a three-dimensional time-dependent model (Yamada 1981, Mellor and Yamada 1982, Yamada 1985). It uses the hydrostatic approximation and a terrain-following coordinate system. HOTMAC solves conservation relations for the horizontal wind components, potential temperature, moisture, turbulent kinetic energy, and the turbulence length scale. HOTMAC describes advection, Coriolis effects, turbulent transfer of heat, momentum, and moisture. It also describes solar and terrestrial radiation effects, turbulent history effects, and the drag and radiation effects of forest canopies. The lower boundary conditions are defined by a surface energy balance and similarity theory. The soil heat flux is obtained by solving a heat conduction equation that ignores lateral heat transfer in the soil. In an urban context the surface energy balance requires an additional term that

represents the heat released by human activities. The additional heat, along with differences in thermal and albedo properties between urban and non-urban surfaces, produces the urban heat island.

At the start of this project, HOTMAC used two major sets of inputs: topography and a single vertical profile of winds, temperatures, and relative humidity. The topography consisted of terrain heights at half-grid intervals over the domain and indices that showed which computational cells were covered with water and which had trees. In the case of trees, the fraction of the area of the cell that was covered by trees was also required. In the instance of cells covered by water, the ground temperature is fixed and the air at the surface is saturated.

The meteorological profile is used to describe the synoptic (large-scale) conditions of winds, temperatures, and moisture. The model is initialized with the potential temperature assumed to be the same in every location for any given height above mean sea level. Potential temperature is the temperature of a parcel of air adiabatically compressed to sea-level pressure. In a well-mixed atmosphere, the potential temperature tends to be constant with height except for very near the surface. On the lateral boundaries the winds, moisture, and temperatures are the result of solving a one-dimensional form of the model in which parameters vary only in the vertical direction. The placement of the boundaries is normally chosen so that all the major terrain influences on the region of interest are included within the computational grid.

Mesoscale models are designed for circumstances in which the local terrain influences are significant and make the meteorology more predictable than might otherwise be the case. The top boundary of the model is fixed at a constant height above sea-level and is a no-flow boundary. The model uses a vertical grid that is linear for a specified number of cells, but then increases parabolically to the top. In a typical application the first 4 cells would be 4 meters high each, after which the cell height would expand from 37 meters for the fifth cell to over 600 meters for the last cell. The horizontal grid is staggered so that the east-west and north-south wind components are calculated at points that are offset one-half grid in the corresponding directions. The model uses the alternating-direction implicit differencing technique, which provides high accuracy and stability. The model uses a nested grid system so that areas of importance can be treated in much greater detail. In the current version, the innermost grid is one-third the scale of the next larger grid. The computational time is dominated by the requirements of the innermost grid so that the outer grids require little computational time. The model forms clouds, but it does not permit precipitation. This version of the code does not treat the radiation effects of clouds. Other versions of the code have been used to describe long-wave radiation from clouds.

HOTMAC has been used successfully in many contexts. It has been used in the geysers region, which is in the Pacific Coast Range near the Pacific Ocean of California. It has been used to describe flow in narrow, deep canyons of western Colorado. It has described the formation and dissipation of clouds during evening hours over the south coast of England. It has successfully described the linked sea breeze between the Pacific Ocean and the Japanese Alps. It has also been used on sub-continental transport problems in the eastern U.S. and the southwestern U.S.

4. Model Development

Early in this project, three days, representing poor, good, and normal air quality were chosen for detailed modeling. All of the days were in the winter of 1987-88. Meteorological inputs were based on the afternoon rawinsonde measurement of the preceding day, which was used to estimate synoptic scale wind and temperature profiles. We used a nested grid system to model the Valley of Mexico and its surrounding terrain. The outer grid has a 6 km spacing and covers the major terrain influences as shown in Figure B.1. The inner grid is enclosed in the red box and embraces the city and the immediately adjacent slopes. The photochemical model domain is enclosed in the blue box. The "urbanized area," as defined by CO emissions, is shown in yellow. The individual characters plotted on the figure are meteorological monitoring sites operated by the SEDESOL. For example, station "Y" is the Hangares station at the airport. The inner grid has a resolution of 2 km. The two white areas in the lower right-hand side are the two 5000-meter-plus volcanoes.

Initially, the urban canopy was approximated by using the estimated distribution of CO emissions defined on a 1 km grid. The relative CO emissions were used to proportion the fraction of the area of a grid cell that was covered by canopy (rooftops), the average soil conductivity, average soil heat capacity, and the urban heat release intensity. The modeling showed that on days with poor ventilation and consistent upper-level winds, the meteorology of the region could be reasonably represented. However, with changing upper-level winds, the model gave poor results.

a. Modifications for Changing Large-Scale Winds

The original version of HOTMAC developed the large-scale winds from the winds used to initialize the model. Essentially, a single wind speed and direction aloft are used to produce the effects of varying large scale pressure systems. In order to have a wind shear above the lowest levels, the model allows the user to specify two wind levels. The result of the coding is to add additional factors in the conservation equations for the two horizontal components so that the wind velocities are nudged toward the desired velocities at the specified levels. The first alteration for time-varying winds was to permit the input winds aloft to be variable with time. The velocities to which the computation is nudged at any given hour would be interpolated in time between the input values at the two nearest times for which measured winds were available.

This approach, however, suffers from two deficiencies: the low-level driving winds are not changed unless the specified levels are quite low and the differences between the measured wind and the large-scale wind are not considered. The lack of low-level wind changes was solved by nudging the lowest-level wind velocities to the average velocities for the lowest 500 meters of the atmosphere. The measured wind normally reflects both the large-scale wind and the local influences of topography and surface features.

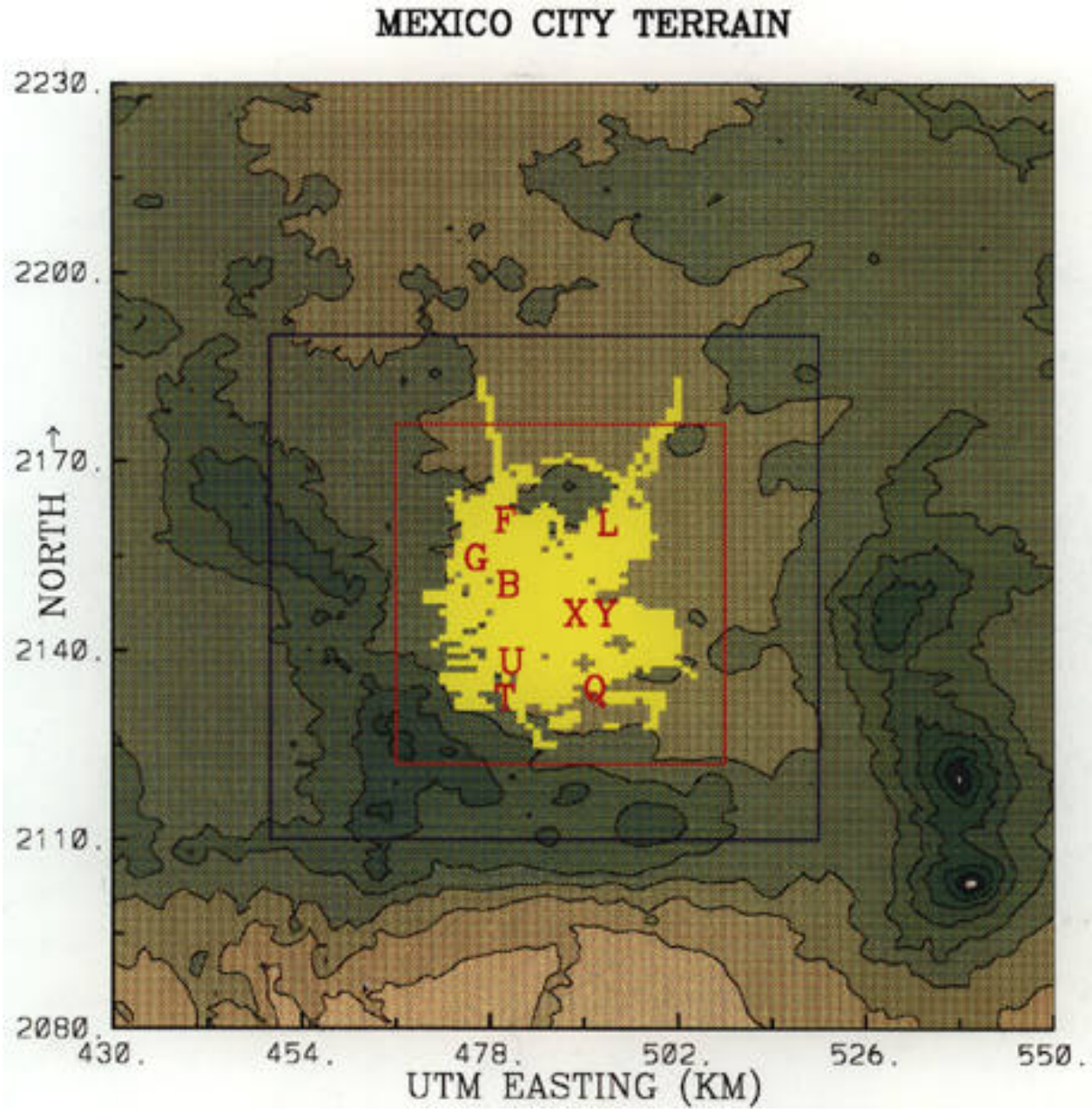

Figure B.1. Modeling domains for the Valley of Mexico air basin. The entire picture comprises the outer grid of the meteorological model. The inner grid is shown by the red box, and the photochemical model domain is shown by the blue box. The urbanized area is depicted in yellow.

b. Modification for Local Wind

The procedure to adjust for the difference between the local and large scale wind was based on using the model to estimate the local wind in the lowest 500 meters. Essentially two model runs are made. In the first run average upper-level conditions are used, and the low-level wind velocities are nudged to very low values to represent no large-scale forcing. Typically this model run is for a simulated one and a half days with one half day to condition the model and one day to provide hourly local wind estimates. The local wind velocities from the model are then subtracted from the measured wind velocities. In the full simulations the modeled local winds are nudged to that difference. This procedure permits the model to reproduce the measurements and make good estimates for other points. It also shows good performance over many days without reinitializing the model.

c. Urban Canopy Description

The buildings, pavement, and heat released by human activities influence the meteorology in urban areas. There are two basic approaches to deal with this effect. One is to use a different roughness length, while the other is to use a canopy. HOTMAC has had a canopy that was developed for forested areas. In the canopy approach alterations are made to the conservation equations for momentum and turbulence to account for the drag effects, while the energy balances are also modified. The energy balance changes involve interception of short- and long-wave radiation by the canopy with associated heating or cooling of the air at the height of the canopy and associated changes at the surface. The original canopy was designed for a forest in which the radiation striking the top of the canopy was not immediately absorbed, but instead, decreased exponentially with distance into the canopy. In addition, there was an implicit assumption that the canopy area perpendicular to horizontal winds was similar to the canopy area projected on the surface. For an urban area, the projected area in the vertical planes is typically much less than that in the horizontal plane. In the current application, the drag coefficient was reduced to account for the differences in vertical and horizontal projected areas. A second change was to allow the canopy to completely intercept radiation falling on it and to allow the canopy to radiate at the temperature of the air at the height of the canopy. Finally, an estimate of the anthropogenic energy released by motor vehicles was put into the energy balance for the lowest few meters of the atmosphere. The current canopy does not have any energy storage.

d. Surface Moisture Treatment

The original version of the model used a very simple treatment of moisture that did not allow the effects of dew formation and other surface moisture features. A new treatment was developed where moisture could accumulate at night on the surface if the temperature reached the dew point. The next day, the sun's heating would be used to dissipate the surface moisture until it had been evaporated. If the surface was dry and the sun was well up, the Bowen ratio, which is the ratio of the sensible heat flux to the latent energy flux, is assumed to be constant. In other words, the energy flux to the atmosphere is apportioned between the heating of the air and evaporation /transpiration of water by a fixed ratio. At other times the evaporation is nil.

e. Surface Coverage Treatment

The original version of the model used only two surface features: water surface and everything else. The model was changed to permit an urban classification, and later it was further altered to accept the results of a satellite-derived surface categorization. The categorization produced 13 categories that are listed in Table B.1.

The satellite data were used to categorize the inner-grid area. Areas outside of the inner grid were described as having mountain vegetation for elevations above 2600 and as having foothills vegetation (category 6) to represent scrub lands for elevations below 2600 meters. The satellite data file gave the fractions of each category in 2 km by 2 km grid cells, which were 1 km offset in each direction from the meteorological grid. The fractional land coverage data were interpolated to the meteorological grid.

For each classification, an estimate was made of the associated surface characteristics: (1) surface albedo, (2) surface thermal emissivity, (3) surface daytime Bowen ratio, (4) soil heat capacity, (5) soil density, and (6) soil thermal diffusivity. The land coverage percentages were used with the category values to estimate the appropriate surface characteristics for each grid cell. In the case of the Bowen ratio, simple area-weighted means, as used for the other parameters, are not appropriate.

The mean daytime Bowen ratio for a cell was calculated as

$$b_{avg} = \frac{\sum_{i=1}^{13} \frac{f_i}{1+\frac{1}{b_i}}}{\sum_{i=1}^{13} \frac{f_i \frac{1}{b_i}}{1+\frac{1}{b_i}}}$$

where b_i is the Bowen ratio for the class while f_i is the fraction of the cell covered by the class. This averaging was chosen to reflect the fact that the total energy released to the atmosphere is proportioned between the sensible heat flux and the latent energy flux. For example, suppose one cell that was split between a very dry portion and a portion that was very wet. A very dry area might have a Bowen ratio of 20, because it

TABLE B.1 Categories Used to Determine Surface Features

Categories
1. vegetation (golf course fairways were placed in this category)
2. mostly bare soil (dry tilled fields and sandy areas are examples)
3. dark soil (irrigated tilled fields would be an example)
4. shadow-volcanic-urban (basalts and shaded urban areas for example)
5. urban lower income (lighter urban areas)
6. vegetation-foothills-city
7. water
8. dark urban material
9. urban material mixture
10. urban (mostly downtown)
11. vegetation mix
12. mountain vegetation
13. a mountain vegetation and rock mixture

would have very little evaporation. A very wet area could have a Bowen ratio of 0.01 because virtually all the solar radiation falling upon it would go into evaporation. We would expect that the overall Bowen ratio for the entire cell would be about 1.0 because half of the solar radiation would be going into evaporation from the wet half, while half would be going into atmospheric heating from the dry half. The above formulation gives a value of a little over 0.9, while an area-weighted average of the two ratios would give a value of about 10 and would suggest a very dry surface.

5. Comparison with Measurements

Measurements are very important to provide model inputs and to help understand the limitations and performance of the models. For the meteorological model there were six types of measurements that were available to provide insight into the model's performance. The measurements are

- surface station winds,
- rawinsonde profiles,
- tethersonde profiles,
- aircraft meteorological profiles,
- aircraft elevated winds, and
- mixing heights derived from light detection and ranging (lidar).

It is important to realize that the model and the measurements are not necessarily attempting to represent the same item. For example, the surface winds are measured at a single site and represent one-hour scalar averages of the wind direction and wind speed. At the same time, the model provides one-hour ensemble mean vector averages of the wind over a 2 km by 2 km grid with a vertical depth appropriate to the grid cell. The model takes the ground level as the street level and includes the buildings as the above-ground canopy. The measurement sites are usually chosen to be in more open areas, but they may be influenced by nearby buildings or trees.

There were two periods in which detailed comparisons were made with a variety of measurements. The first period was February 21 through February 22, 1991, which was a period with a good scope of measurements and was also a period in which high O_3 concentrations occurred in the southwest portion of the city (on February 22). This period represents a classical pollution episode. The second period is from February 25 through February 28, 1991. There were fewer measurements available during this period, and the highest O_3 occurred in the downtown region on February 28.

During the first period, the simulations were begun with information from the late afternoon and early evening rawinsonde measurements at the airport. Rawinsonde measurements are made by launching a balloon with a radio transmitter and following the transmitter with a radio direction finder. The transmitter radios back the pressure and dry-bulb and wet-bulb temperatures, while the direction finder gives the balloon's location. The analyzed measurements give the height, pressure, wind direction, wind speed, temperature, and relative humidity. The balloons are designed to rise at a rate of about 200 meters per minute. In the Mexico City work, the data were available at increments of about 75 meters in height. About 7 rawinsonde flights were made each day. During both periods, the upper-level winds at 2000 and 3000 meters above the surface were based on the rawinsonde measurements.

During the first period, the low-level wind data were obtained by averaging the winds between 250 meters and 750 meters from the tethersonde measurements that were made at the Polytechnic site. Wind speeds, wind directions, pressure, and wet-bulb and dry-bulb temperature are measured continuously as the cable is slowly reeled out. Approximately one hour is used to allow the tethersonde to reach the maximum height of 1 km. In contrast, the rawinsonde takes a much shorter time to traverse the same height and produces data at much larger intervals. The model requires an ensemble mean wind, and thus the tethersonde provides a better approximation of the required input. For the second period where relatively few tethersonde profiles were available the rawinsonde profiles were used.

The model begins with the temperature being horizontally uniform; this is characteristic of most afternoons in which the atmosphere is well-mixed. Normally, the sounding profile taken at about 5:00 p.m. was used to start the simulation. The temperature and relative humidity profiles from the sounding were used to define an approximate profile for input to the model.

a. Comparison to Surface Station Winds

The model produces volume-averaged, ensemble mean vector winds. These winds are interpolated between grid cells to the monitoring locations. The measurements, which were provided by SEDESOL, represent scalar-averaged wind speeds and directions. In the scalar averaging of the directions the previous wind direction is considered. For example, if the wind were from 350 degrees one minute and 5 degrees the next; 360 degrees would be added to the 5 degrees to make 365 degrees for averaging purposes. In addition to the uncertainty caused by the averaging techniques, stations may experience local influences that would be too fine a scale for the model.

Two kinds of displays were developed to help understand the model performance: hourly plots in which the model wind vectors are shown along with the measured winds and station locations, and daily time-profile plots in which either the wind direction or the wind speed is shown in comparison to the measurements. In both cases the terrain is also shown as well as the locations of the sites. Figures B.2 through B.5 show hourly comparisons for the morning, afternoon, morning transition and evening for February 22. The dark green in the lower left hand corner of the figures represents the mountains to the southwest of the city; only the inner grid is shown. The symbol Y represents the Hangares station of the SEDESOL network, which is located at the airport. The mountains in the upper central area are Pico de Tres Padres, which are north of the city center. The blue arrows show the modeled wind speed and direction, while the red arrows show the measured wind speed and direction. The modeled values are for 26 meters in the terrain-following coordinate system, which corresponds to about 40 meters above the ground. This height was chosen because it is the first height above the highest point of the canopy for which calculations were made. The 6:00 a.m. slope winds as evidenced by stations U and T, which are closest to the mountains, are well represented. Station B is not well represented, but it generally seems to show anomalous behavior. The city stations such as X and Y show a somewhat different behavior, which is not what might be expected because of

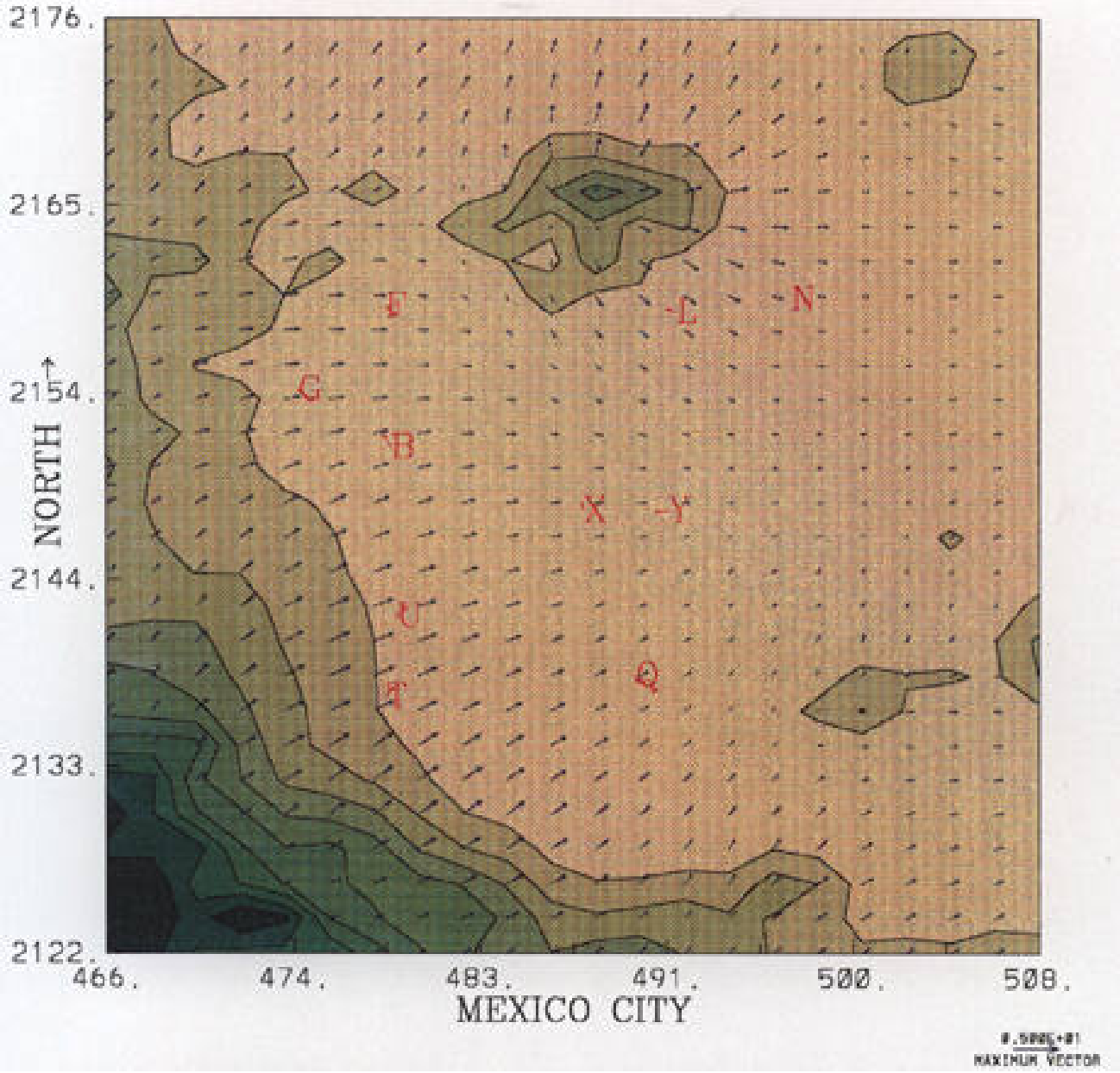

Figure B.2. Comparison of measured winds (red) to computed winds (blue) for 6:00 a.m., February 22, 1991, with station locations and topography.

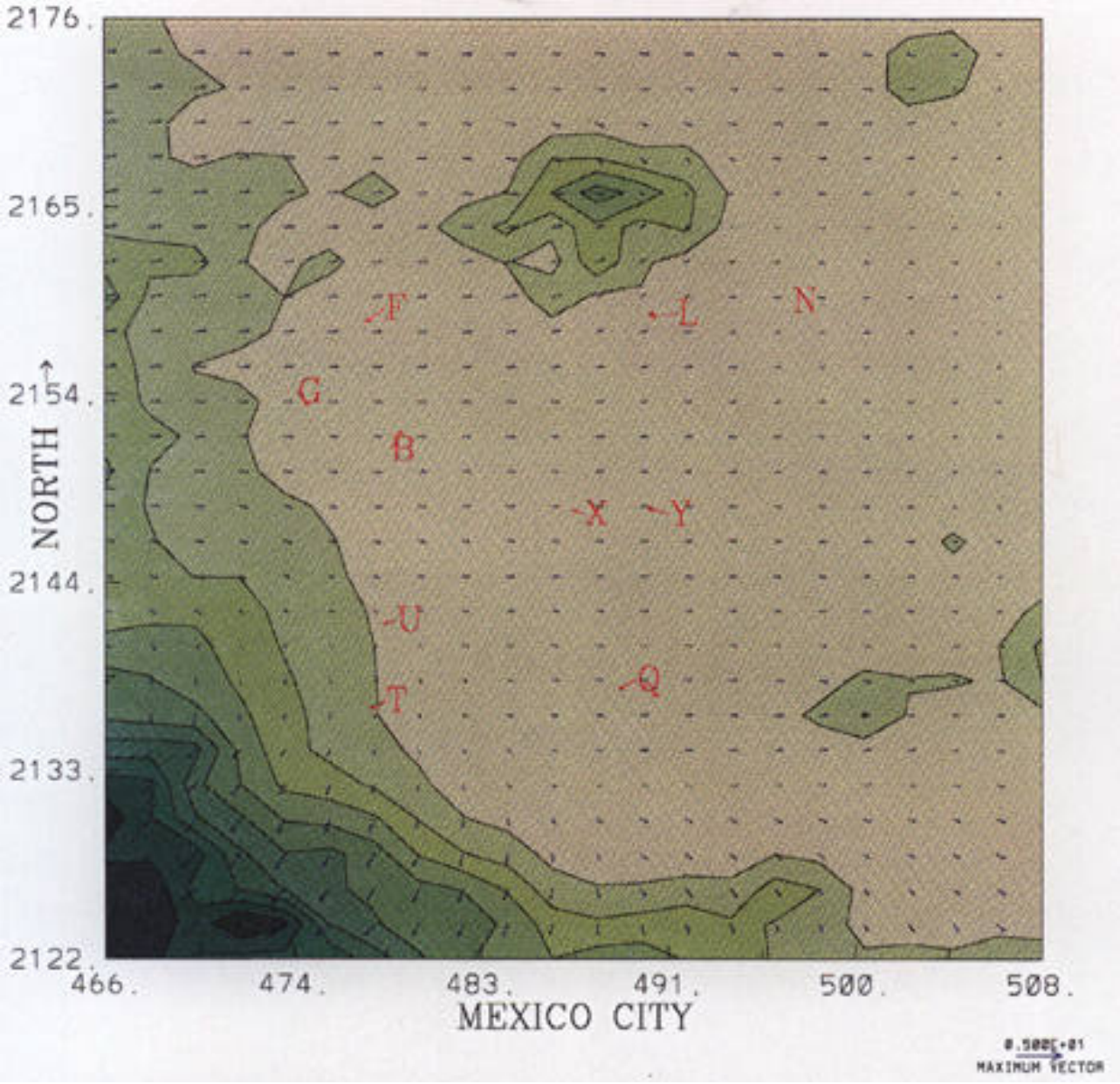

Figure B.3. Comparison of measured winds (red) to computed winds (blue) for 10:00 a.m., February 22, 1991, with station locations and topography.

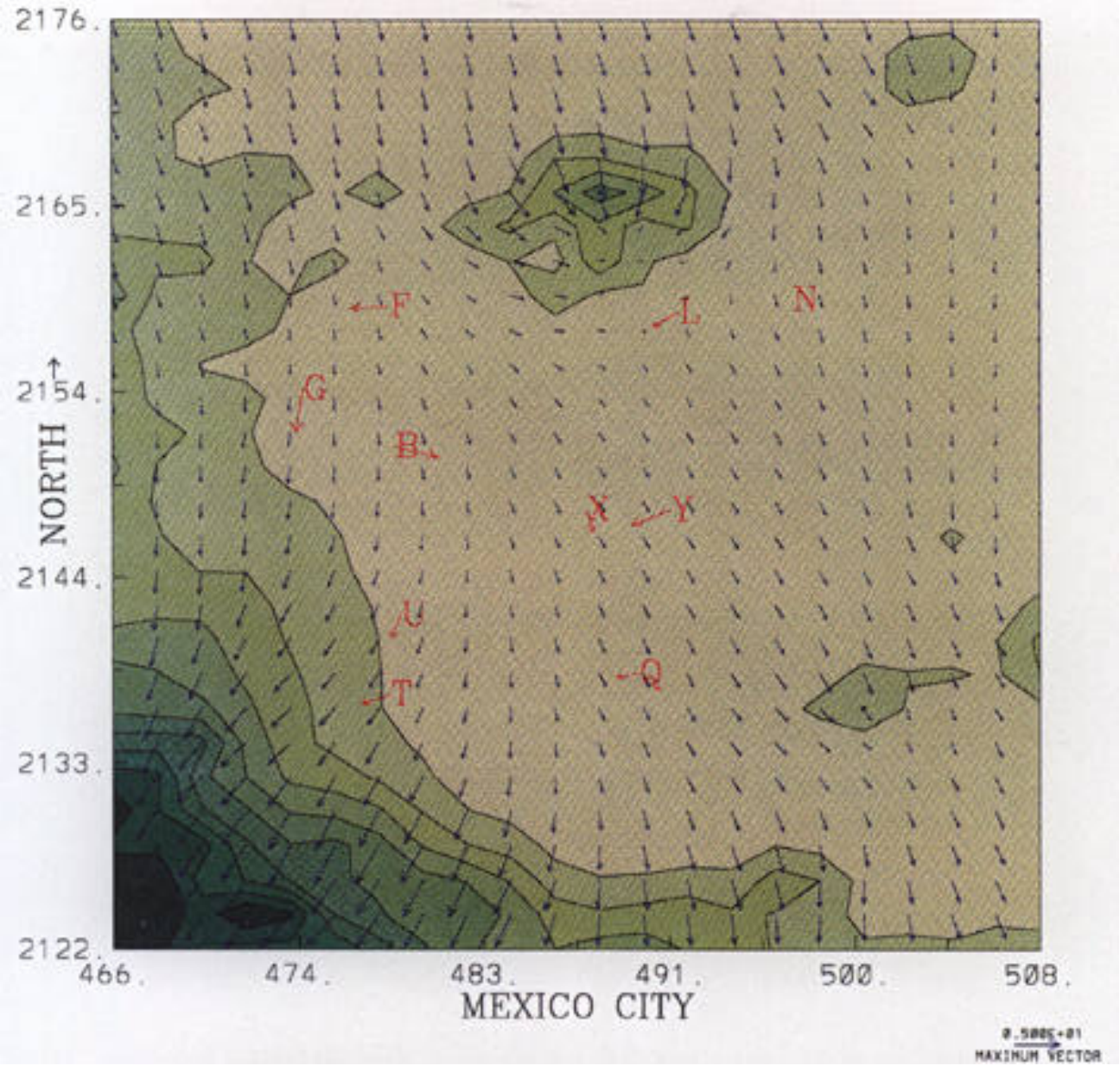

Figure B.4. Comparison of measured winds (red) to computed winds (blue) for 1:00 p.m., February 22, 1991, with station locations and topography.

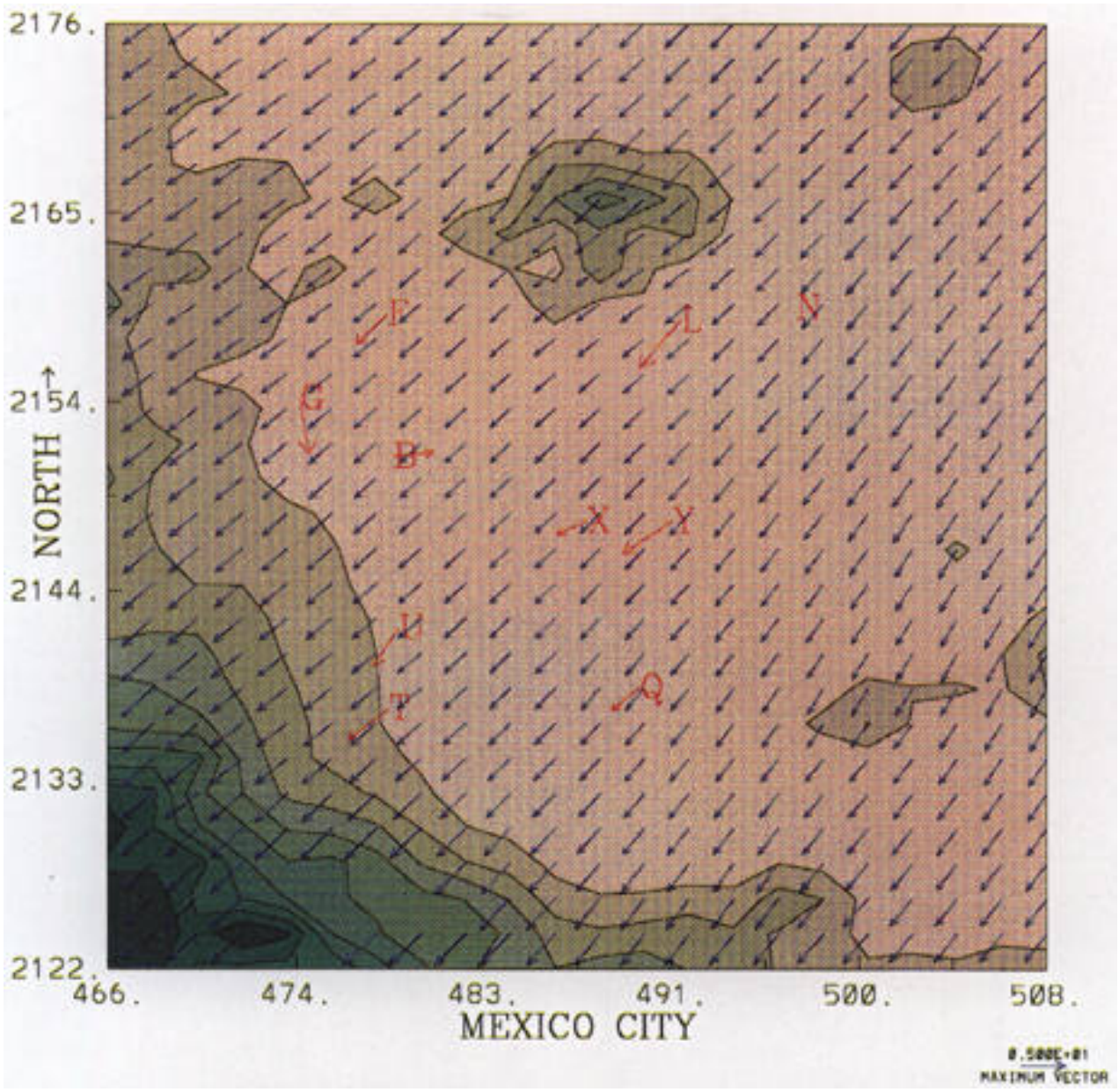

Figure B.5. Comparison of measured winds (red) to computed winds (blue) for 9:00 p.m., February 22, 1991, with station locations and topography.

the likely local effects. There is also some suggestion in the data that there is more wind convergence over the city than the model shows, as seen by winds from the west on the west side of the city and winds from the east on the east side of the city. The transition to up-slope flows occurs at about 10:00 a.m., and the model is showing a less-developed transition than are the measurements. Figure B.4 shows the afternoon flows at 1:00 p.m. with fully developed slope winds. At 9:00 p.m. strong winds out of the northwest dominate the flow fields, and there is good agreement between the model and the measurements. This wind is likely the result of a coupled sea breeze and valley breeze from the Gulf of Mexico. Model simulations with the Regional Atmospheric Modeling System (RAMS) model and a large enough domain to include both oceans predict the occurrence of these winds. The RAMS model was developed by Roger Pielke and his colleagues at Colorado State University; it is a three-dimensional prognostic meteorological model, and it is designed to use input from the National Meteorological Center's gridded analyses of meteorological conditions. These four figures demonstrate the variety of wind conditions that can occur in the valley. They also show that the model does a reasonably good job of representing the major features.

Figure B.6 shows the time profiles of wind directions at all sites on February 22, while Figure B.7 shows the time profile of wind speeds at all sites on February 22. In Figure B.6 the entire model domain is shown so that the two white points on the lower right-hand side are the two 5000-meter-plus, volcanoes, the central green splotch is Pico de Tres Padres, and the red Y is the airport. The model shows good behavior for stations U and T, although there are some large fluctuations in the measurements that may be the result of afternoon clouds, which are not represented in the model.

The wind speeds shown in Figure B.7 represent a good agreement in the early morning hours and the late evening hours, but they underestimate the increase in the late morning and afternoon winds. Part of this difference may be related to the difference between vector-averaged winds and scalar-averaged speeds. For an extreme example, suppose that the wind for one minute was from the north at 2 meters per second and then it shifted to the south for the next minute. The vector averaged wind for the two minutes would be zero, while the scalar averaged winds would be 2 meters per second. Actual experiments as reported by Dr. Hector G. Riveros R. of the Instituto de Física at the Mexican National University (UNAM) show that the scalar averages can be much greater than the vector averages during circumstances where the mean winds are light, and the turbulent fluctuations are large. From an air transport point of view the vector average is the more relevant because the critical question is how long the same air mass remains near the source and experiences increased concentrations.

Figures B.8 and B.9 show the comparisons between measured and modeled wind direction profiles for February 25 and February 28 respectively, and Figures B.10 and B.11 show the comparisons for wind speeds. The simulations show relatively good agreement with measurements despite the fact that the model was initialized with rawinsonde data and the fact that the simulation extends for a relatively long period. The wind speed comparisons show a similar behavior to that found on February 22.

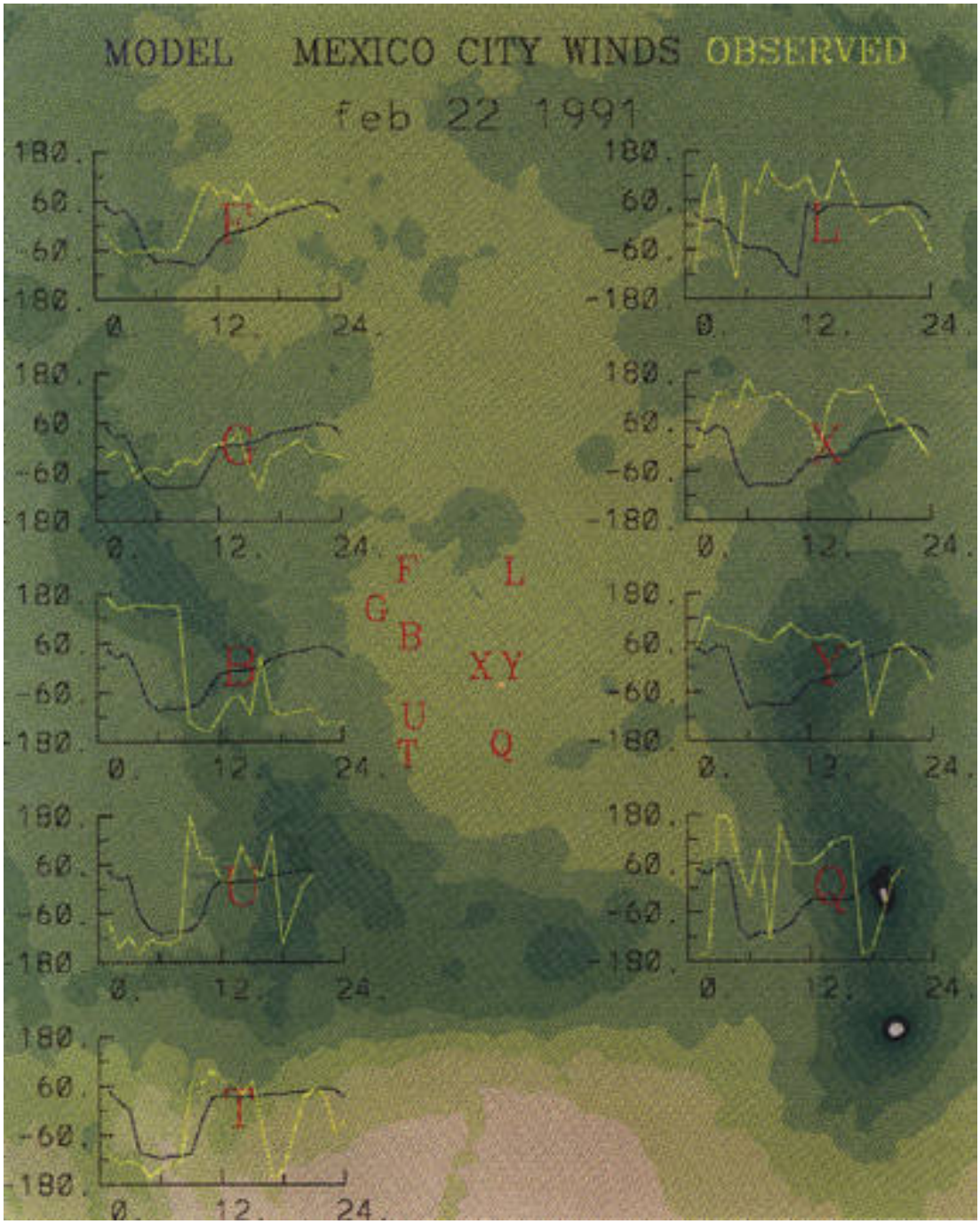

Figure B.6. Comparison of measured hourly wind directions (yellow) to computed hourly wind directions (blue) on February 22, 1991, with station locations and topography.

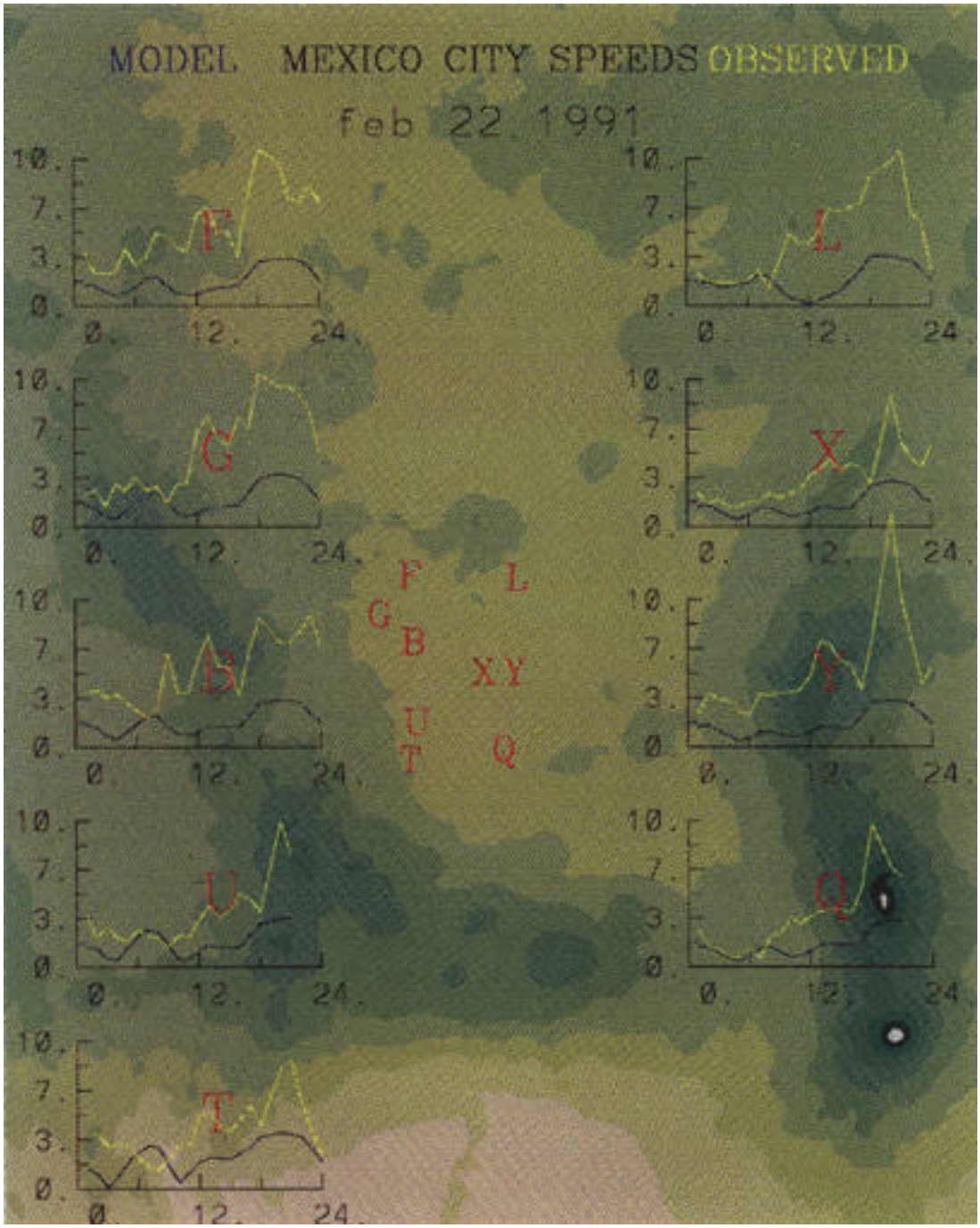

Figure B.7. Comparison of measured hourly wind speeds (yellow) to computed hourly wind speeds (blue) on February 22, 1991, with station locations and topography.

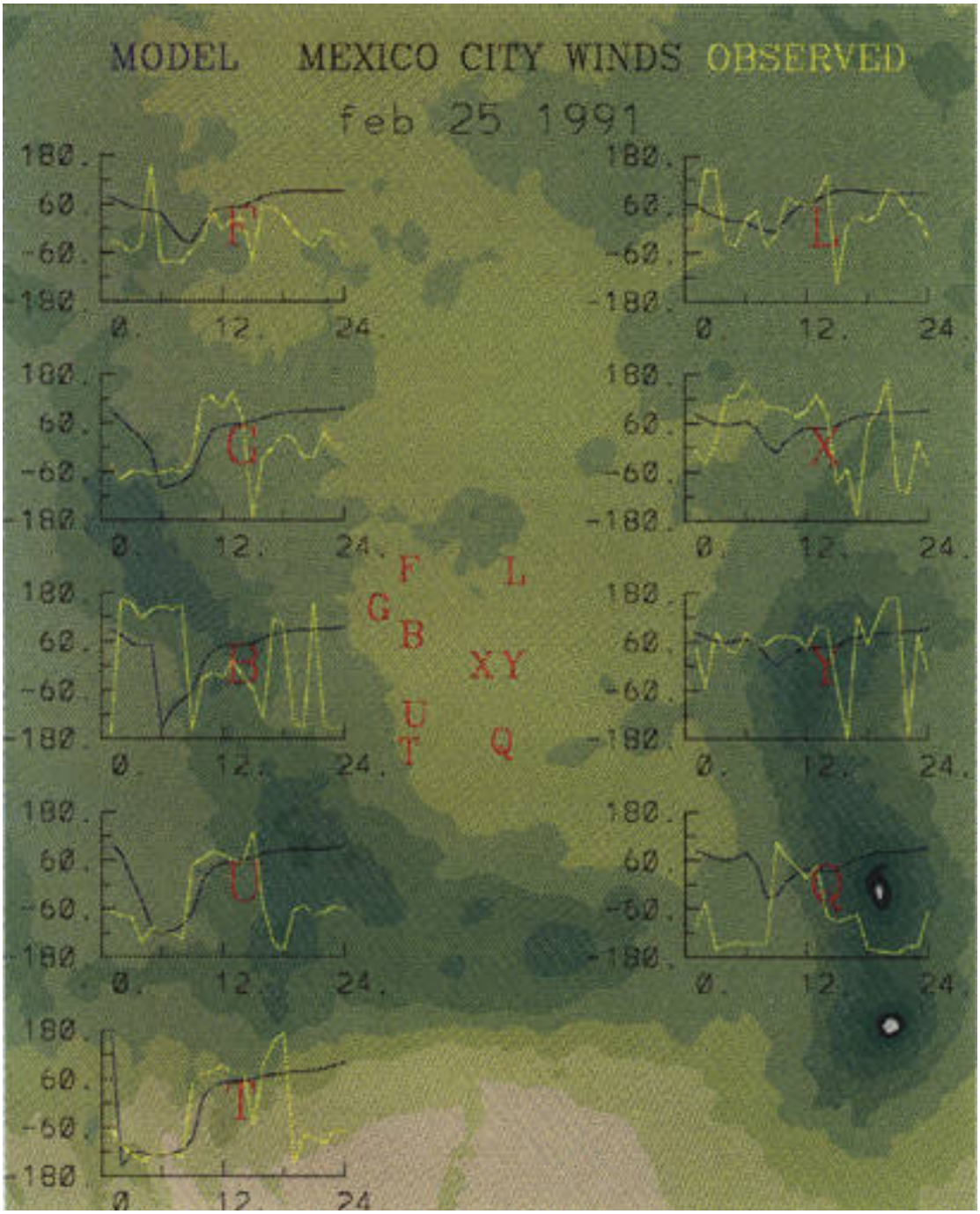

Figure B.8. Comparison of measured hourly wind directions (yellow) to computed hourly wind directions (blue) on February 25, 1991, with station locations and topography.

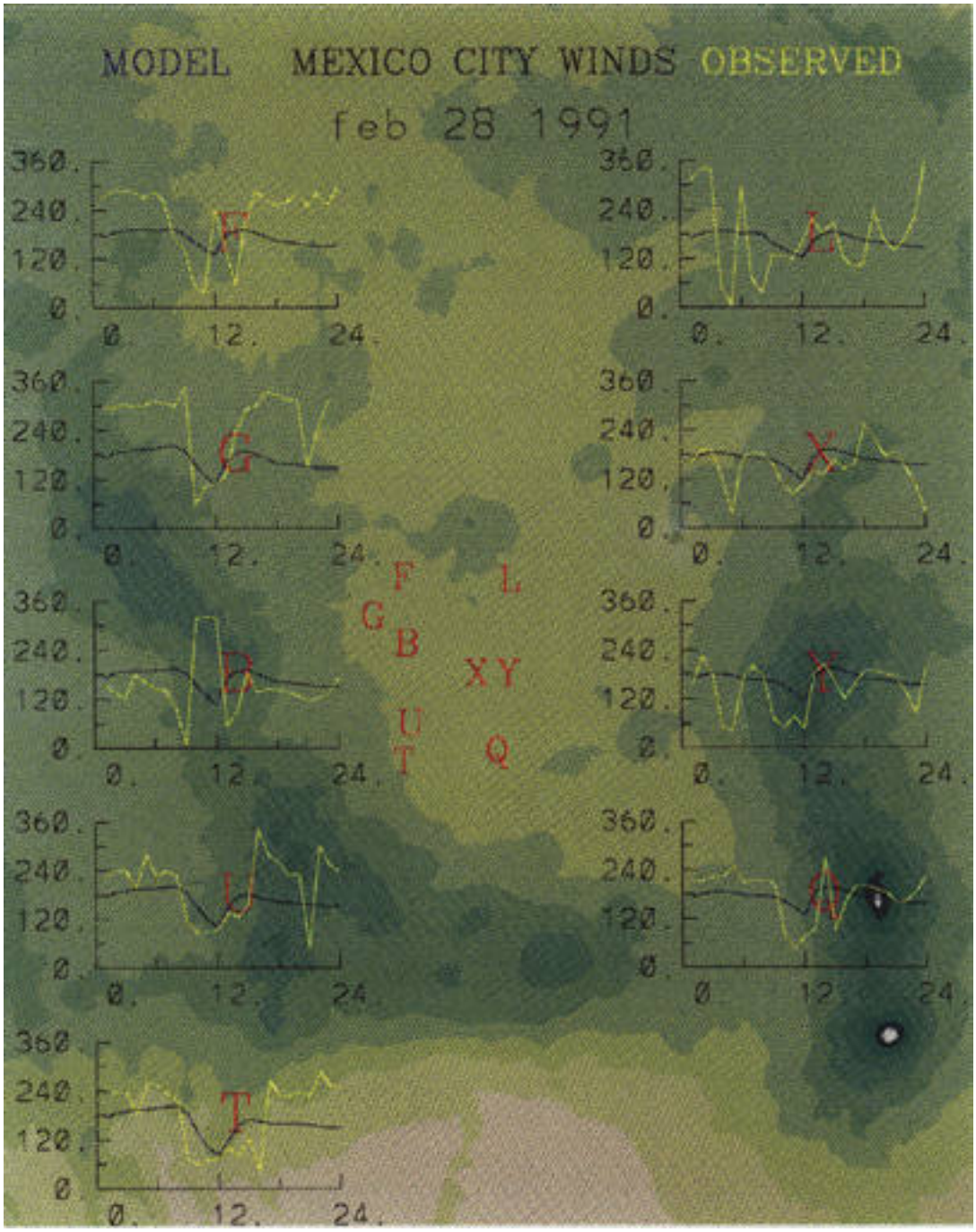

Figure B.9. Comparison of measured hourly wind directions (yellow) to computed hourly wind directions (blue) on February 28, 1991, with station locations and topography.

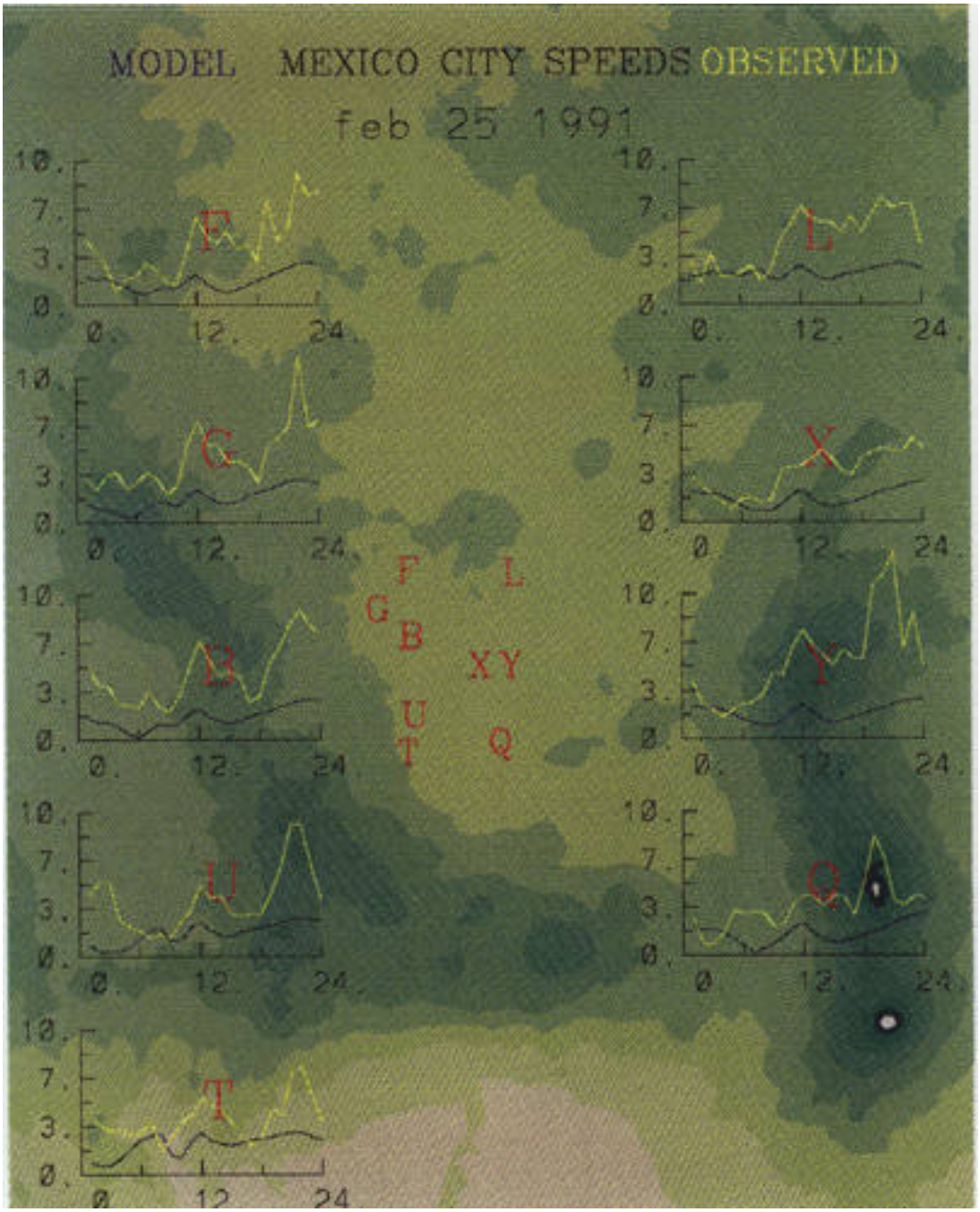

Figure B.10. Comparison of measured hourly wind speeds (yellow) to computed hourly wind speeds (blue) on February 25, 1991, with station locations and topography.

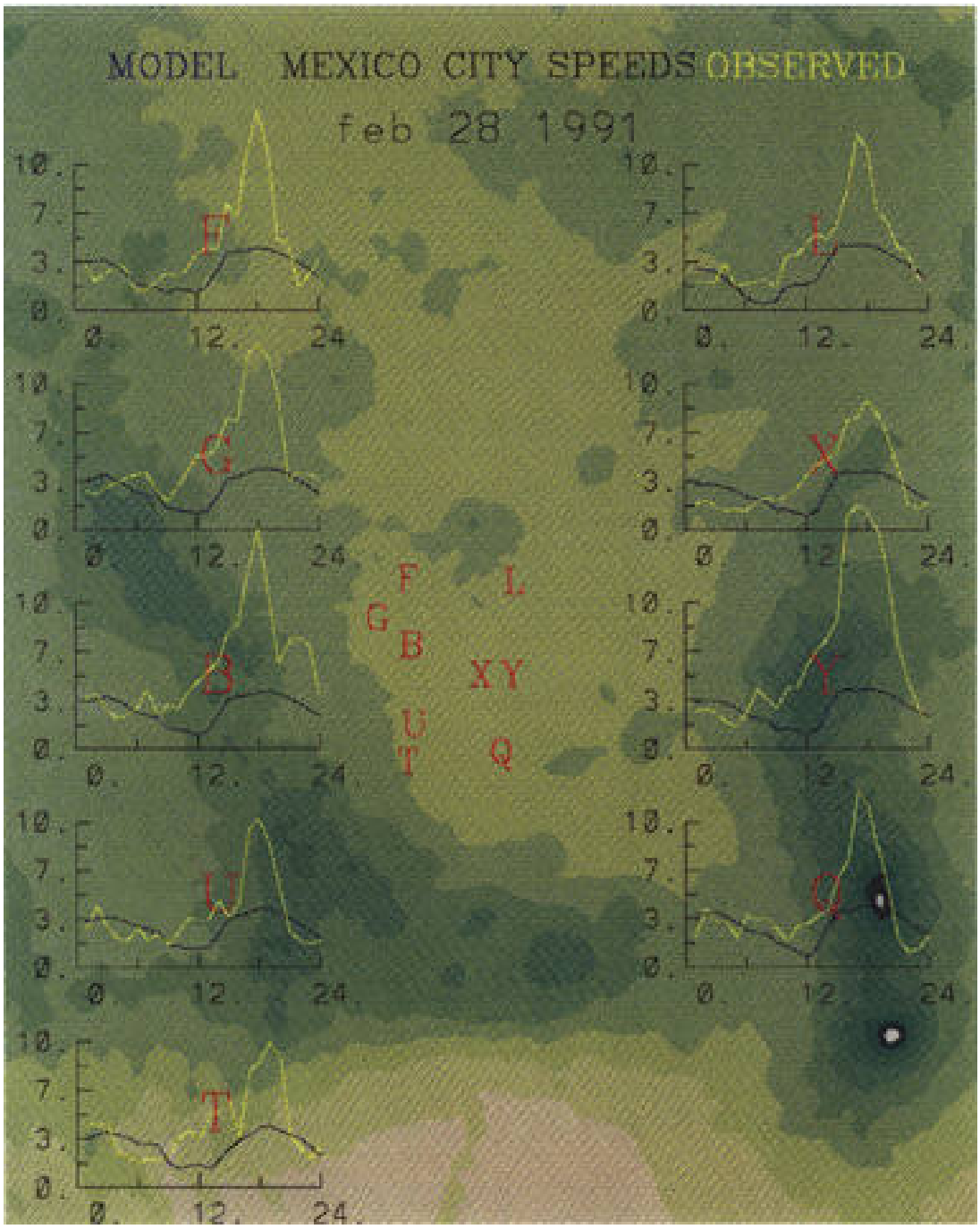

Figure B.11. Comparison of measured hourly wind speeds (yellow) to computed hourly wind speeds (blue) on February 28, 1991, with station locations and topography.

b. Rawinsonde Profiles

One concern in the comparison of model winds to the rawinsonde winds is the relatively short time over which the rawinsonde measurements are made. The difficulty of a brief measurement period is that it may not be very representative of the average conditions that the model is asked to predict. This concern is particularly important during the daytime, when the wind fluctuations are large. To address this concern, plots were made in which two standard deviations of the wind components were added or subtracted from each modeled wind component. Figure B.12 is an example of such a comparison for 2:00 p.m. on February 22, 1991. The solid line shows the measured wind directions by the rawinsonde, the dotted line shows the model prediction, and the dashed lines show the modeled directions with two standard deviations added or subtracted from the horizontal wind components. At the bottom of the figure the dashed lines indicate that essentially any wind direction is consistent with the model because the turbulent fluctuations are so large. Since the standard deviations are provided by the model, we can see that the measured winds are consistent with the model results up to 2.3 km above the surface. In a similar fashion, the modeled wind speeds are consistent with the measurements shown in Figure B.13 below 2.0 km and above 0.2 km. Near the surface there is a high-speed tail in the measurements, which is likely to be either a very local effect, or perhaps a result of the balloon being launched from a point other than the assumed point. The high-speed tail is a frequent feature in the rawinsonde measurements. Figure B.14 shows the comparison between modeled and measured winds at 3:00 a.m. In this case there are differences that reach a maximum of about 70 degrees at 200 m. The very low turbulence is apparent as the dashed lines collapse onto the dotted line. High levels of turbulence remain at the surface and also appear in the layer from 1 to 2 km where the high wind shear is important. The wind-speed comparison is shown in Figure B.15 and shows a similar behavior to the wind directions.

Figure B.16 shows the comparison between modeled and measured potential temperature at 3:00 a.m. on February 22. A well-mixed atmosphere would show as a vertical line on this type of a plot. Both curves show a stable atmosphere near the surface, but the measured atmosphere is considerably more stable. There is some evidence that the modeled long-wave radiation parameters are producing a slight overestimation of long-wave radiation. The afternoon potential temperature is shown in Figure B.17 and shows a very similar behavior in both the model and the measurements.

Figure B.18 shows the comparison between the modeled and measured water vapor at 3:00 a.m. while Figure B.19 shows the same comparison for 2:00 p.m. In the morning comparison the model misses some of the lower level variation, while in the afternoon, the comparison is good. The increased water vapor levels near the surface in both the model and the measurements are associated with evaporation or transpiration at the surface.

The problem of representative upper-level data is an important one, and the wind simulations suggest the rawinsondes are telling us less than we would like them to. This problem is important, not just for Mexico City air quality; it is also important for weather forecasting and air quality analyses throughout the world because rawinsondes are relied upon for most meteorological and air quality analyses.

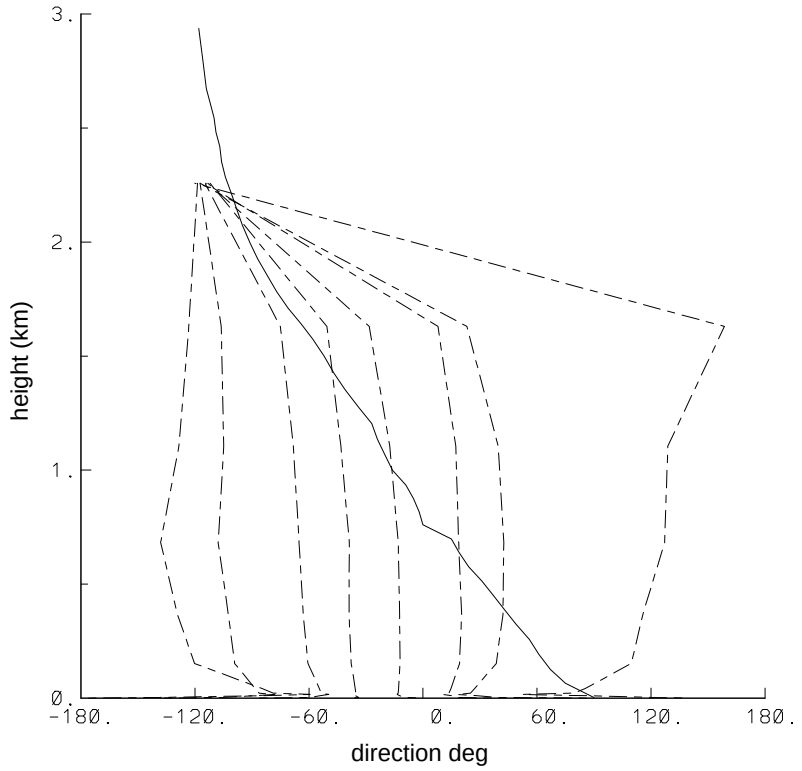

Figure B.12. Comparison of the measured wind direction profile (solid) to the model mean profile (dotted) and the model mean profile with two standard deviations added to or subtracted from the horizontal wind components (dashed) for 2:00 p.m. on February 22, 1991, at the Mexico City Airport.

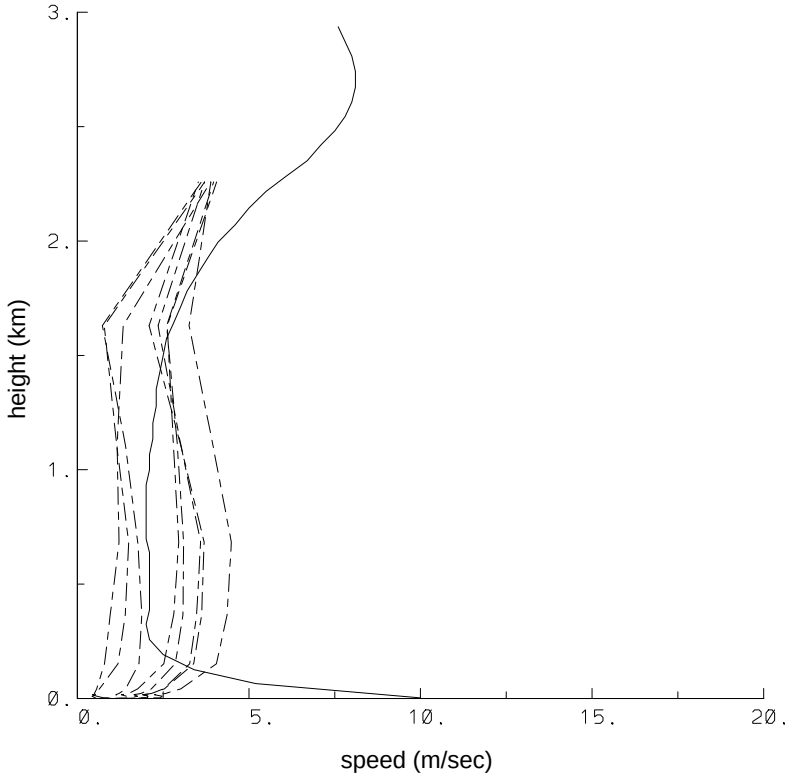

Figure B.13. Comparison of the measured wind speed profile (solid) to the model mean profile (dotted) and the model mean profile with two standard deviations added to or subtracted from the horizontal wind components (dashed) for 2:00 p.m. on February 22, 1991, at the Mexico City Airport.

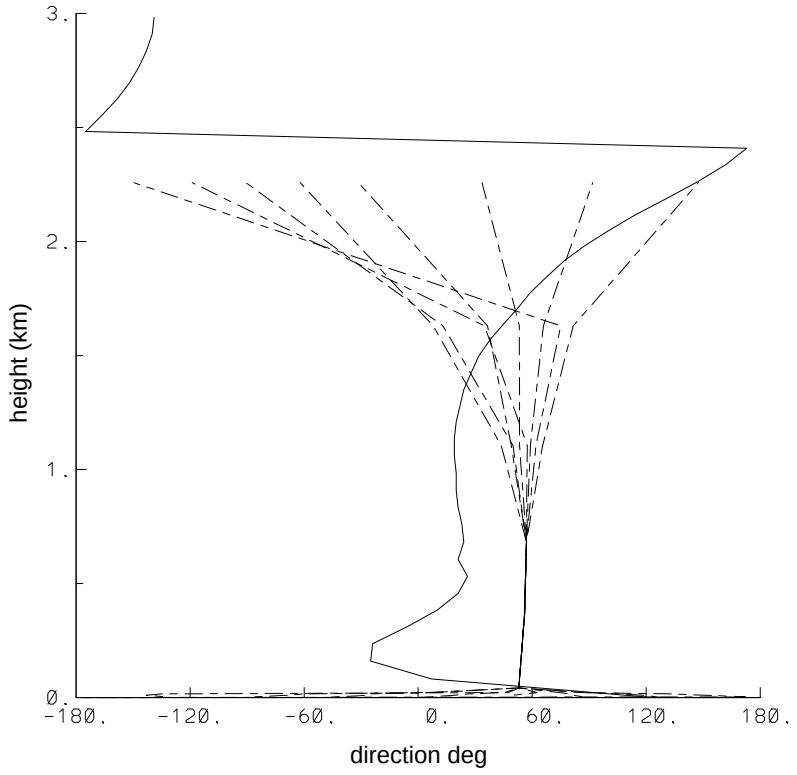

Figure B.14. Comparison of the measured wind direction profile (solid) to the model mean profile (dotted) and the model mean profile with two standard deviations added to or subtracted from the horizontal wind components (dashed) for 3:00 a.m. on February 22, 1991, at the Mexico City Airport.

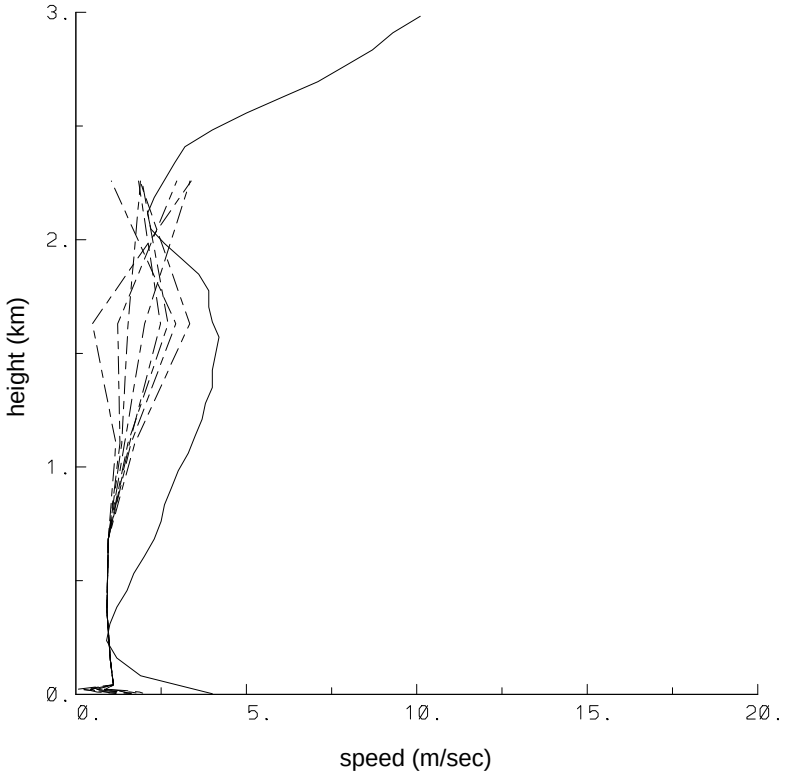

Figure B.15. Comparison of the measured wind speed profile (solid) to the model mean profile (dotted) and the model mean profile with two standard deviations added to or subtracted from the horizontal wind components (dashed) for 3:00 a.m. on February 22, 1991, at the Mexico City Airport.

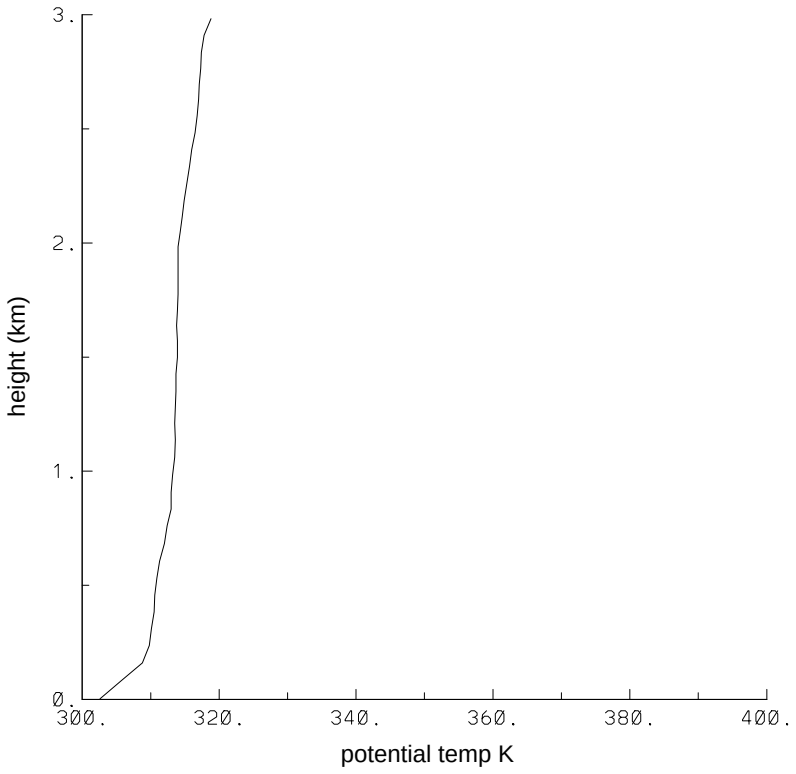

Figure B.16. Comparison of the measured potential temperature profile (solid) and to the modeled potential temperature (dotted) for 3:00 a.m. on February 22, 1991, at the Mexico City Airport.

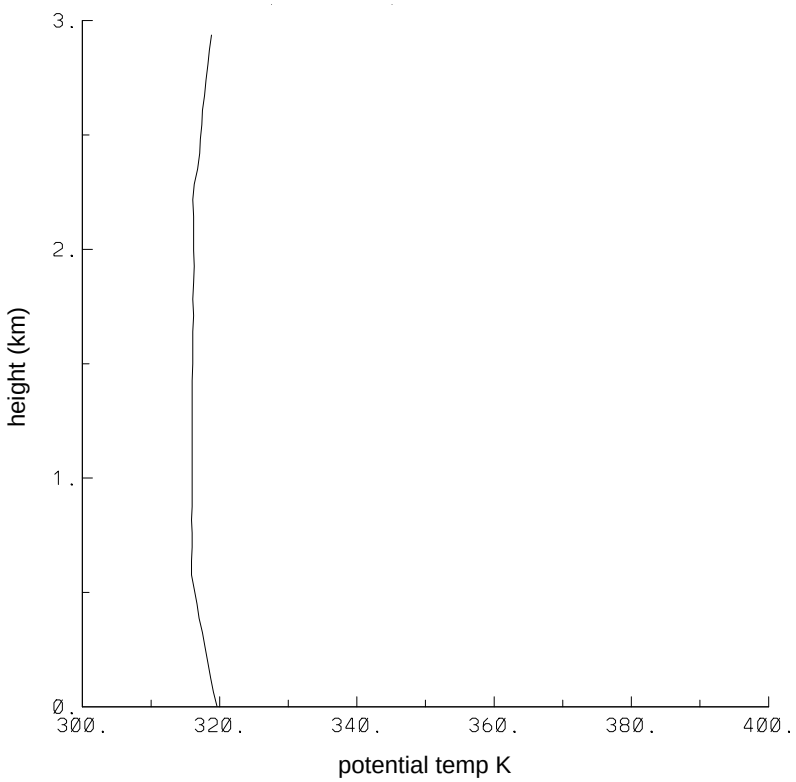

Figure B.17. Comparison of the measured potential temperature profile (solid) and to the modeled potential temperature profile (dotted) for 2:00 p.m. on February 22, 1991, at the Mexico City Airport.

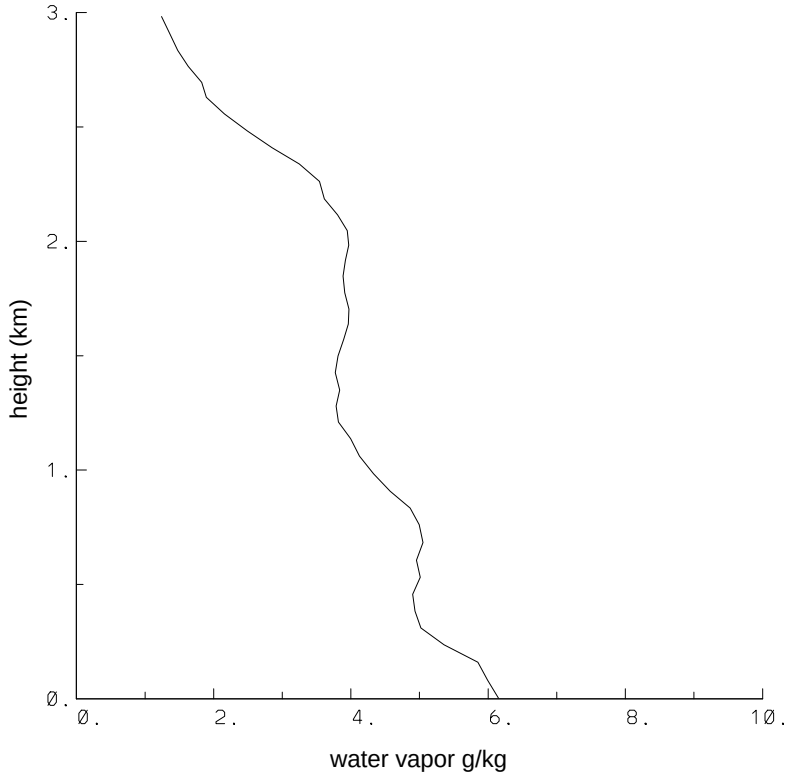

Figure B.18. Comparison of the measured water vapor profile (solid) and to the modeled water vapor profile (dotted) for 3:00 a.m. on February 22, 1991, at the Mexico City Airport.

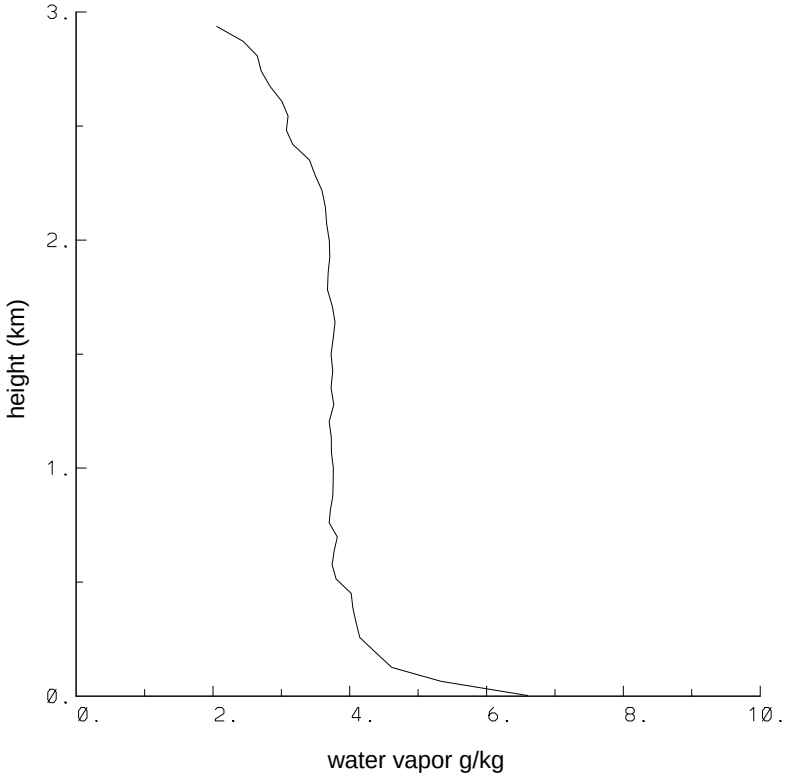

Figure B.19. Comparison of the measured water vapor profile (solid) to the modeled water vapor profile (dotted) for 2:00 p.m. on February 22, 1991, at the Mexico City Airport.

c. Tethersonde Profiles

For the simulation of February 20-22, 1991, tethersonde measurements were used in the derivation of the synoptic-scale winds in the model for the lowest 750 meters of the atmosphere. Actually the average winds for the layer between 250 and 750 meters above ground were used to estimate the synoptic-scale winds. The actual, modeled winds will be influenced by the thermal winds in addition to the synoptic-scale winds, so that the comparison between the tethersonde measurements and the modeled winds is still appropriate. Figure B.20 shows the wind directions as measured by the tethersonde for about 3:00 a.m. on February 22. There are considerable fluctuations in the tethersonde winds, but the model is generally within the designated range. Figure B.21 shows a similar and good comparison for the wind speeds. Figure B.22 shows a comparison of modeled and measured potential temperature at the same time. The modeled value is somewhat warmer than the measured temperature, but it shows a similar pattern.

Figure B.23 shows the tethersonde wind direction as compared to the model prediction at 10:00 a.m. Figure B.24 shows the tethersonde wind direction for the period beginning at 10:59 a.m. as compared to the 11:00 a.m. modeled wind direction. In Figure B.23 there are large fluctuations below 400 meters and relatively few fluctuations above that level. In Figure B.24 there are large fluctuations throughout. The 10:06 sounding was actually used to derive the wind input for the 11:00 a.m. model run. The 11:00 a.m. runs, which are shown in Figure B.24, are a better fit to the 10:06 measurements of Figure B.23. Similar behavior is shown in Figures B.25 and B.26, which show the tethersonde speeds at 10:06 a.m. and 10:59 a.m. respectively, as compared to the model results for 10:00 a.m. and 11:00 a.m. The model results show a rapid change associated with the changes in driving winds. In Figure B.26 the measured speed fluctuations also show reduced levels above 400 meters.

d. Aircraft-measured Meteorological Profiles

There were four days during the two periods of interest, the 21st, 22nd, 26th, and 27th of February 1991, in which vertical profiles were measured by the aircraft. In each case, the plane took off in midmorning and climbed out to the northeast. The comparisons are made with the profiles calculated by the model for the airport location. The comparison of wind directions is shown for all four days in Figures B.27 through B.30. In a similar fashion, the speed comparisons are shown in Figures B.31 through B.34. In each case the dashed lines represent the modeled profiles. Generally the model provides a reasonable representation of the measurements, although it does tend to give lower wind speeds near 1 km, where a frequently higher speed wind occurs. There is no direct input of these winds into the model because the model uses only the averaged winds below 750 meters and the winds at 2000 and 3000 meters above the surface. The effect of these higher winds might explain some of the discrepancy between the modeled and measured surface winds in the afternoon. After the mixing height goes above 700 meters, the effect of these winds will be felt at the surface. The other feature of note (which is consistent with the tethersonde observations) is the marked fluctuations within the mixed layer. The modeled values represent ensemble means and thus

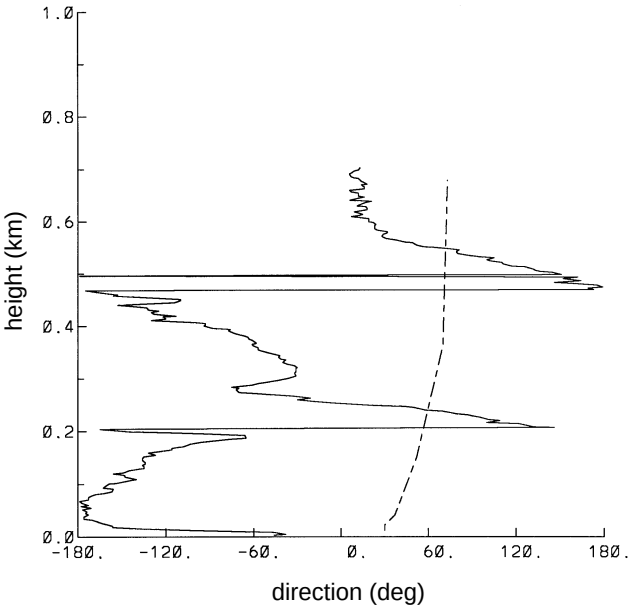

Figure B.20. Comparison of the tethersonde measured wind direction profile (solid) to the modeled wind direction profile (dashed) at 3:00 a.m. on February 22, 1991, at the Polytechnical University site.

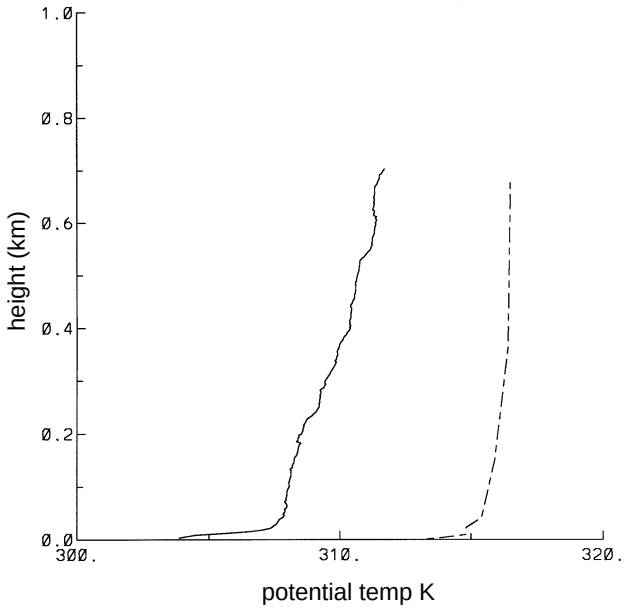

Figure B.22. Comparison of the tethersonde measured potential temperature profile (solid) to the modeled potential temperature profile (dashed) at 3:00 a.m. on February 22, 1991, at the Polytechnical University site.

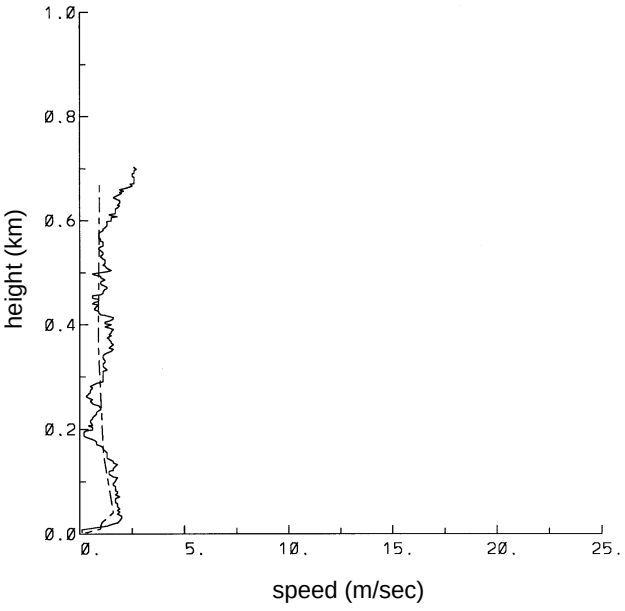

Figure B.21. Comparison of the tethersonde measured wind speed profile (solid) to the modeled wind speed (dashed) at 3:00 a.m. on February 22, 1991, at the Polytechnical University site.

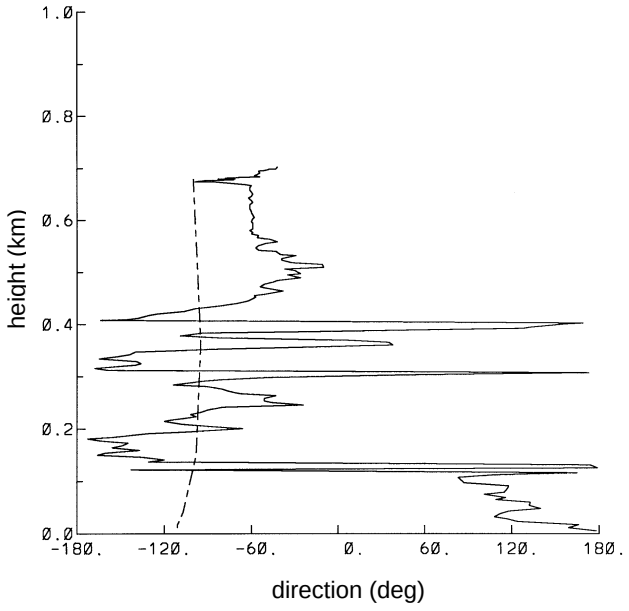

Figure B.23. Comparison of the tethersonde measured wind direction profile beginning at 10:06 a.m. (solid) to the modeled wind direction profile (dashed) at 10:00 a.m. on February 22, 1991, at the Polytechnical University site.

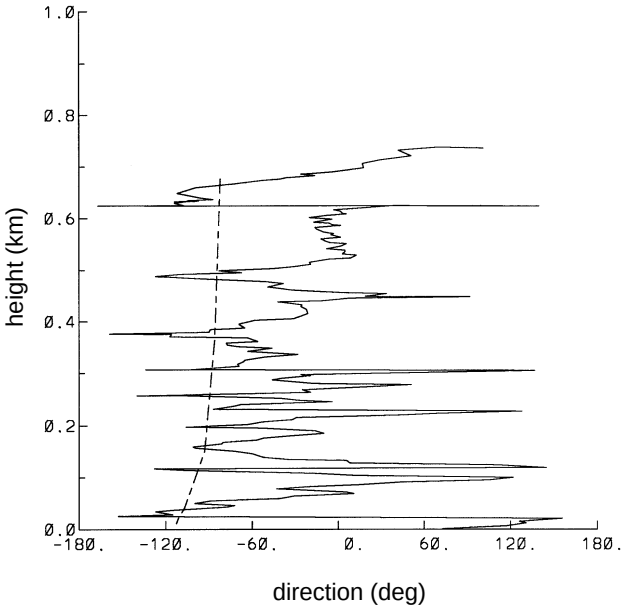

Figure B.24. Comparison of the tethersonde measured wind direction profile beginning at 10:59 a.m. (solid) to the modeled wind direction profile (dashed) at 11 a.m. on February 22, 1991, at the Polytechnical University site.

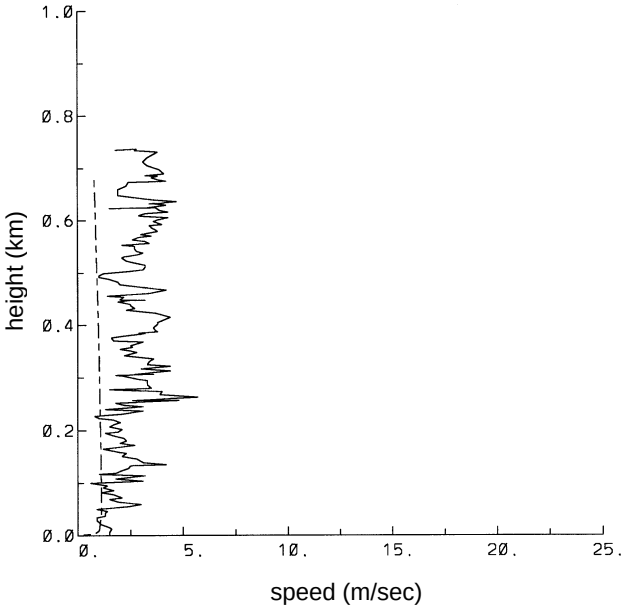

Figure B.26. Comparison of the tethersonde measured wind speed profile beginning at 10:59 a.m. (solid) to the modeled wind speed profile (dashed) at 11 a.m. on February 22, 1991, at the Polytechnical University site.

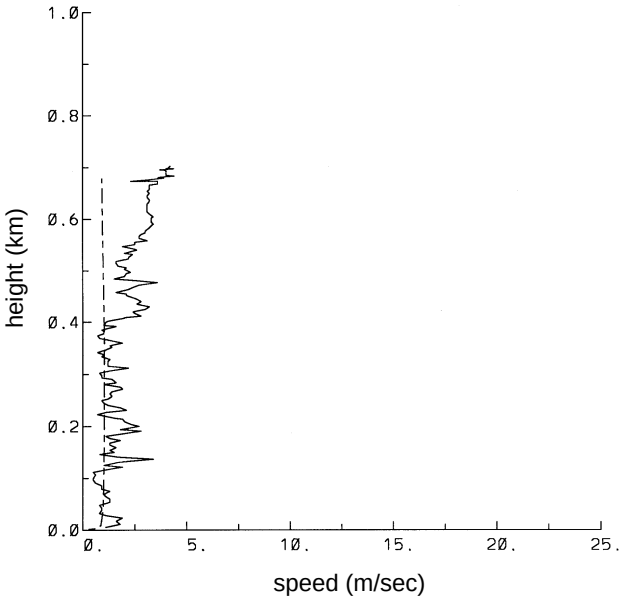

Figure B.25. Comparison of the tethersonde measured wind speed profile beginning at 10:06 a.m. (solid) to the modeled wind speed profile (dashed) at 10:00 a.m. on February 22, 1991, at the Polytechnical University site.

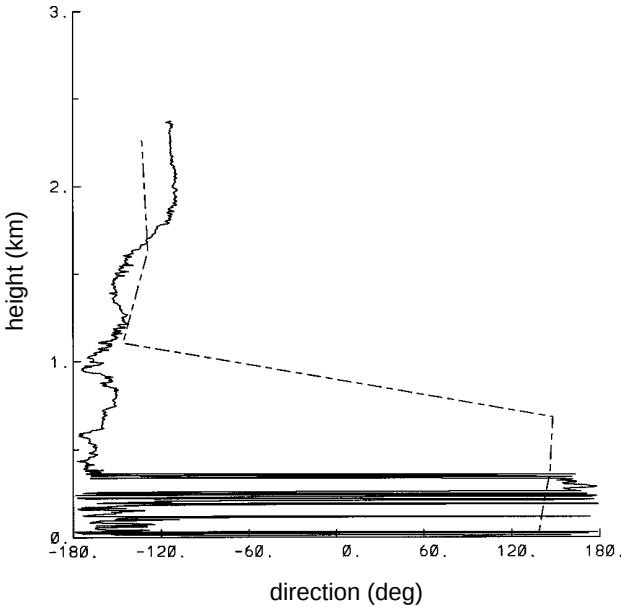

Figure B.27. Comparison of the aircraft measured wind direction profile (solid) to the modeled wind direction profile (dashed) at 9:00 a.m. on February 21, 1991.

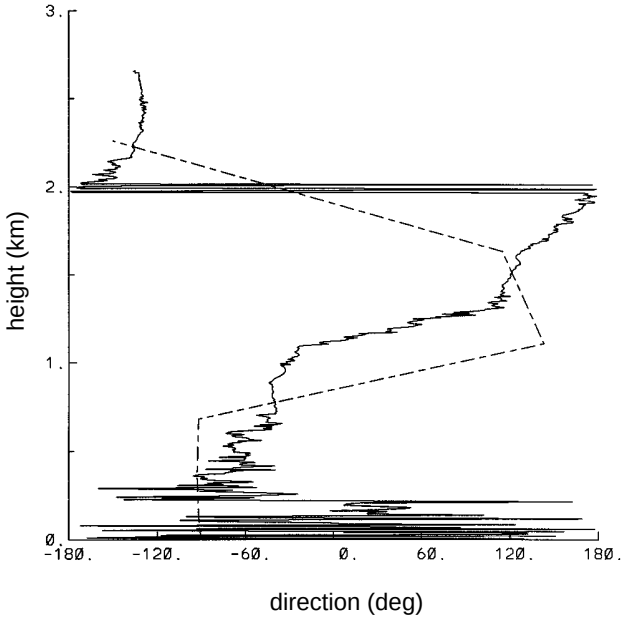

Figure B.28. Comparison of the aircraft measured wind direction profile (solid) to the modeled wind direction profile (dashed) at 10:00 a.m. on February 22, 1991.

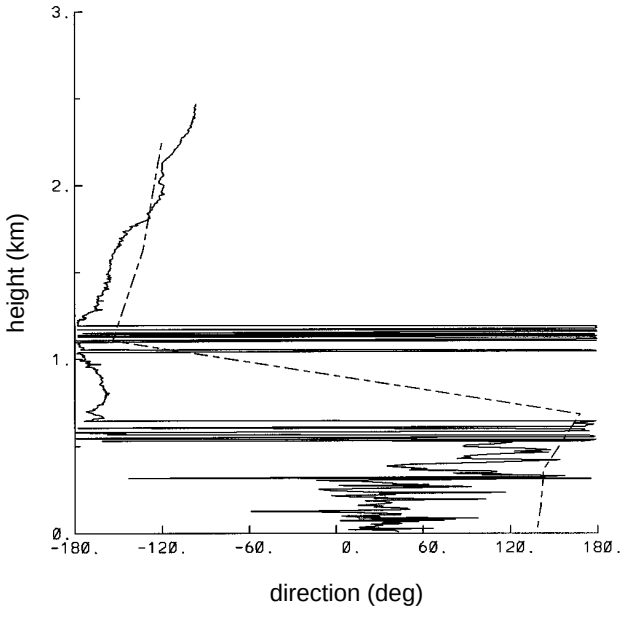

Figure B.29. Comparison of the aircraft measured wind direction profile (solid) to the modeled wind direction profile (dashed) at 10:00 a.m. on February 26, 1991.

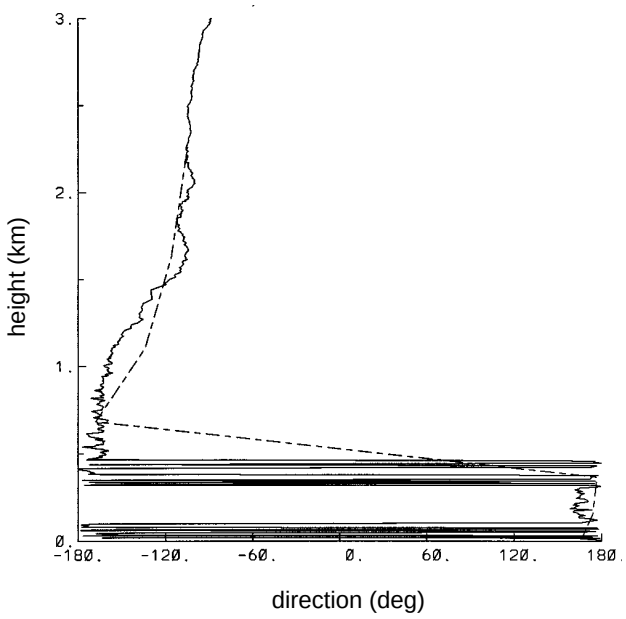

Figure B.30. Comparison of the aircraft measured wind direction profile (solid) to the modeled wind direction profile (dashed) at 8:00 a.m. on February 27, 1991.

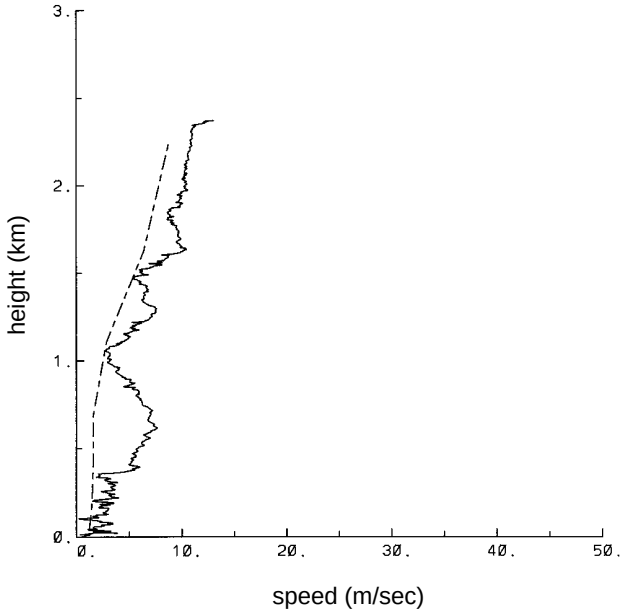

Figure B.31. Comparison of the aircraft measured wind speed profile (solid) to the modeled wind speed profile (dashed) at 9:00 a.m. on February 21, 1991.

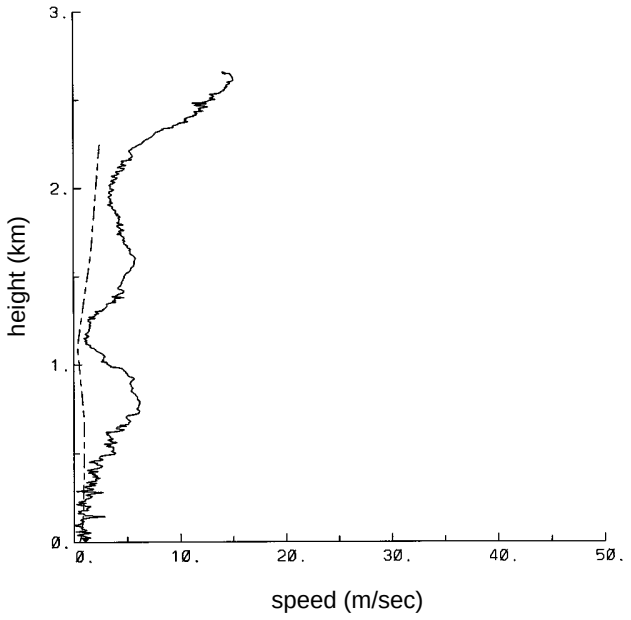

Figure B.32. Comparison of the aircraft measured wind speed profile (solid) to the modeled wind speed profile (dashed) at 10:00 a.m. on February 22, 1991.

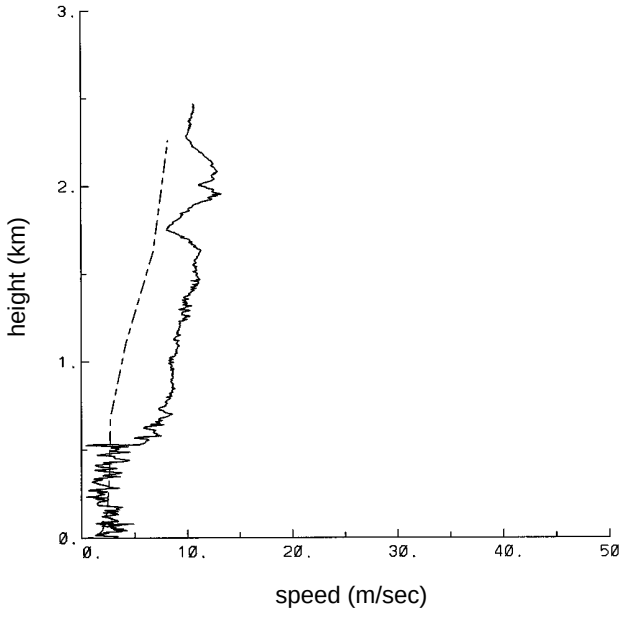

Figure B.33. Comparison of the aircraft measured wind speed profile (solid) to the modeled wind speed profile (dashed) at 10:00 a.m. on February 26, 1991.

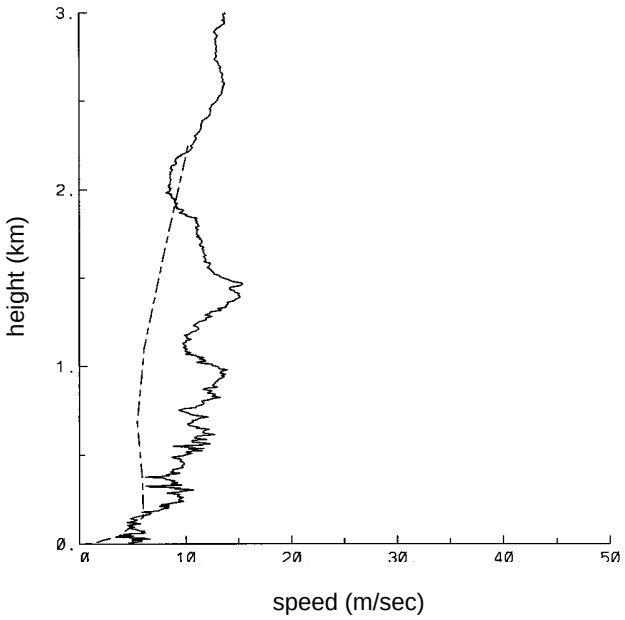

Figure B.34. Comparison of the aircraft measured wind speed profile (solid) to the modeled wind speed profile (dashed) at 8 a.m. on February 27, 1991.

do not show the fluctuations, although similar values would be expected from the modeled turbulence.

e. Aircraft-measured Elevated Winds

There were three days in the relevant periods—February 21, 22, and 27—in which aircraft measurements of winds were available at about 500 meters above the surface. Figures B.35 through B.37 show the comparisons of wind directions for these days, while Figure B.38 through B.40 show the comparisons of wind speeds. Generally the wind directions are well represented, but the speeds are less accurately modeled. In Figure B.38 the model fails to show the marked increase in wind speed on the eastern side of the city. In Figure B.39 the modeled winds are too light, while in Figure B.40 the modeled winds are too strong.

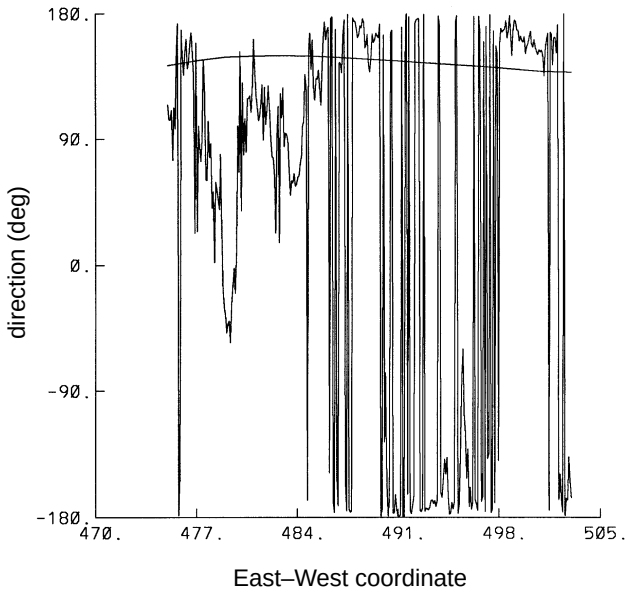

Figure B.35. Comparison of the aircraft measured wind directions on a west-to-east pass of the city at 2710 meters above sea level to the modeled wind directions at 10:00 a.m. on February 21, 1991.

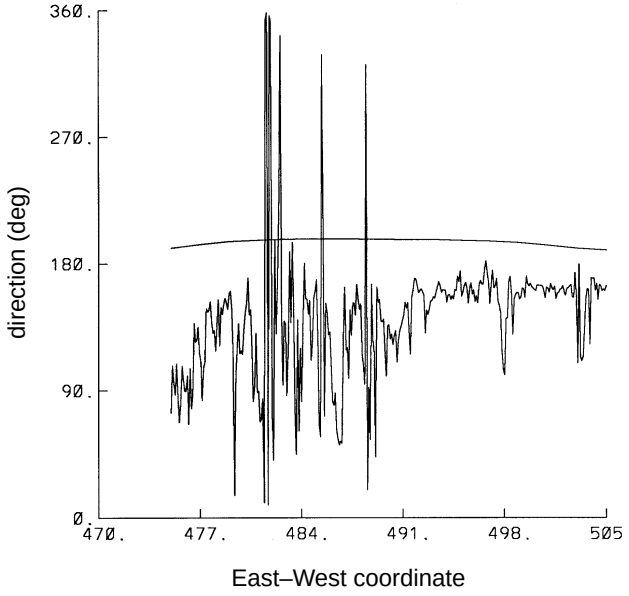

Figure B.37. Comparison of the aircraft measured wind directions on a west-to-east pass of the city at 2710 meters above sea level to the modeled wind directions at 10:00 a.m. on February 27, 1991.

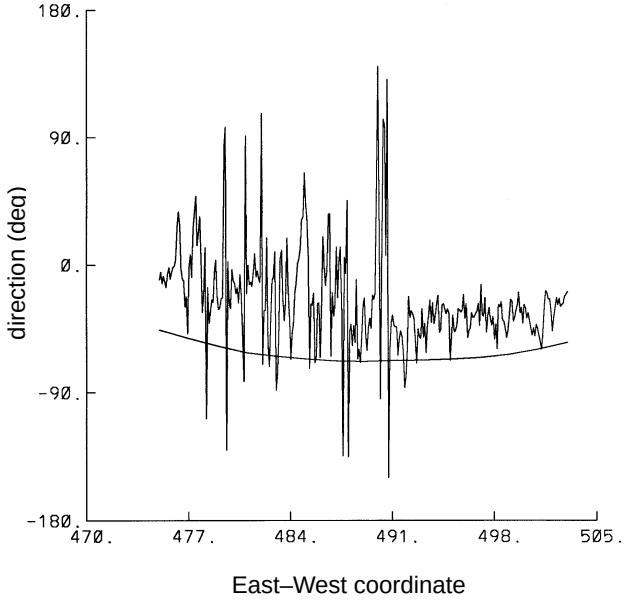

Figure B.36. Comparison of the aircraft measured wind directions on a west-to-east pass of the city at 2710 meters above sea level to the modeled wind directions at 11:00 a.m. on February 22, 1991.

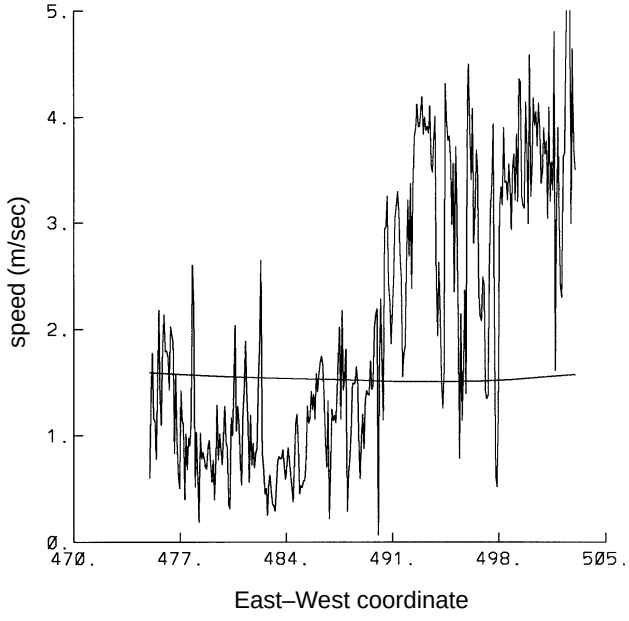

Figure B.38. Comparison of the aircraft measured wind speeds on a west-to-east pass of the city at 2710 meters above sea level to the modeled wind speeds at 10:00 a.m. on February 21, 1991.

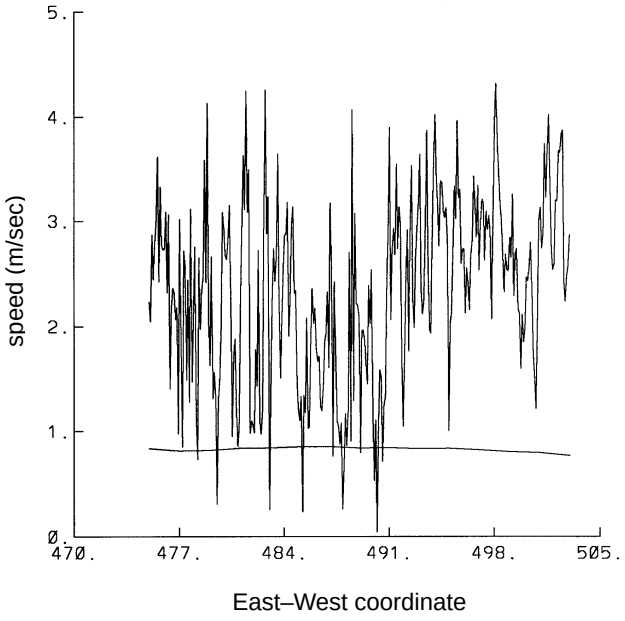

Figure B.39. Comparison of the aircraft measured wind speeds on a west-to-east pass of the city at 2710 meters above sea level to the modeled wind speeds at 11:00 a.m. on February 22, 1991.

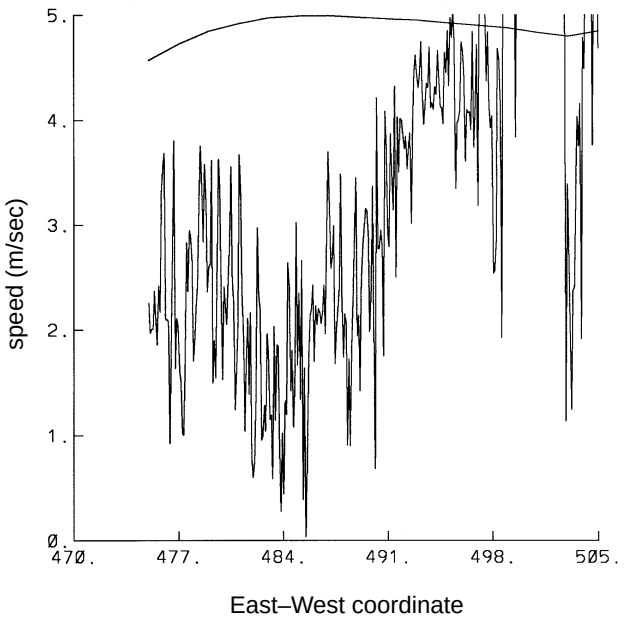

Figure B.40. Comparison of the aircraft measured wind speeds on a west-to-east pass of the city at 2710 meters above sea level to the modeled wind speeds at 10:00 a.m. on February 27, 1991.

f. Lidar-derived Mixing Heights

There were four days in which lidar-derived mixing heights were available in the period of interest. The lidar-derived mixing heights were determined as the height at which 50% of the horizontal area has a signal characteristic of the clean air aloft. There were two sites used in the four days. During February 22, the lidar was at the Centro de Investigación y Estudios Avanzados (CINVESTAV) site, which is a few kilometers north of the city center. On February 26-28, the lidar was at the UNAM site, which is on the southern boundary of the city. The UNAM site is about 100 meters above the level of the city, and the mixing height measurements are relative to the height of the site. The actual line of sight is over the city, which is at a lower elevation, so that the mixing heights would be expected to be about 100 meters higher than those reported. Typically, the lidar cannot identify structures below about 100 meters because of line-of-sight restrictions imposed by nearby objects.

Figure B.41 displays the comparison between the model and the measurements for February 22, while Figures B.42 through B.44 report the comparisons for February 26-28, respectively. The agreement for February 22 is excellent; the principal disagreements are in the night when the lidar minimum heights may be important and one point in the late afternoon when clouds could have influenced the comparison. The agreements for February 26-28 are not as good. In particular, the measurements show a much slower increase in the mixing height in the midmorning.

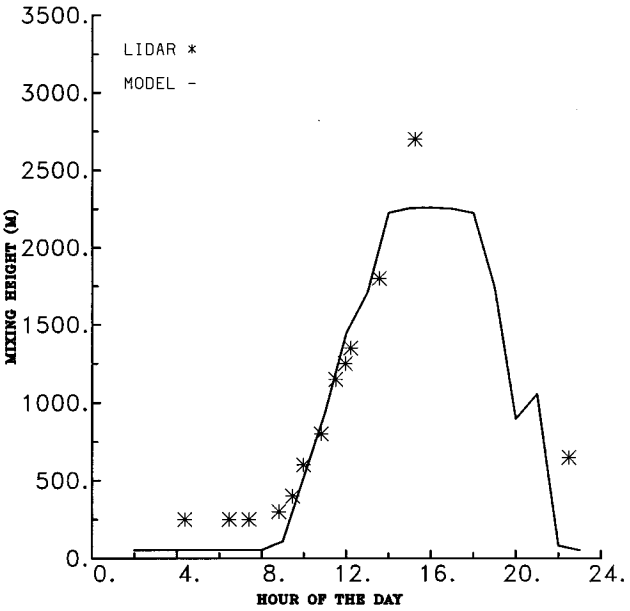

Figure B.41. Comparison of the lidar measured mixing heights (asterisks) to the modeled mixing heights (line) for February 22, 1991.

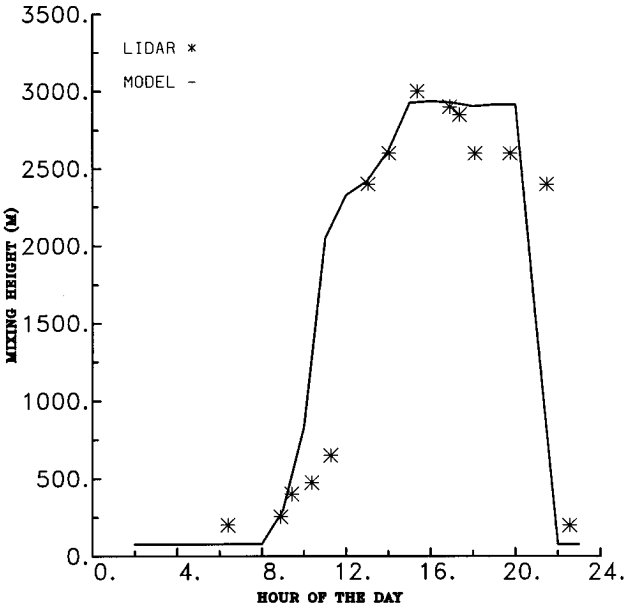

Figure B.42. Comparison of the lidar measured mixing heights (asterisks) to the modeled mixing heights (line) for February 26, 1991.

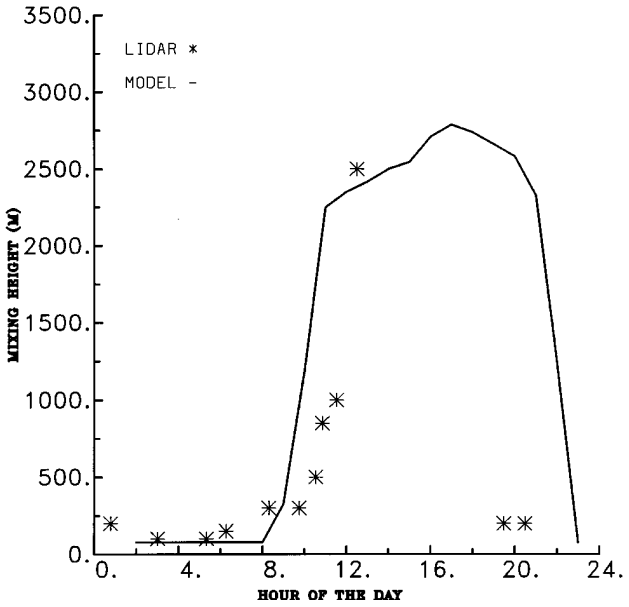

Figure B.43. Comparison of the lidar measured mixing heights (asterisks) to the modeled mixing heights (line) for February 27, 1991.

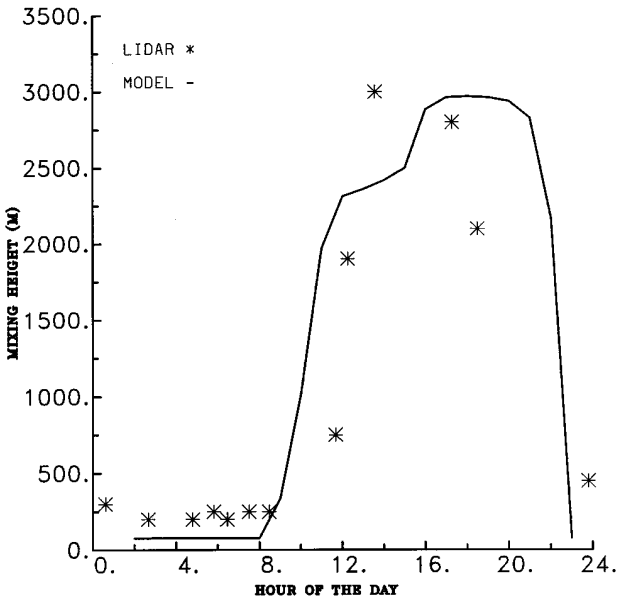

Figure B.44. Comparison of the lidar measured mixing heights (asterisks) to the modeled mixing heights (line) for February 28, 1991.

6. Performance Summary

Researchers (Tesche et al. 1990) funded by the California Air Resources Board, have suggested procedures for evaluating the performance of air quality models. They suggested many graphical outputs and a suite of statistical measures. Included among the statistical measures are

- model means,
- mean observation,
- standard deviation of model estimates,
- standard deviation of observations,
- least squares regression statistics,
- root mean square error,
- systematic root mean square error,
- unsystematic root mean square error,
- index of agreement,
- skill error, and
- skill variance.

Many of these terms are well understood, but some may require explanation. Specifically the regression is of the form

$$\hat{\phi}_{pi} = a + b\ \phi_{oi}$$

so that the predictions, $\hat{\phi}_{pi}$ are regressed against the observations, ϕ_{oi} with intercept a and regression coefficient b. The systematic root mean square error is then defined as

$$RMSE_s = \left[\frac{1}{N}\sum_{i=1}^{N}(\hat{\phi}_{pi} - \phi_{oi})^2\right]^{1/2}$$

while the unsystematic root mean square is

$$RMSE_u = \left[\frac{1}{N}\sum_{i=1}^{N}(\hat{\phi}_{pi} - \phi_{pi})^2\right]^{1/2} .$$

The index of agreement is given by

$$I = 1 - \left[\frac{N(RMSE)^2}{\sum_{i=1}^{N}(|P'_i| + |O'_i|)^2}\right]$$

with $P'_i = \phi_{pi} - \phi_o$, and $O'_i = \phi_{oi} - \phi_o$. The range of I is from 0 to 1 with 1 representing perfect agreement. The skill error is given by

$$SE = \frac{RMSE_u}{\sigma_o}$$

while the skill variance is given by:

$$SV = \frac{\sigma_p}{\sigma_o} .$$

The computation of these statistical parameters is straight forward for the wind speeds and mixing layer heights, but wind directions pose a more difficult problem. Because of the difficulty with circular data, techniques developed by Mardia (1972) were used to calculate a regression relationship which is analogous to the standard regression on a line. Table B.2 summarizes the statistics for wind speeds at the monitoring stations for six days:

Note that the bulk of the disagreement is represented by the systematic error.

Table B.3 summarizes the statistics for wind directions at the monitoring stations for six days:

The correlation coefficient is not shown since it is not calculated for circular data. Generally the model captures the major meteorological features; the winds respond well to major changes in forcing winds. The slope winds develop appropriately and couple well with the large-scale conditions. There are some areas, however, which could be improved. For instance, the

TABLE B.2 Wind Speeds at the Monitoring Stations Over a Six-Day Period

Wind-Speed Statistics	
Model mean	2.4
Observation mean	4.8
Standard deviation of predictions	1.2
Standard deviation of observations	3.0
Regression intercept	1.8
Regression coefficient	0.14
Correlation coefficient	0.32
Root mean square error	3.7
Systematic root mean square error	3.5
Unsystematic root mean square error	1.2
Index of agreement	0.49
Skill error	0.40
Skill variance	0.42

TABLE B.3 Statistics for Wind Directions at the Monitoring Stations Over a Six-Day Period

Wind Direction Statistics	
Model mean	161
Observation mean	203
Standard deviation of predictions	74
Standard deviation of observations	94
Regression intercept	79
Regression coefficient	.42
Correlation coefficient	xx
Root mean square error	87
Systematic root mean square error	80
Unsystematic root mean square error	72
Index of agreement	0.73
Skill error	0.96
Skill variance	0.79

model does not have quite as much convergence over the city as it should, and it also looks as though the temperatures do not drop as much at night as they should. The rapid rise in mixing heights in the February 25-28 simulations is of concern and is probably related to the temperature behavior. The wind speeds seem to be a little low. The light wind speeds could be a function of the way layer-averaged winds are used as input, or they may reflect the fact that the model is currently not using some of the information from the soundings in the range from 750 meters to 2000 meters above ground. In a layer where winds are turning with heights averaging over 250-750 meters, the wind speeds may actually be artificially reduced.

7. Applications

The major applications of the meteorological model were (1) to drive the photochemical models and (2) to drive the dispersion modeling. These are discussed in detail in sections C and D of this volume. However, another interesting application was to investigate the potential effect on air pollution of major terrain modifications near Mexico City. Some groups have advocated cutting a pathway for air motion through the Sierra de Ajusco to the southwest of Mexico City. HOTMAC was used to investigate this proposal by simulating wind fields before and after terrain modification.

The Sierra de Ajusco is dominated by two peaks reaching nearly 4000 m in height. This range forms a massive wall that blocks air moving to the southwest. With February 22, 1991, and the original terrain serving as the base case, the terrain input file to HOTMAC was modified for two test cases. The results were then compared with the original solutions for the same period. The two test cases considered were the opening of a channel directed northeast-southwest and the removal of the tops of the two highest peaks in the Sierra de Ajusco. Figure B.45a depicts the original terrain used in the HOTMAC model, while Figure B.45b shows the terrain

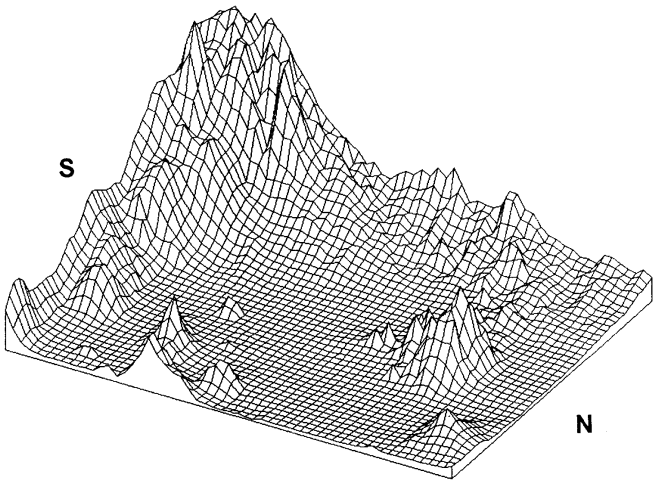

(a)

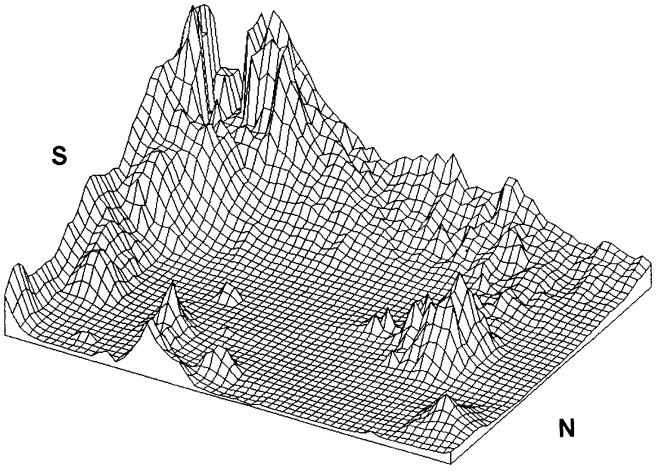

(b)

Figure B.45. (a) Three-dimensional depiction of the fine-grid topography used in the HOTMAC base case simulation. (b) Three-dimensional depiction of the fine-grid topography used in the channel opening simulation.

after the channel had been opened. The channel opening would require moving more than 6 cubic kilometers of earth.

The effect of the modifications was examined by comparing the calculated winds at three sites for the three cases. The sites chosen are: Xalostoc (site L in Figure B.1), Merced (site X in Figure B.1), and Pedregal (site T in Figure B.1). These sites lie along a northeast-southwest line ending at Pedregal, which had the highest O_3 concentrations in the city on February 22, 1991. Figure B.46abc shows the simulated vertical profiles of the winds for the three sites at 5:00 a.m. The differences between the three cases base case (1), channel opening (2), and cutoff peaks (3) are very small. There is a difference in wind directions at Xalostoc near the surface, and there are differences in both wind speed and wind direction at Pedregal at about 20 meters height. In the case of Xalostoc the winds are very light so that a change in wind direction is insignificant, while at Pedregal, the differences suggest a slightly weaker drainage wind.

Figure B.47abc shows the simulated wind profiles for the three sites and three cases at 12:00 noon. Once again the differences are quite small. The terrain modifications produced no significant effect on the winds of the basin, but it must be pointed out that the terrain modification was very small when compared with the physical dimension of the mountain range. Nonetheless, this application illustrates how proposed solutions to Mexico City's air pollution problem can be evaluated in an economical and appropriate manner.

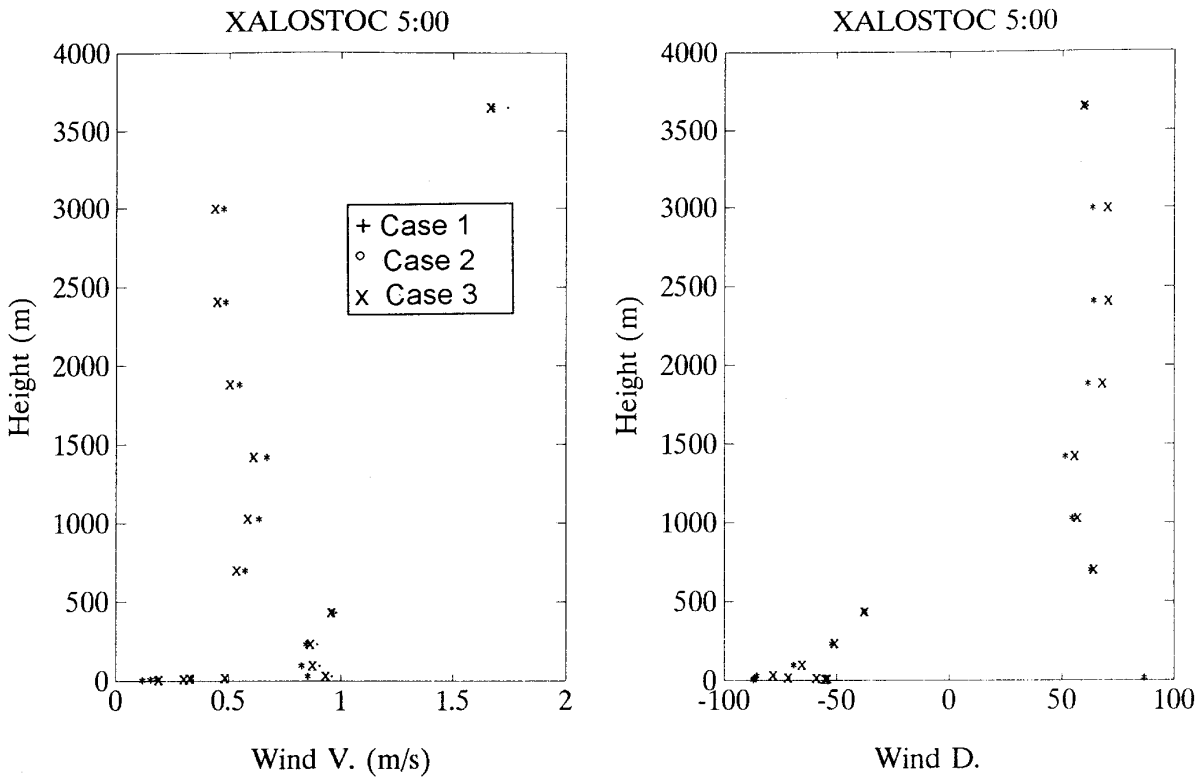
XALOSTOC 5:00
Height (m)
Wind V. (m/s)
+ Case 1
° Case 2
x Case 3
XALOSTOC 5:00
Height (m)
Wind D.

(a)

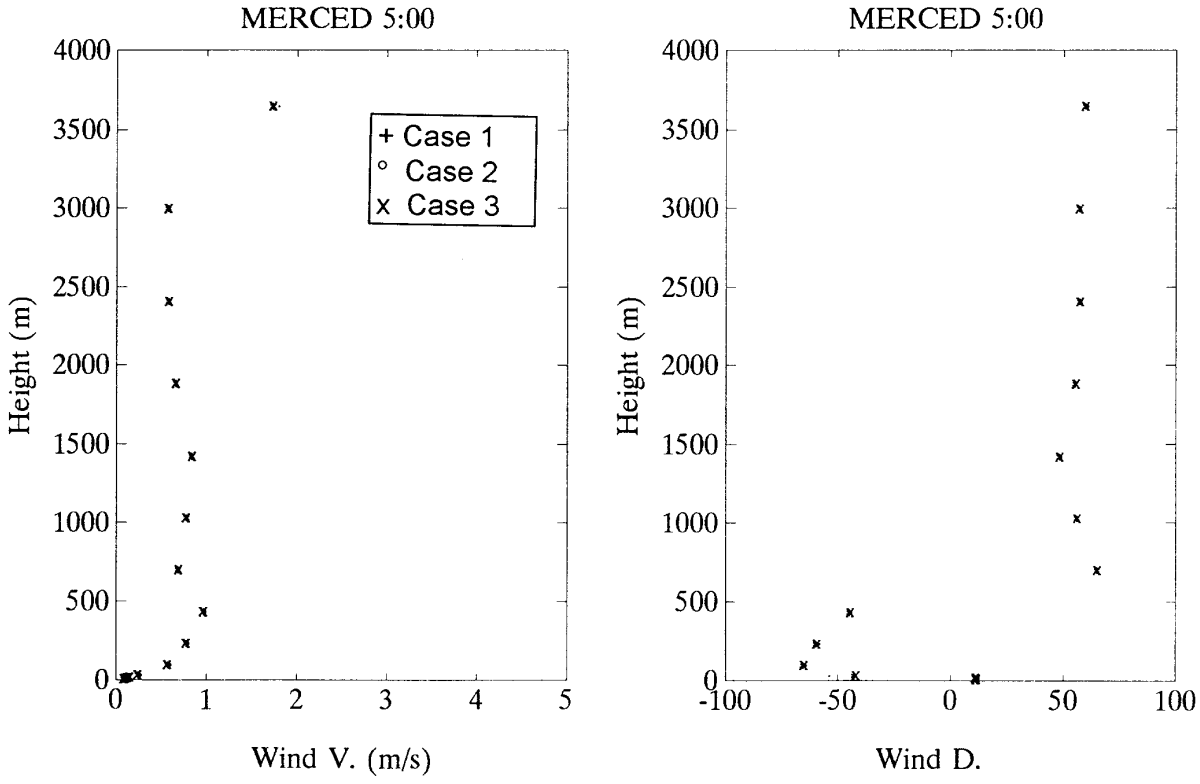
MERCED 5:00
Height (m)
Wind V. (m/s)
+ Case 1
° Case 2
x Case 3
MERCED 5:00
Height (m)
Wind D.

(b)

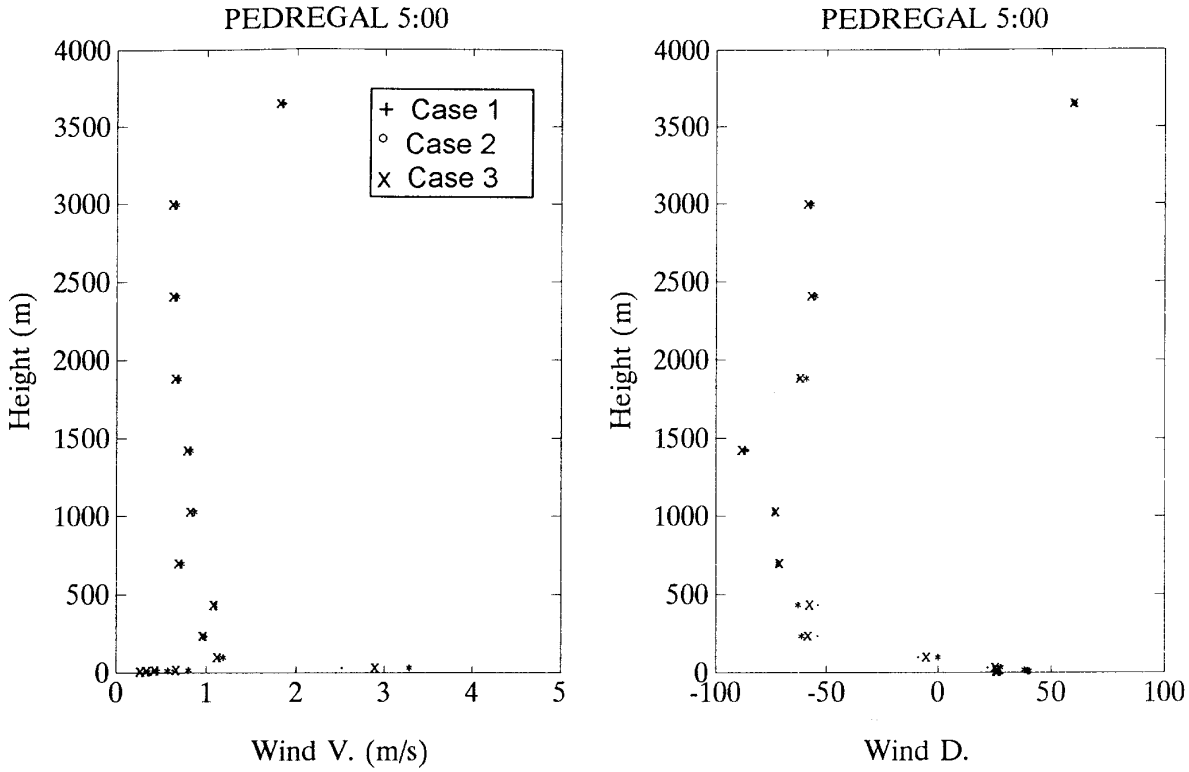

(c)

Figure B.46. Simulated vertical-wind profiles for February 22, 1991, at 5:00 a.m. (a) Xalostoc, (b) Merced, and (c) Pedregal.

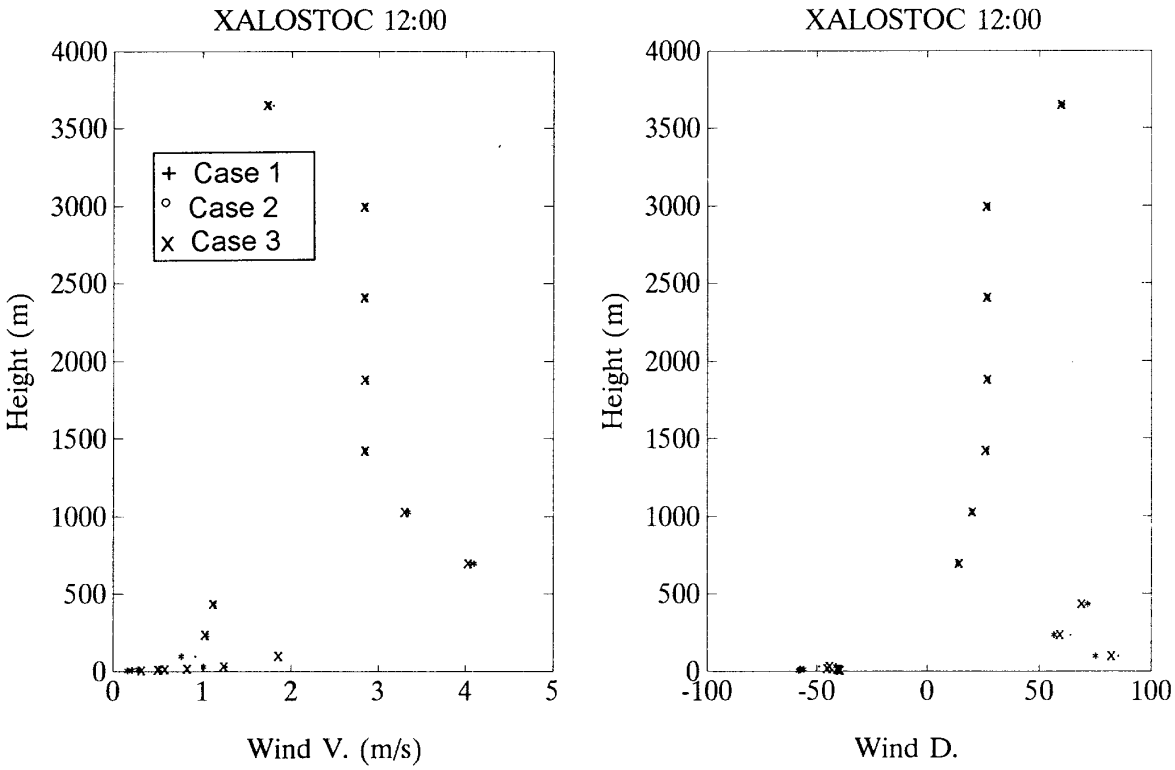
XALOSTOC 12:00
+ Case 1
° Case 2
x Case 3
Height (m)
Wind V. (m/s)
XALOSTOC 12:00
Height (m)
Wind D.

(a)

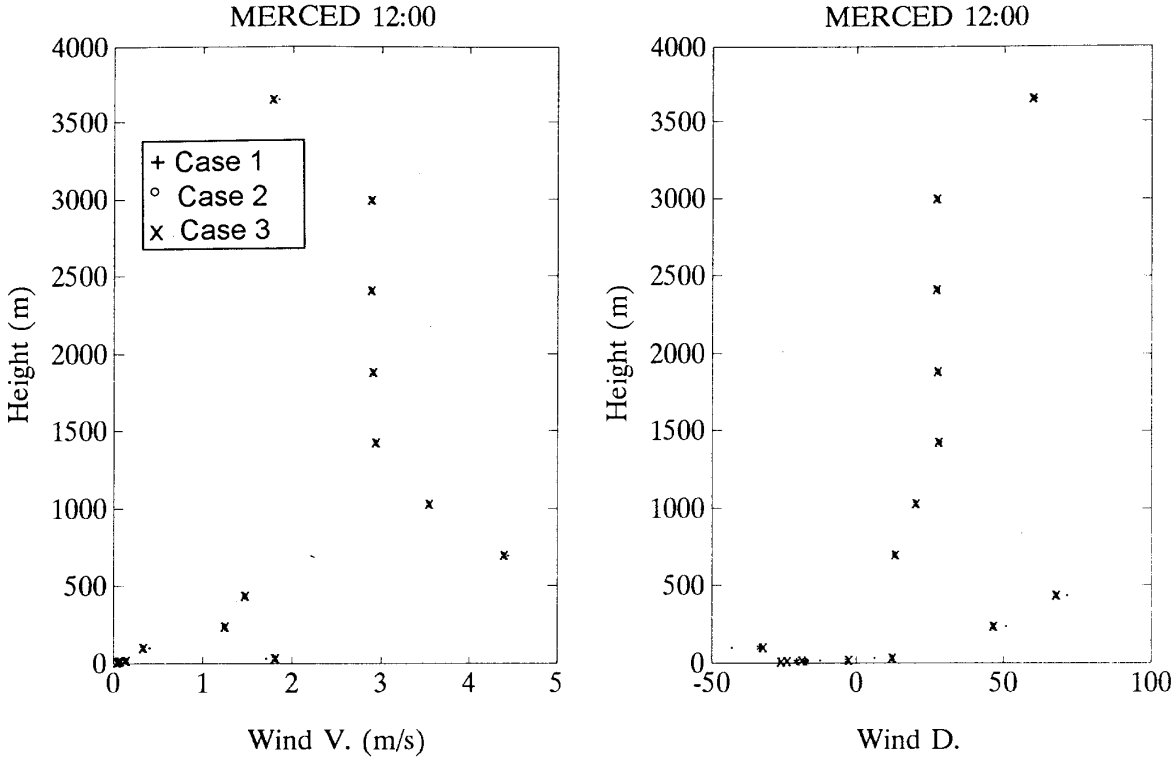
MERCED 12:00
+ Case 1
° Case 2
x Case 3
Height (m)
Wind V. (m/s)
MERCED 12:00
Height (m)
Wind D.

(b)

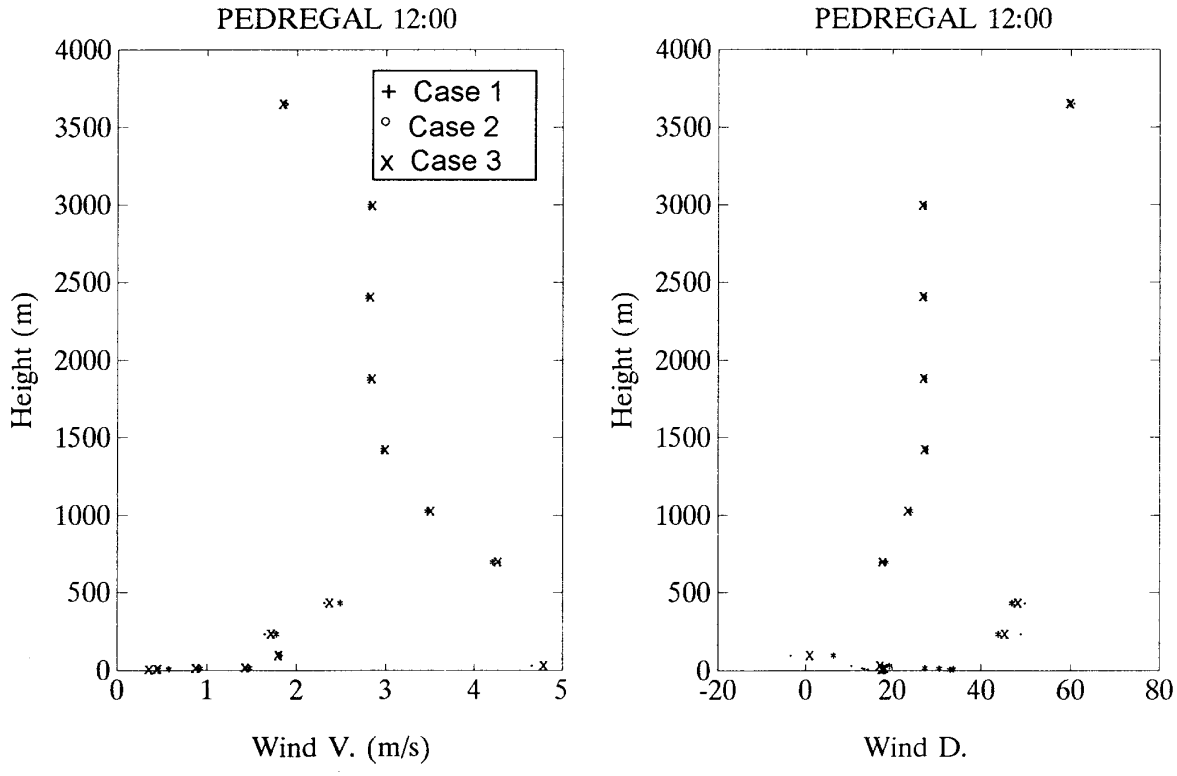

(c)

Figure B.47. Simulated vertical-wind profiles for February 22, 1991, at noon. (a) Xalostoc, (b) Merced, and (c) Pedregal.

C. DISPERSION MODELING

1. Objectives

The dispersion modeling has three objectives:

- to provide a test of the modeling system against measured data, to provide insight into the transport variables used in the photochemical modeling;
- to estimate fractional changes in CO that cannot be estimated reliably by a linear rollback because of changes in the spatial or temporal pattern of emissions; and
- to estimate the importance of changes in emissions that could effect the SO_2 concentrations in the city.

2. Background

Dispersion modeling blends the emissions with the meteorology to produce concentrations of nonreactive pollutants. Typically, dispersion modeling is used to represent the average conditions and the high concentrations that occur over a year. It is normally not expected to reproduce the hourly concentrations at the exact positions at which they occur. Small differences between the modeled wind and the actual wind can produce large differences in concentrations from point sources. (Browne 1981) In the urban context the situation is somewhat improved because the sources tend to be more uniform and thus less sensitive to the wind directions. The emission sources, however, can be hard to identify or may vary rapidly over time.

The two pollutants that were principally modeled with the dispersion model were CO and SO_2. The CO is produced by low-level sources such as vehicles and small boilers. Measured concentrations can be very sensitive to the presence of local sources near the monitor. The SO_2 is produced by low-level sources such as diesel trucks, but it is also produced by industrial sources such as power plants. Sources that emit from tall stacks are difficult to model precisely because small changes in wind directions or conditions that affect how high the materials rise above the stacks may produce major changes in concentrations measured at a monitor. (Browne 1981) In Mexico City the problem is further compounded by the high terrain, which can deflect the material to different locations. In some instances, models endorsed by the U.S. Environmental Protection Agency (EPA) have failed to display a positive correlation with hour-by-hour and site by site measurements. (Weil and Brower 1982) However, the models usually show approximately correct peak concentrations and average concentrations and are thus appropriate for air quality planning purposes.

3. Description of the Dispersion Model

The dispersion model is RAPTAD, a Monte Carlo dispersion and transport code. (Yamada and Bunker, 1988) Pseudoparticles are transported with instantaneous velocities that include the mean wind field and the turbulence velocities. The turbulence velocity is generated randomly so that it is consistent with the standard deviation of the wind at the particle location. The location of each pseudoparticle represents the center of mass of a concentration distribution for each puff. A puff is a volume of polluted air emitted at a discrete time like a puff of smoke from a steam locomotive. The total concentration at any point is obtained by adding the

concentration contributions of each puff at that point (a kernel method). The Monte Carlo kernel method requires that a functional form for the distribution kernel be chosen and that parameters that describe the width, breadth, and depth of the distribution be calculated. The approach used here is to assume a Gaussian distribution where particle position variances are determined from the time integration of the velocity variances encountered over the history of the puff. The position variances are estimated based on the random force theory of turbulent diffusion (Lee and Stone, 1982). The random force theory is also known as the Brownian-motion analogy, or the Langevin model. An equation is written that describes the motion of particles under the influence of random accelerations and a resistive force term. Lee and Stone extend the theory to the treatment of clusters of particles from finite-size, finite-duration sources.

The system has many advantages for applications involving complex terrain. The use of a higher-order turbulence model means that there are three-dimensional time-dependent wind fields and turbulence fields available for the representation of dispersion and transport. Transport can be treated in more detail because important terrain influences are represented in both the mean fields and the turbulence fields. Consider the situation depicted in Figure C.1. A nighttime situation is depicted in which the pollution, represented by the red dots, is being released in the upper end of a canyon. The flow in the canyon bottom is down-canyon because of the cold air draining down hill. The flow aloft is depicted as up-canyon. A normal Gaussian puff model would follow the mean wind down the canyon and ignore the material that dispersed upward and was taken up-canyon by the winds aloft. The situation can be treated either by a Monte Carlo kernel model such as RAPTAD, or it could be treated by a random particle model that did not use a kernel. Other random particle codes calculate concentrations by counting random particles in cells. The cell approach, however, has the disadvantage that the cell sizes must be carefully chosen, and they must vary in size. If the cell size is too small, the concentrations will be very noisy with some cells having no particles and thus no concentrations, while an adjacent cell may have very large concentrations if it has one or two particles in its small volume. If the cells are too large, the concentrations will be smeared out in an unrealistic fashion. The kernel system, as used by RAPTAD, avoids this problem because the pollution associated with a particle is not concentrated at a point but extends over a volume surrounding a point. The volume around the point is calculated based on the turbulence history of the particle. In an afternoon turbulent circumstance, the volume expands very rapidly, while at night it expands very slowly.

A second example of the importance of a more sophisticated treatment of dispersion is afforded by the following example. A tracer material was released for one hour in a valley in Utah with 65 monitors used to record the concentrations. During the night very few monitors actually recorded significant amounts of tracer because the plume remained narrow as a result of nighttime conditions. However, the concentration profile recorded at 10 km downwind extended for several hours. Gaussian puff calculations gave low concentrations for all hours except one. RAPTAD gave concentrations that remained high for a few hours. The Gaussian puff model moved all the material with

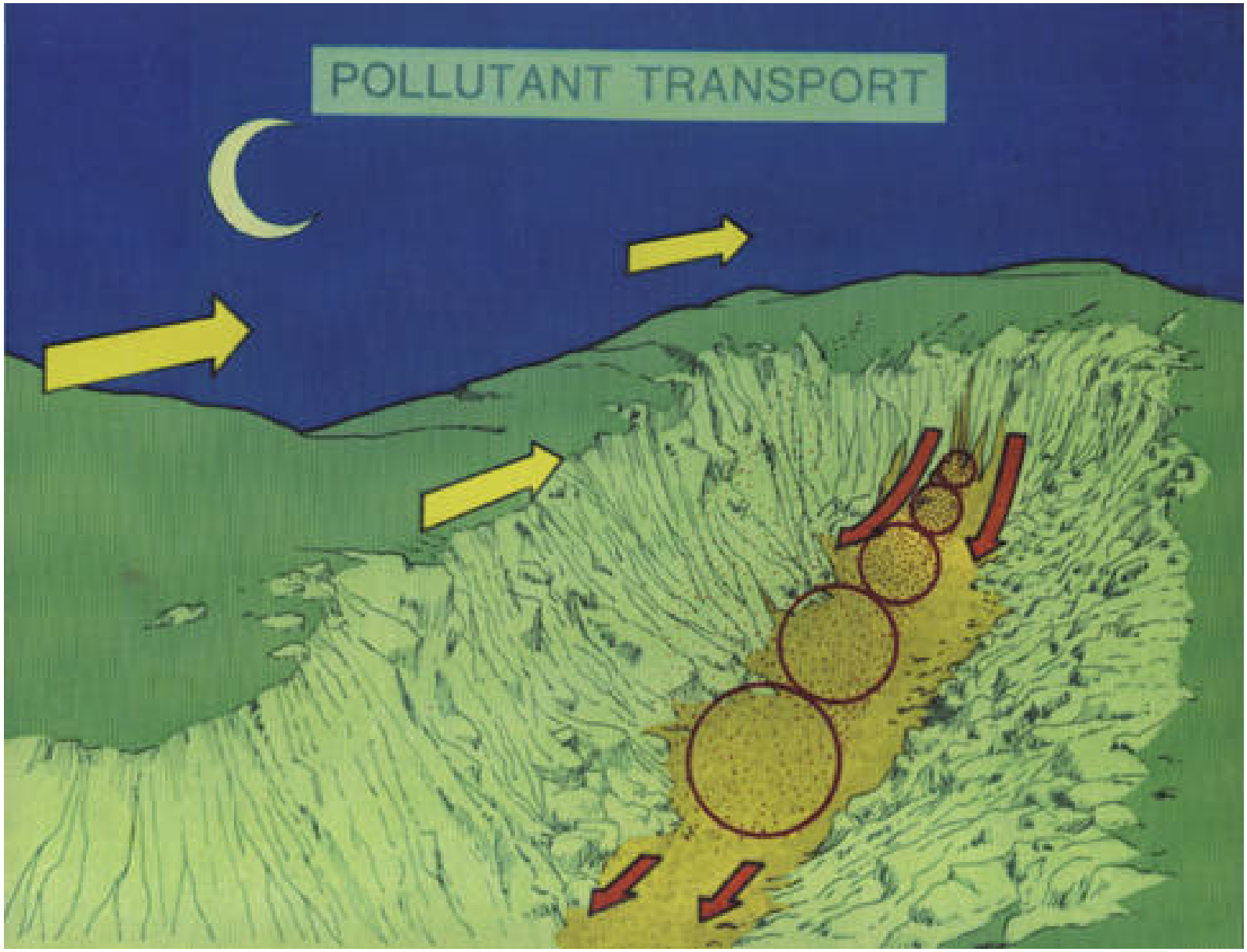

Figure C.1. Depiction of the dispersion and transport of materials released from the upper end of a canyon during the nighttime.

the same wind speed. In actuality, some of the material near the ground moved very slowly, while some aloft moved much more rapidly. RAPTAD was able to treat the wind-speed differences and provide a much better description of the actual pollution behavior.

4. Model Development

Initially the dispersion model had several limitations:

- the kernel growth was based on a simplistic model that was inappropriate for rapidly changing turbulence conditions,
- emission rates did not vary over the day,
- only one source was treated,
- the plume rise was treated simplistically, and
- the effect of vertical variations in stability was not reflected in the size of the particle kernel.

Turbulence conditions can change very rapidly shortly after sunrise, or when a layer aloft is captured by a growing mixed layer. Changing emission rates are very important for mobile sources. There are many sources that contribute to poor air quality in Mexico City. The contribution of industrial sources with large boilers to the air quality at any given time depends upon the heights obtained through buoyant plume rise. Unrepresentative plume rise calculations can lead to poor estimates. Finally, the volume that is calculated to surround a pseudoparticle is based on the circumstances experienced by the pseudoparticle. If materials are transported in a mixed layer, the turbulence may be quite high, but there may be a stable layer aloft in which there is little turbulence. It is inappropriate to let the pseudoparticle volume extend into the stable layer above.

a. Improved Spread Parameters

From the random force theory of turbulent diffusion, we have the following expression for the spread parameter in the y direction:

$$\sigma_y^2 = \left[\sigma_{yo}^2 + 2\sigma_{yo}\cdot\partial\sigma\cdot\bar{S} + (\partial\sigma)^2\right],$$

where

$$\partial\sigma = \sqrt{2}\cdot\sigma_v\cdot t_{Ly}\sqrt{\frac{\Delta t}{t_{Ly}} - 1 + \exp\left(-\frac{\Delta t}{t_{Ly}}\right)}.$$

The parameter $\bar{S}$ results from the spatial averaging over the plume width. It is given by:

$$\bar{S} = \frac{2}{\xi^2}[\xi - 1 + \exp(-\xi)],$$

with,

$$\xi = \frac{3.25_{y_o}}{L},$$

with the Eulerian length scale L approximated as:

$$L = \frac{\sigma_v\cdot t_{Ly}}{0.39}.$$

In this formulation, we only concern ourselves with the incremental change that occurs to a finite puff during a single time step. We need only assume that the turbulence conditions are constant over a single time step.

b. Time Varying Emissions

The model was altered to accept hourly emissions. The procedure specifies the total number of hours on the days to be simulated and then hourly emissions are read in. Each time is in hours from midnight of the start of the simulation, so that different emissions could be used at the same time on different days. Emission changes less frequent than hourly could also be

used. Within the hour there is a linear interpolation with time between the last hour and the next one. Typically, all the mobile sources are assumed to have the same time profile of emissions, while the stationary sources are treated with a different profile. Two separate RAPTAD runs are made to treat each of these source types, and the results are combined with a simple code that adds the contributions at each monitor site.

c. Extension to Multiple Sources

With the original code, multiple sources were treated by combining the results from multiple runs. However, if each emission cell is considered as a different source, the problem becomes unwieldy. Consequently, the code was modified to deal with a large number of emission sources having the same time profile. The first step is to prepare a file that gives cumulative frequency distribution of the emissions for all the sources. For example, suppose we had only three sources, and the first cell had 10% of the total emissions, the second had 30% of the total emissions, and the third had 60% of the emissions. The cumulative frequency distribution would have a line at 0.1 for the first cell, a line at 0.4 for the second cell, and a line at 1.0 for the third cell. Thus, cells one and two represent 40% of the total emissions, while cells one, two, and three represent 100% of the total emissions. What the model does is to release more particles in cells that represent more emissions. The total emissions are divided equally among the particles to be released in any given hour. When a particle is to be released, the model selects a random number between 0 and 1. It then selects the cell that is above the random number, but is closest to it. For example, suppose the random number were 0.33. This is less than 0.4, so cell 2 would be chosen and the psuedoparticle would be released from the center of cell two. If the random number were 0.05, cell one would be chosen and the particle released from it. The larger the fraction of emissions in any cell the more likely the particles are to be released from that cell. For the mobile source emission inventory there are hundreds of cells in the cumulative distribution. The new input includes the cumulative distribution of emissions, the easting and northing coordinates of the cell, and for large point sources the stack parameters associated with the source.

d. Improved Plume Rise Description

The original plume rise description covered only neutral and stable conditions. In the revised model, a considerable elaboration has been developed based on Briggs' work (Briggs, 1984). The model now includes two different treatments for stable conditions, a treatment for elevated inversion layers aloft, a convective turbulence treatment, and two neutral stability treatments. The smallest applicable plume rise is picked as the limiting condition in each case. The plume rise is still based on bulk properties of the atmosphere and does not make full use of the meteorological model outputs that are available.

e. Mixing Heights and Vertical Restrictions on the Plume Kernel

One problem with the kernel approach is that the kernel is based only on the turbulence parameters experienced by the pseudoparticles. A pseudoparticle released at the surface in a

well-mixed layer will tend to travel in the layer and not experience the more stable layers aloft. Consequently, one may calculate a vertical spread parameter that is too large if there is a strong inversion layer aloft. This concern was addressed by limiting the growth of the vertical spread of particles in the mixed layer to be less than the height of the mixed layer. In cases where the mixed layer height limits the vertical spread of the kernel, the model uses a vertically uniform distribution instead of a Gaussian distribution. This treatment is very similar to that used by Gaussian puff models except that we are using it for individual pseudoparticle kernels rather than the plume as a whole.

One problem with this approach is how to calculate the mixed layer height based on the HOTMAC meteorological outputs. Fortunately, the use of HOTMAC and RAPTAD is ideal for testing an old formulation or for developing and testing a new formulation. We examined the potential temperature formulation that defines the mixing height as the height at which the potential temperature is equal to the potential temperature near the surface. We released particles near the surface and plotted their heights, and we also plotted the heights of the mixed height based on the potential temperature formulation. Ideally the calculated mixing heights should represent the upper limit of the particle positions. We found that the potential temperature representation seemed to overestimate the height of the mixing layer.

Next, we considered a formulation in which we defined the mixing height by the height at which the fluctuations in the vertical velocity, σ_w, dropped below some specified level. This system tended to do a much better job for the midmorning-through-afternoon heights, but it sometimes had difficulties with early morning situations. We remedied this defect by using a formulation where we defined the mixing height by the height at which the potential temperature first began to increase in the early morning. In the early morning, relatively small values of σ_w, are adequate to transport material upward across the thin layers; however, in the afternoon large values of σ_w are required to move the material across the deep layers. Figure C.2 displays the particle positions as seen from above at 10:00 a.m. from an early morning release on February 22. Only the fine grid is shown; the bounding lines show what will be displayed in the vertical position plots. For example, the particles that are displayed in Figure C.3 are those which are found between Universal Transverse Mercator northing coordinates (UTMY) 2140. and 2160, while the particles displayed in Figure C.4 are those found between easting coordinates (UTMX) 479. and 499. The various lines in Figure C.3 correspond to the mixing height calculated from the various meteorological grids that fall within the UTMY lines. The heights show an increase over higher terrain. For example, note the bump in Figure C.4 at UTMY 2165, which corresponds to Pico de Tres Padres as shown in Figure C.2.

f. Improvements to Model Speed

In order to provide the level of detail needed close to the sources, many particles must be released. However, as the plumes from individual sources merge and mix, less detail is needed. Moving and calculating the concentrations associated with many particles requires computer time. We have dealt with this problem by reducing the number of particles once they are an

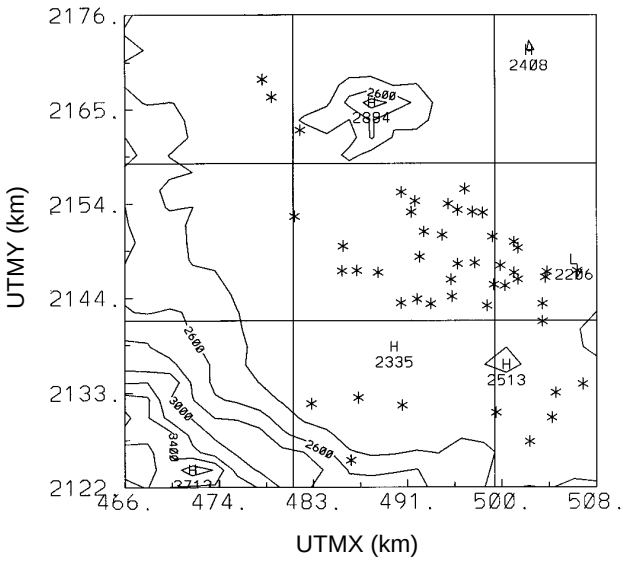

Figure C.2. Calculated pseudoparticle positions displayed on a contour map of the fine-grid area for 10:00 a.m. on February 22, 1991, after an early morning release.

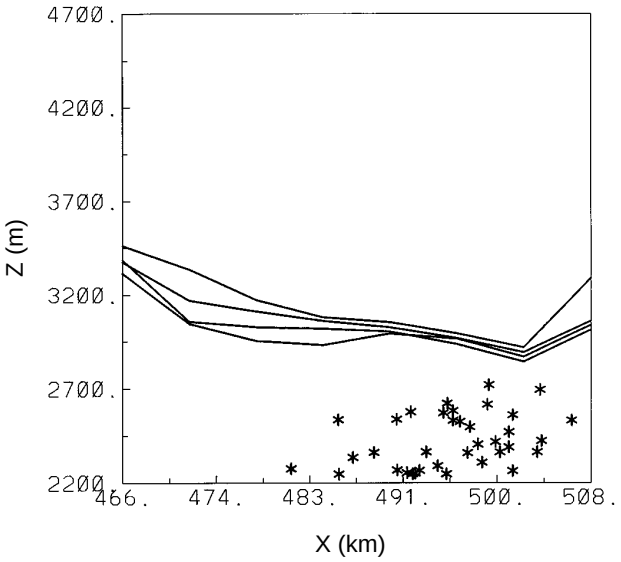

Figure C.3. Calculated vertical positions above ground of pseudoparticles (asterisks) and modeled mixing heights (lines) for all pseudoparticles with UTM northing positions between 2140 and 2160 km.

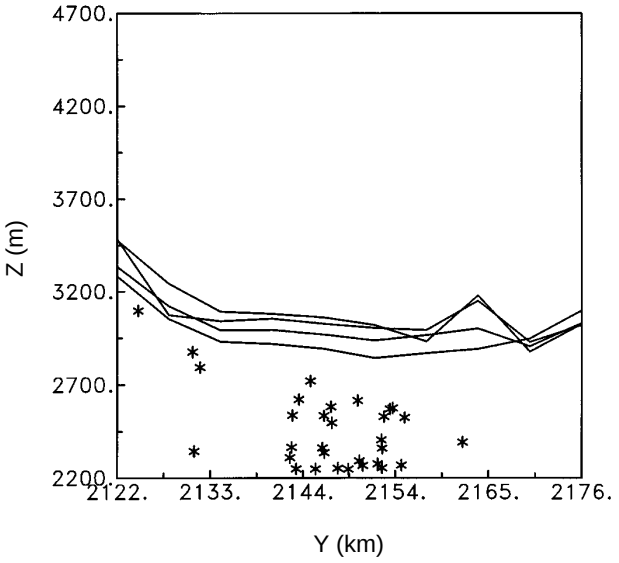

Figure C.4. Calculated vertical positions above ground of pseudoparticles (asterisks) and modeled mixing heights (lines) for all pseudoparticles with UTM easting positions between 479 and 499 km.

hour and a half old. As we drop most of the particles, we increase the emissions associated with the remaining particles correspondingly. This saves us a great deal of computation time while retaining the capability to treat the important near-source behavior. We have also done other things to increase the speed of the model. These include calculating the concentrations at intervals of several time steps instead of after each time step and using a table look-up instead of a direct calculation of the exponentials in the Gaussian distributions.

5. Comparison of Model Results to Measurements

Two principal data sets were available for testing the performance of the dispersion model: the National Center for Atmospheric Research (NCAR) aircraft measurements and the

SEDESOL surface monitoring results. The aircraft measurements provided a general context that is very important to model verification, while the SEDESOL stations provided the concentrations at the surface where the people are. Good performance aloft is important for what it tells about the meteorology that is used by the photochemical model. The photochemistry develops over time so that near-source concentrations are less important than general bulk concentrations.

The direct application of the dispersion model is to the SEDESOL measurements, because they are used to determine the air quality. The dispersion model can calculate either concentrations on a specified grid or at specific locations. In this context, we chose to calculate concentrations at the SEDESOL monitoring sites. Furthermore, since the monitoring day chosen by SEDESOL is from 7:00 p.m. one day until 6:00 p.m. the next, the same period was chosen for the RAPTAD simulations. The simulations were begun on February 20, at 7:00 p.m. for the first period and continued until early morning on February 23. For the second period simulations were begun at 7:00 p.m. on February 24 and continued until early morning on the first of March. In each case the first day has been ignored to avoid results dominated by initial conditions.

a. Aircraft CO and SO_2 Comparisons

We have used two kinds of aircraft measurements: vertical profiles and horizontal tracings. We have modeled the vertical profiles by calculating the concentrations at intervals of 150 meters from the surface up to 1500 meters. We have used the coordinates of the Hangares monitor (station Y) as representative of the profiles, although the aircraft takes off from the runway and climbs out to the northeast. Figure C.5 shows a comparison of the measured CO profile on February 22 with a profile calculated for the airport. Figure C.6 shows the measured CO profile and a profile calculated for a point 9 km east of the airport. The values calculated for the airport show concentrations that are too high near the surface, while the modeled values east of the airport show much lower concentration. The model does not reproduce the high concentrations measured 0.5 km and higher above the surface. Neither the model nor the measurements show a pattern that would be expected for limited mixing conditions. Figures C.7, C.8, and C.9 show measured and calculated vertical profiles for CO on February 21, 26, and 27, respectively. Figure C.7 is particularly interesting because the measurements show an increase above 1.5 km

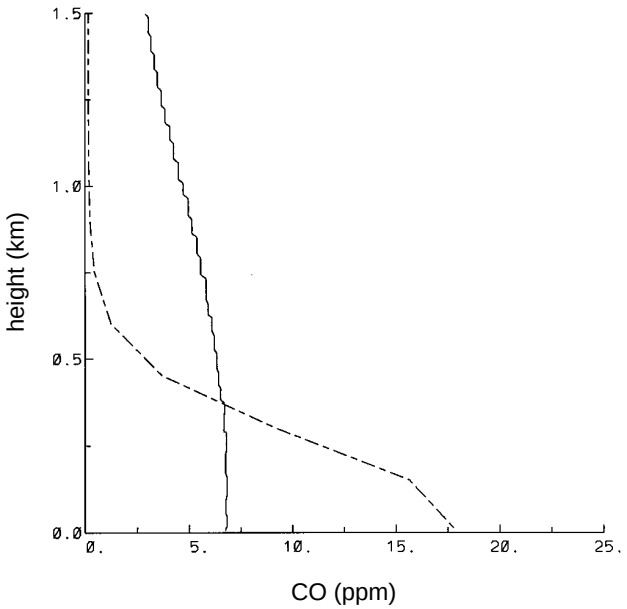

Figure C.5. Comparison of aircraft measured CO concentrations after takeoff from the Mexico City Airport with modeled vertical CO profiles (dashed line) from the airport for 10:00 a.m. on February 22, 1991.

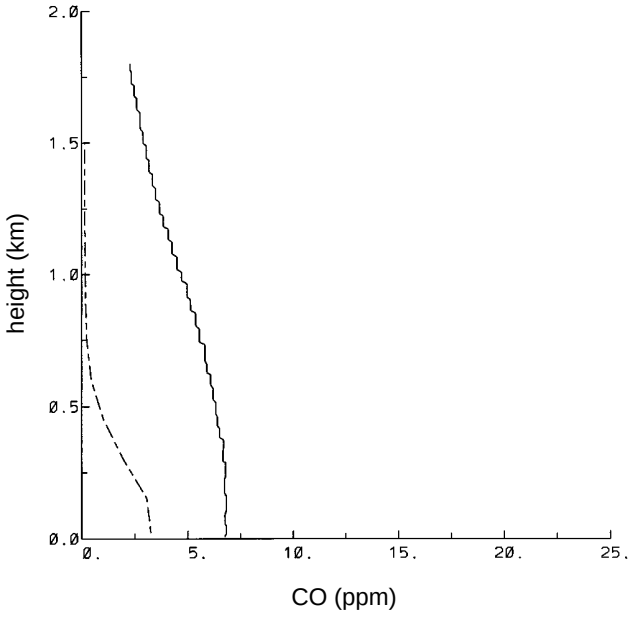

Figure C.6. Comparison of aircraft measured CO concentrations after takeoff from the Mexico City Airport with modeled vertical CO profiles (dashed line) for a point 9:00 km east of the airport for 10:00 a.m. on February 22, 1991.

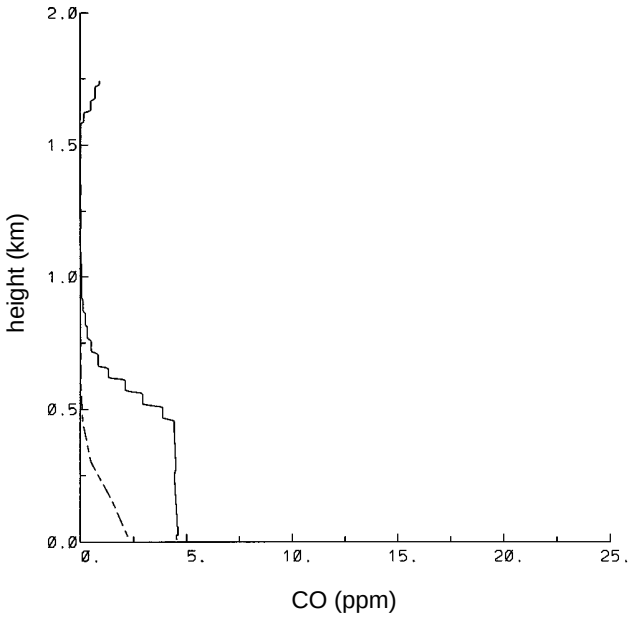

Figure C.7. Comparison of aircraft measured CO concentrations after takeoff from the Mexico City Airport with modeled vertical CO profiles (dashed line) from the airport for 10:00 a.m. on February 21, 1991.

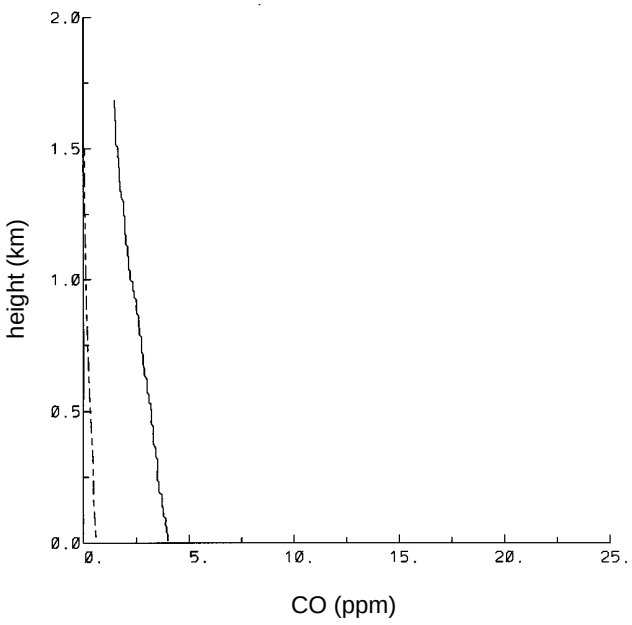

Figure C.8. Comparison of aircraft measured CO concentrations after takeoff from the Mexico City Airport with modeled vertical CO profiles (dashed line) from the airport for 8:00 a.m. on February 26, 1991.

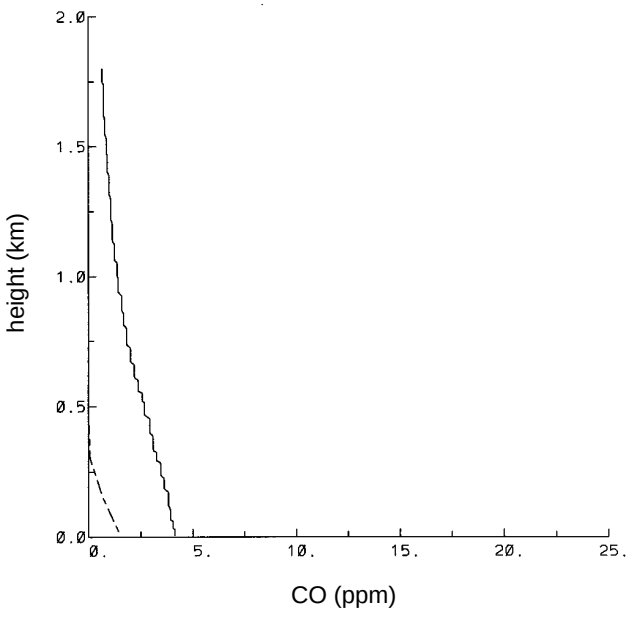

Figure C.9. Comparison of aircraft measured CO concentrations after takeoff from the Mexico City Airport with modeled vertical CO profiles (dashed line) from the airport for 8:00 a.m. on February 27, 1991.

that might be indicative of material carried up the slopes to the southwest and returned via the southwest winds aloft. Unfortunately points above 1.5 km were not modeled. Figure C.7 is the only profile that shows anything like a classic mixed layer in either the modeled or measured results.

Figure C.10 shows a measured vs. calculated CO comparison for a horizontal traverse from west to east over the center of the city at 500 meters above the surface on February 22. The modeled results are for only four points at easting coordinates of 475., 485., 495., and 504. The measurements and the model show a similar pattern, although the measurements show higher concentrations on either side of the city. The modeled results include no background CO concentrations. A typical background in a remote area would be about 0.2 parts per million, but an appropriate background for Mexico City might be somewhat different. Figure C.11 shows a similar comparison for February 21, and Figure C.12 shows the comparison for February 26.

Figure C.13 shows the vertical profile comparison for SO_2 at the airport on February 22, 1991. The calculation shows a pattern similar to the measurements, but the calculated concentrations are slightly underestimated. An earlier version of the SO_2 inventory gave a significant overestimate for the modeled profiles; the differences between the two inventories has not been resolved. Figure C.14 gives the vertical profiles for February 21 at the airport. In this instance the concentrations are very close near the surface, but the model underestimates the observations aloft. Figure C.15 shows the comparison for February 26 at the airport, while Figure C.16 shows the comparison for February 27.

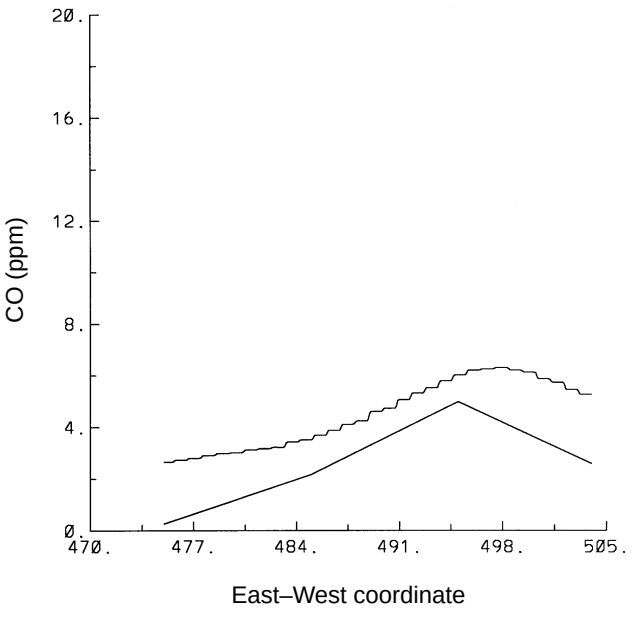

Figure C.10. Comparison of aircraft measured CO concentrations on a west-to-east traverse of the center of the city to modeled concentrations at four points along the traverse for 11:00 a.m. on February 22, 1991.

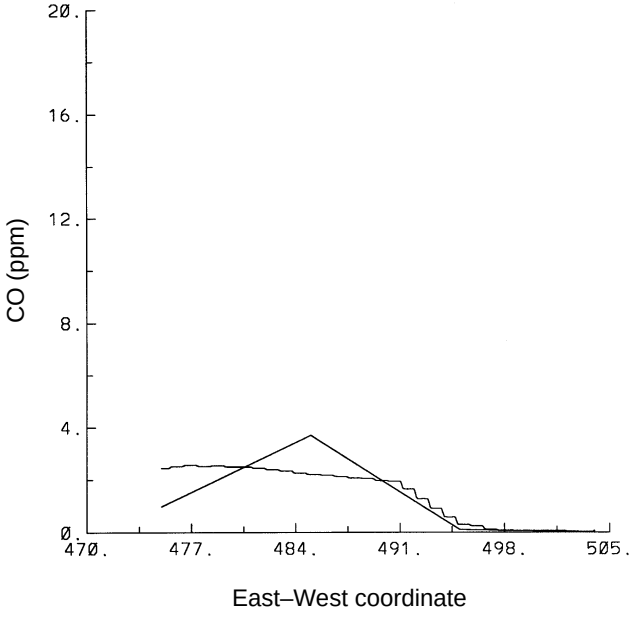

Figure C.11. Comparison of aircraft measured CO concentrations on a west-to-east traverse of the center of the city to modeled concentrations at four points along the traverse for 10:00 a.m. on February 21, 1991.

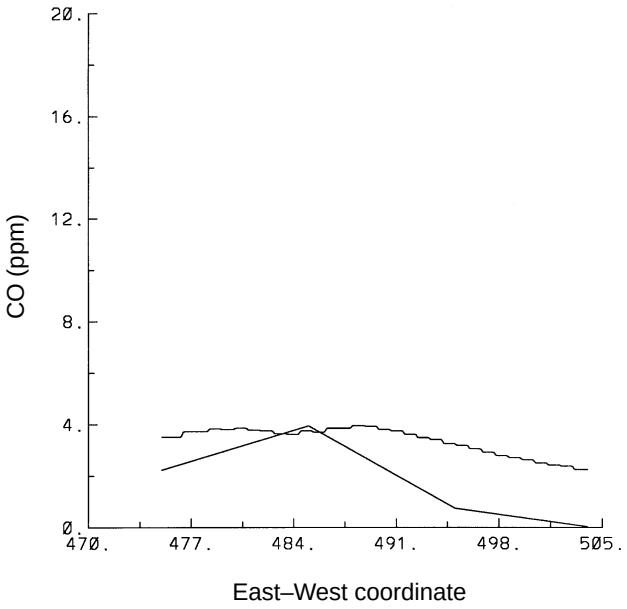

Figure C.12. Comparison of aircraft measured CO concentrations on a west-to-east traverse of the center of the city to modeled concentrations at four points along the traverse for 11:00 a.m. on February 26, 1991.

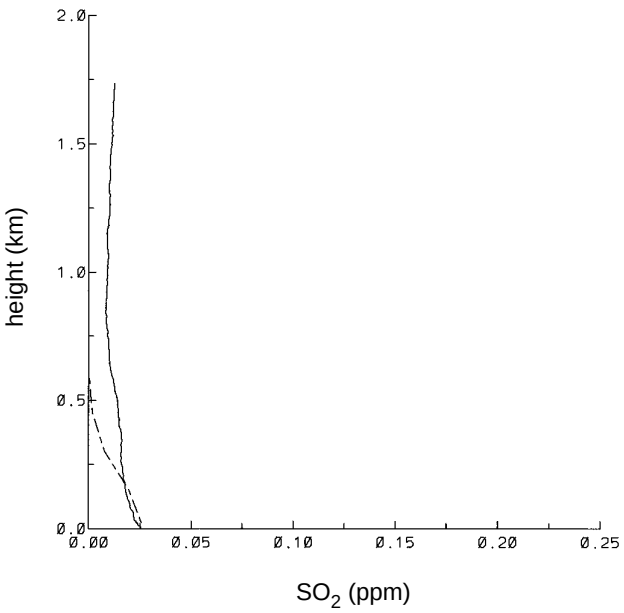

Figure C.14. Comparison of aircraft measured SO_2 concentrations after takeoff from the Mexico City Airport with modeled vertical SO_2 profiles (dashed line) from the airport for 10:00 a.m. on February 21, 1991.

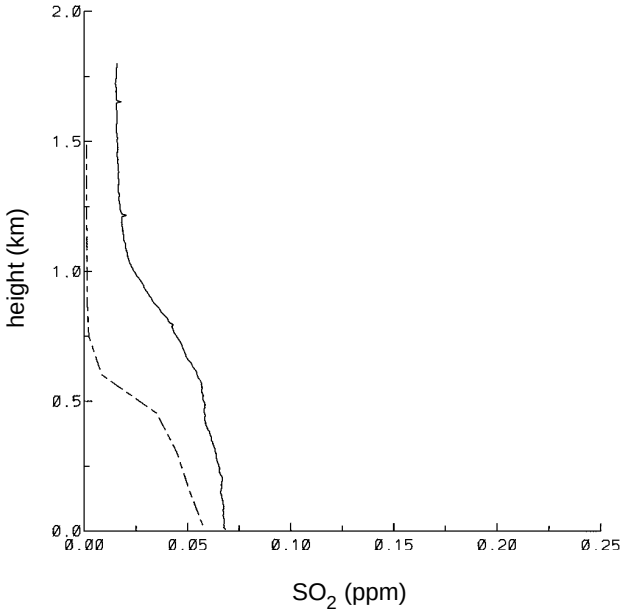

Figure C.13. Comparison of aircraft measured SO_2 concentrations after takeoff from the Mexico City Airport with modeled vertical SO_2 profiles (dashed line) from the airport for 10:00 a.m. on February 22, 1991.

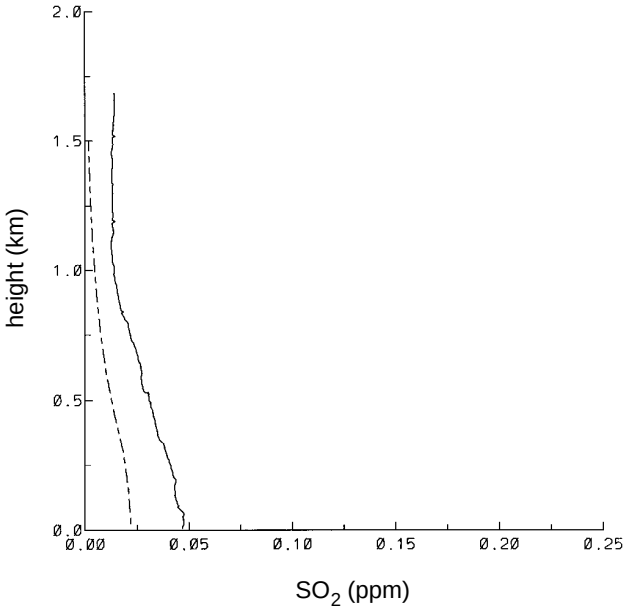

Figure C.15. Comparison of aircraft measured SO_2 concentrations after takeoff from the Mexico City Airport with modeled vertical SO_2 profiles (dashed line) from the airport for 10:00 a.m. on February 26, 1991.

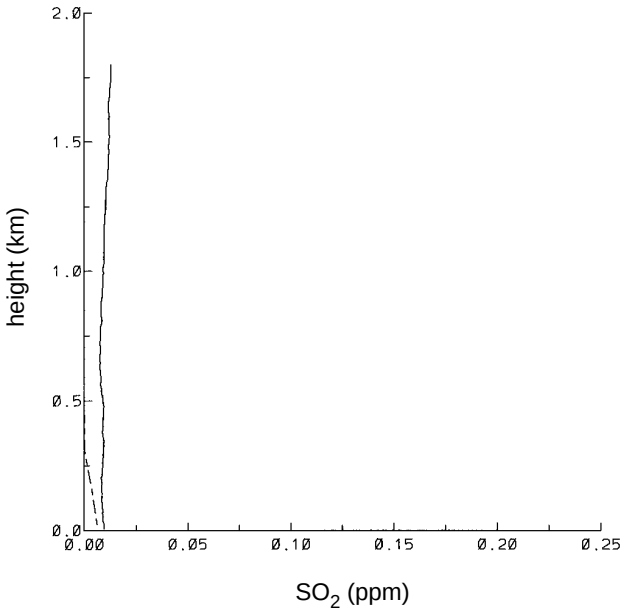

Figure C.16. Comparison of aircraft measured SO_2 concentrations after takeoff from the Mexico City Airport with modeled vertical SO_2 profiles (dashed line) from the airport for 8:00 a.m. on February 27, 1991.

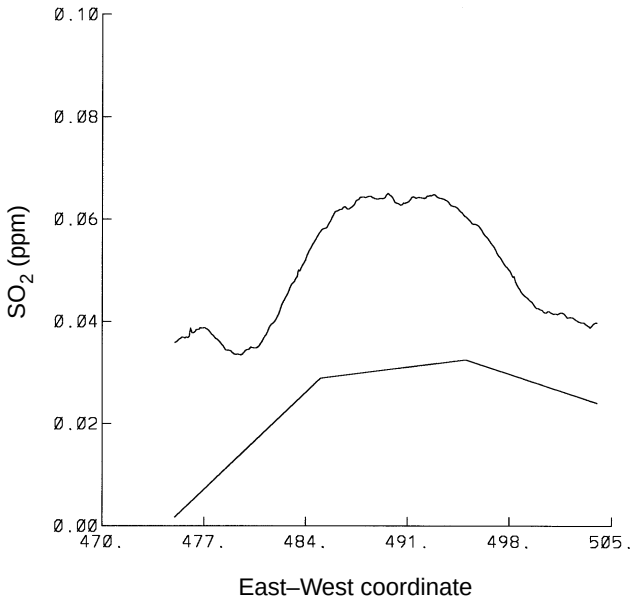

Figure C.17. Comparison of aircraft measured SO_2 concentrations on a west-to-east traverse of the center of the city to modeled concentrations at four points along the traverse for 11:00 a.m. on February 22, 1991.

Again the concentrations aloft are underestimated, but even the actual concentrations are relatively low at about 0.02 ppm.

Figure C.17 shows the SO_2 comparison for a horizontal traverse from west to east over the center of the city at 500 meters above the surface on February 22. The modeled results are for only four points at easting coordinates of 475., 485., 495., and 504. The measurements and the model show a similar pattern, although the measurements show higher concentrations on either side of the city. The modeled results include no background SO_2 concentrations. Figure C.18 shows the comparison for February 21, while Figure C.19 shows the comparison for February 26. In most cases the concentrations are low, and the model results slightly underestimate the observations. On February 22 the concentrations are the highest of the three days, and the model reproduces that pattern, but the estimations are about half of the observations. Once again the earlier inventory gave much higher modeled values.

b. Surface CO and SO_2 Comparisons

Figure C.20 reports the model-measurement comparison at several SEDESOL monitoring stations for CO for February 22, 1991. Figures C.21 through C.23 report the CO comparisons for February 26 through February 28, respectively. Generally the model appears to show the correct behavior although there are cases when the model misses a peak or puts one in that should not be there. There are also some cases in which the measurements have strange behavior. For example, station P shows relatively high concentrations at all times as does station Q. There has been concern that the stations have a 2.5 ppm offset to avoid numerical processing problems

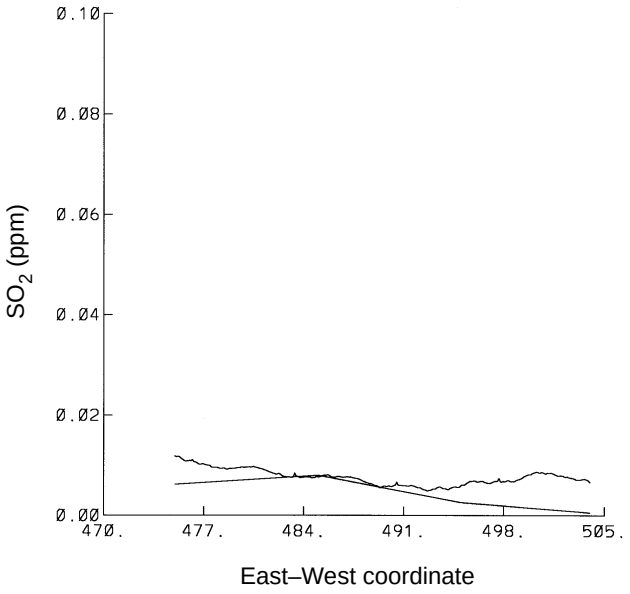

Figure C.18. Comparison of aircraft measured SO_2 concentrations on a west-to-east traverse of the center of the city to modeled concentrations at four points along the traverse for 10:00 a.m. on February 21, 1991.

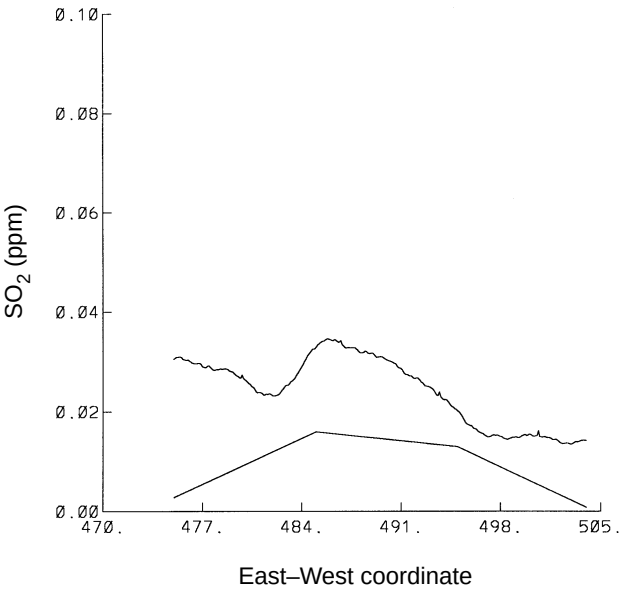

Figure C.19. Comparison of aircraft measured SO_2 concentrations on a west-to-east traverse of the center of the city to modeled concentrations at four points along the traverse for 11:00 a.m. on February 26, 1991.

associated with scatter around a zero base line; however, these stations do not seem to have a uniform offset.

Figure C.24 reports the comparison between modeled and measured SO_2 on February 22, 1991. Figures C.25 through C.27 report similar comparisons for February 26-28, respectively. Again the model shows behavior similar to the measurements, although the newer inventory has produced underestimates that were not found with the older inventory. Of particular interest is the difference between Figure C.20 for CO and Figure C.24 for SO_2. Figure C.24 reports early morning peaks in both the model and the measured results that are not reflected in the CO comparisons. These could be the result of terrain-induced mixing of elevated plumes.

6. Performance Summary

In section B.6 we described suggested statistical measures for evaluating model performance. Because they were considering gridded model predictions, the researchers who advocated these measures suggested a different set of measures to evaluate the performance of models in predicting concentrations. Since we are using receptor model predictions, we chose to use the same measures as described in B.6, even though these measures are likely to provide a somewhat more pessimistic view of model performance. Table C.1 summarizes the statistics for the comparison between modeled and measured CO concentrations.

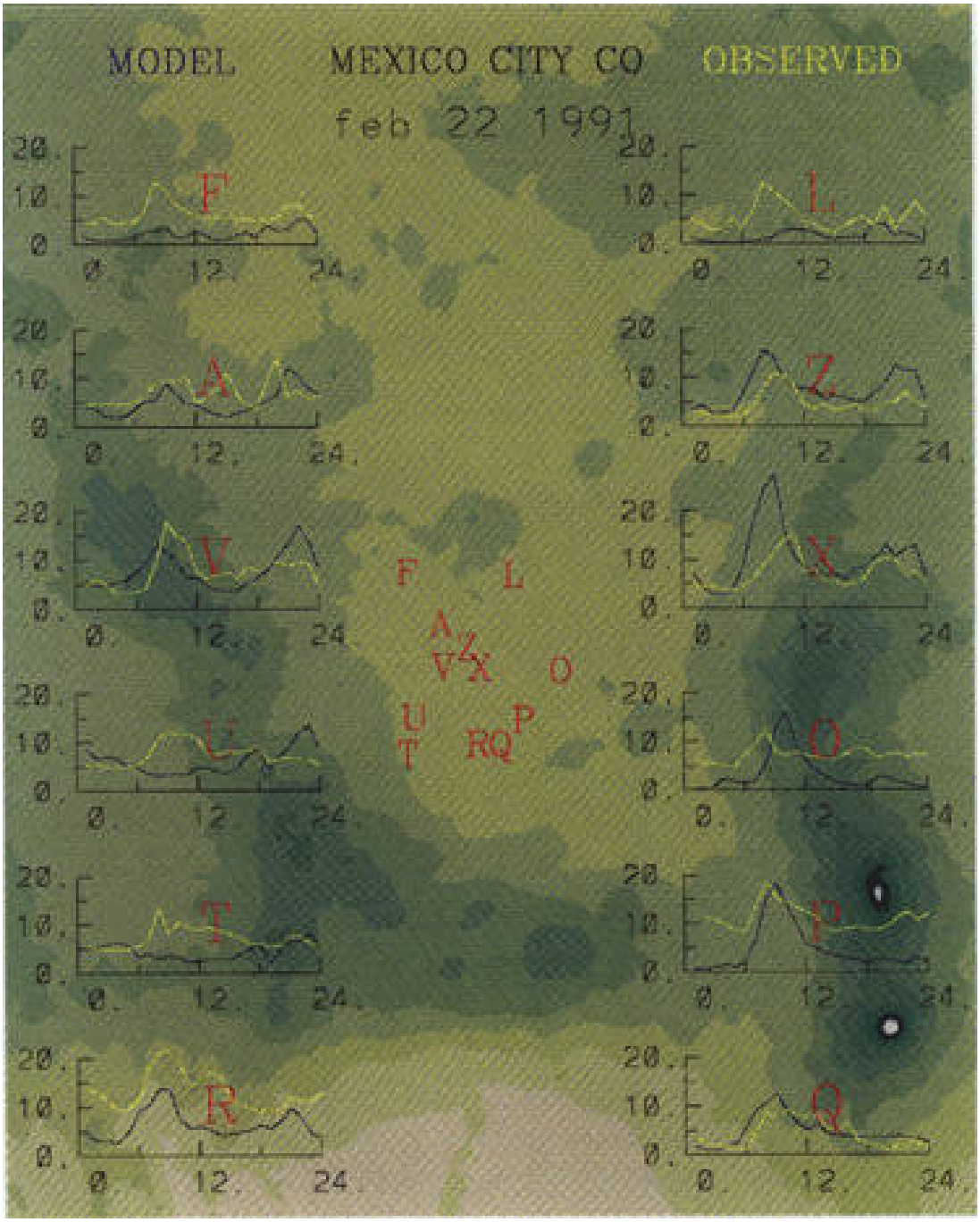

Figure C.20. Comparison of hourly measured CO concentrations (yellow) from the SEDESOL surface monitoring network with modeled ones (blue) with station locations for February 22, 1991.

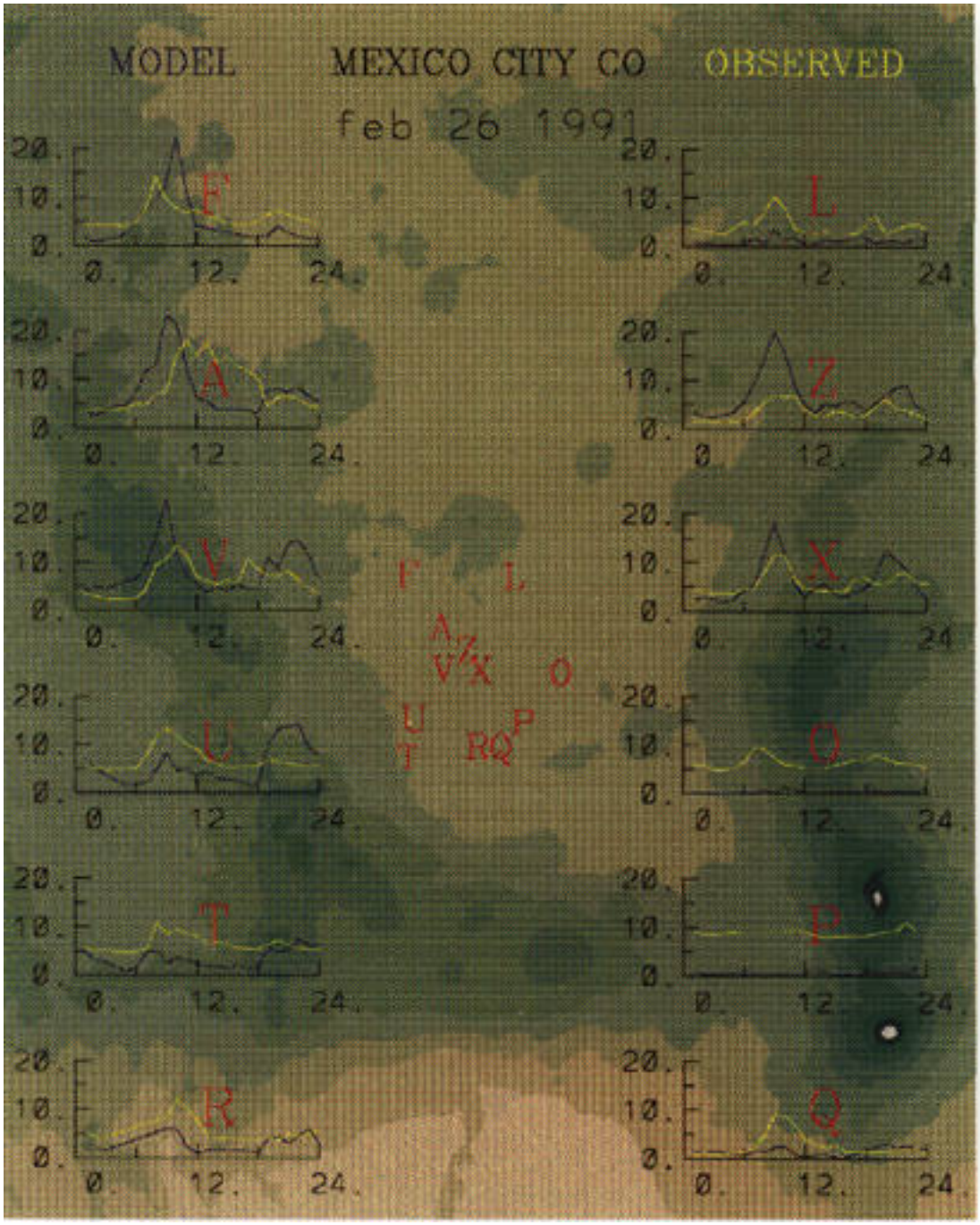

Figure C.21. Comparison of hourly measured CO concentrations (yellow) from the SEDESOL surface monitoring network with modeled ones (blue) with station locations for February 26, 1991.

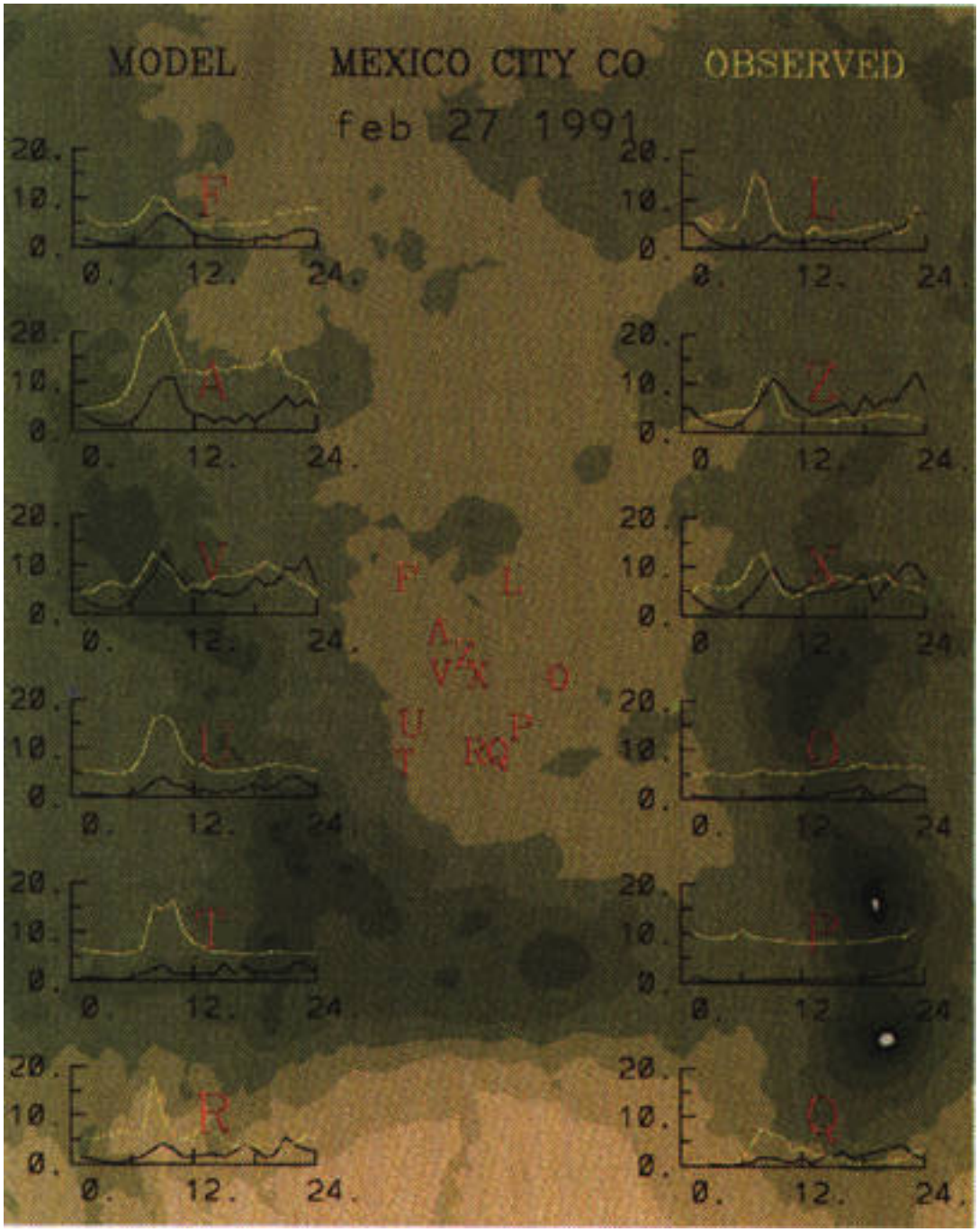

Figure C.22. Comparison of hourly measured CO concentrations (yellow) from the SEDESOL surface monitoring network with modeled ones (blue) with station locations for February 27, 1991.

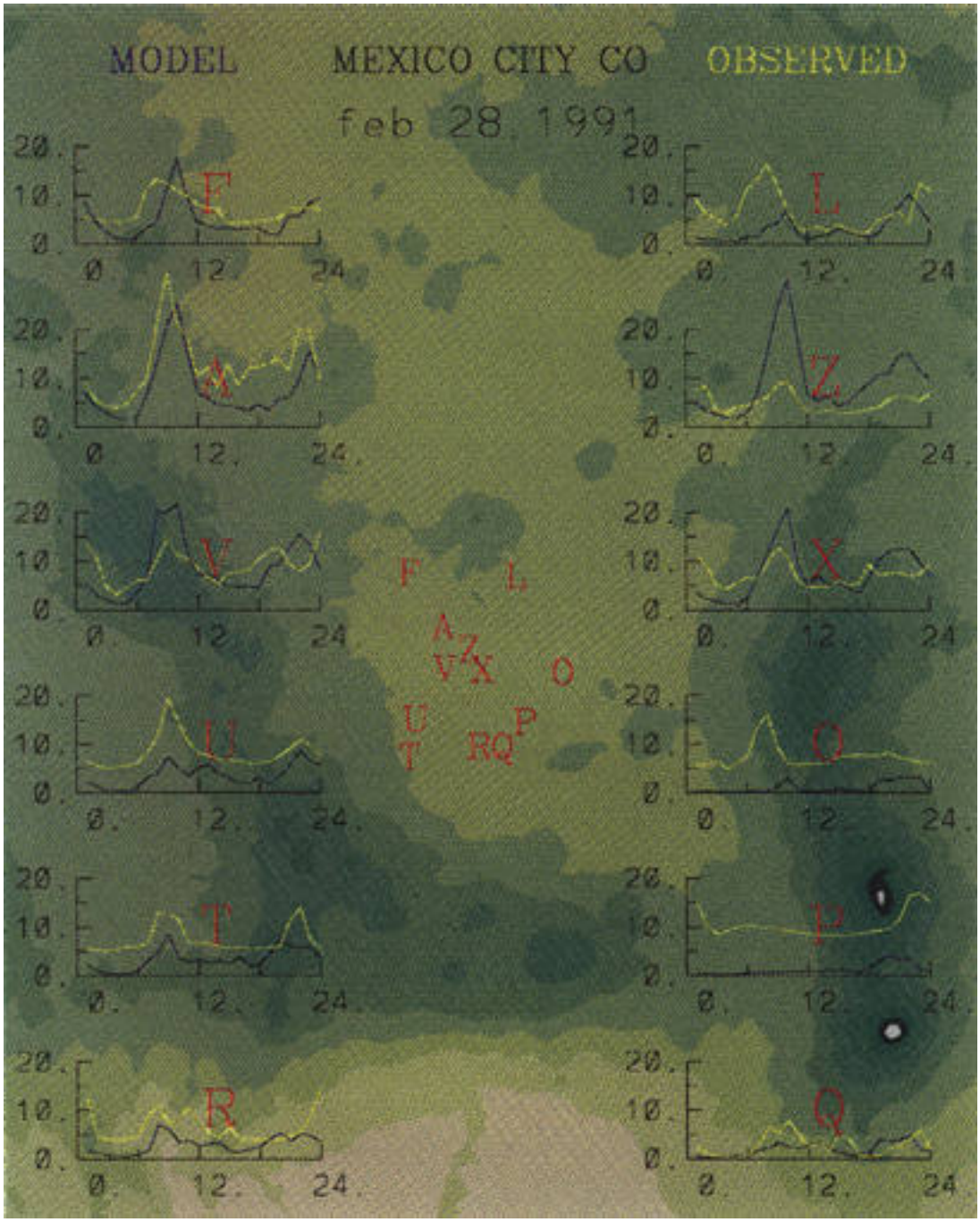

Figure C.23. Comparison of hourly measured CO concentrations (yellow) from the SEDESOL surface monitoring network with modeled ones (blue) with station locations for February 28, 1991.

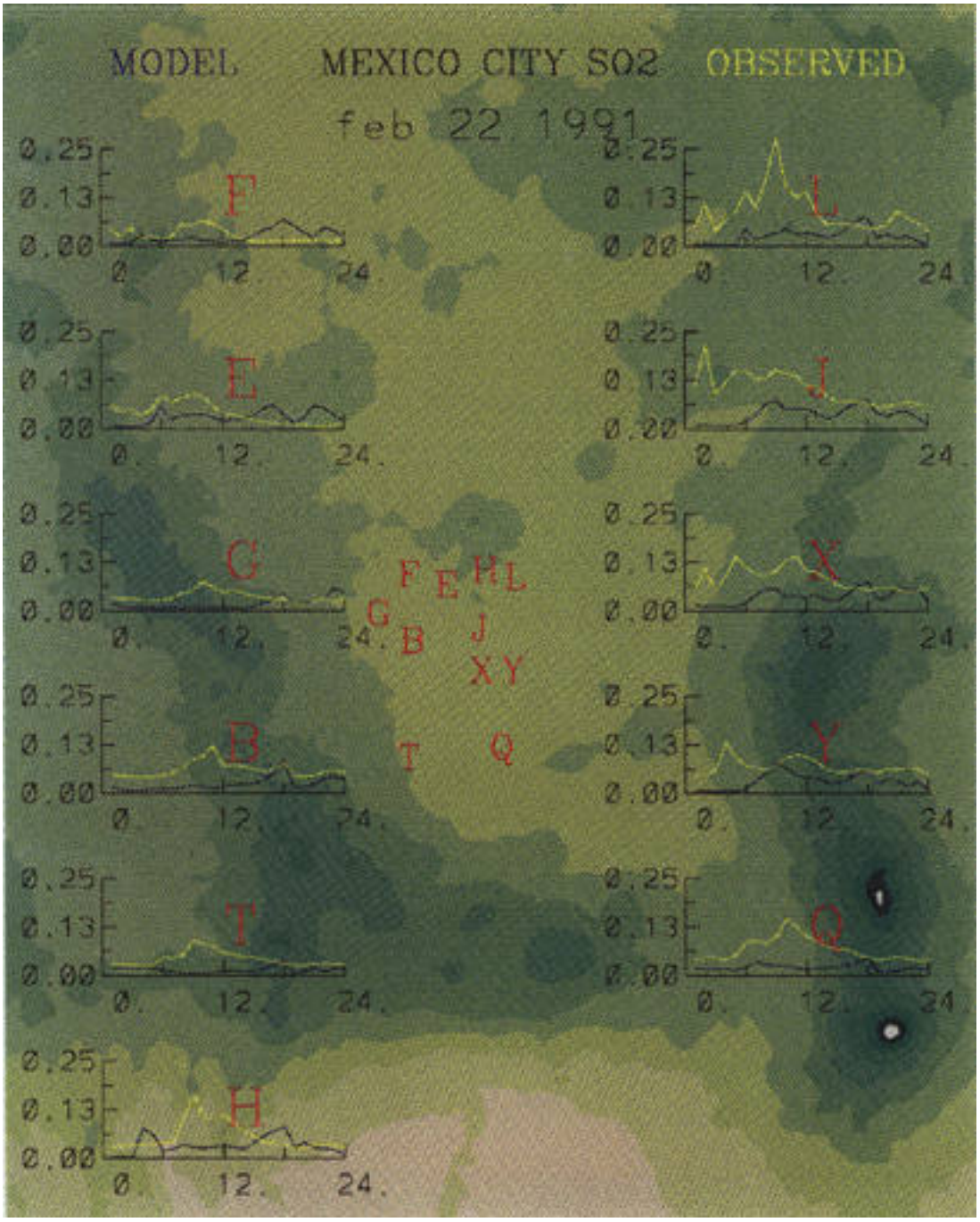

Figure C.24. Comparison of hourly measured SO_2 concentrations (yellow) from the SEDESOL surface monitoring network with modeled ones (blue) with station locations for February 22, 1991.

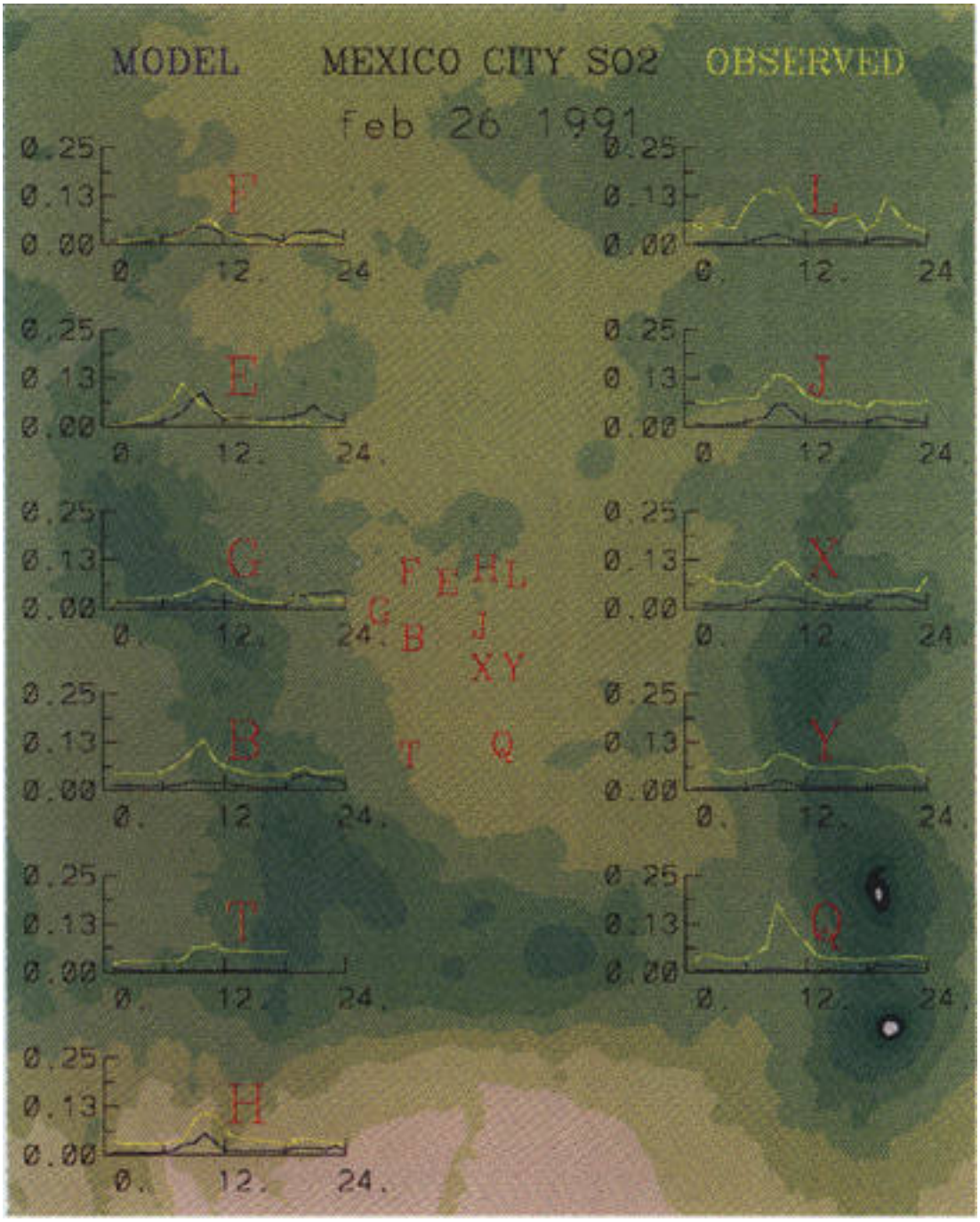

Figure C.25. Comparison of hourly measured SO_2 concentrations (yellow) from the SEDESOL surface monitoring network with modeled ones (blue) with station locations for February 26, 1991.

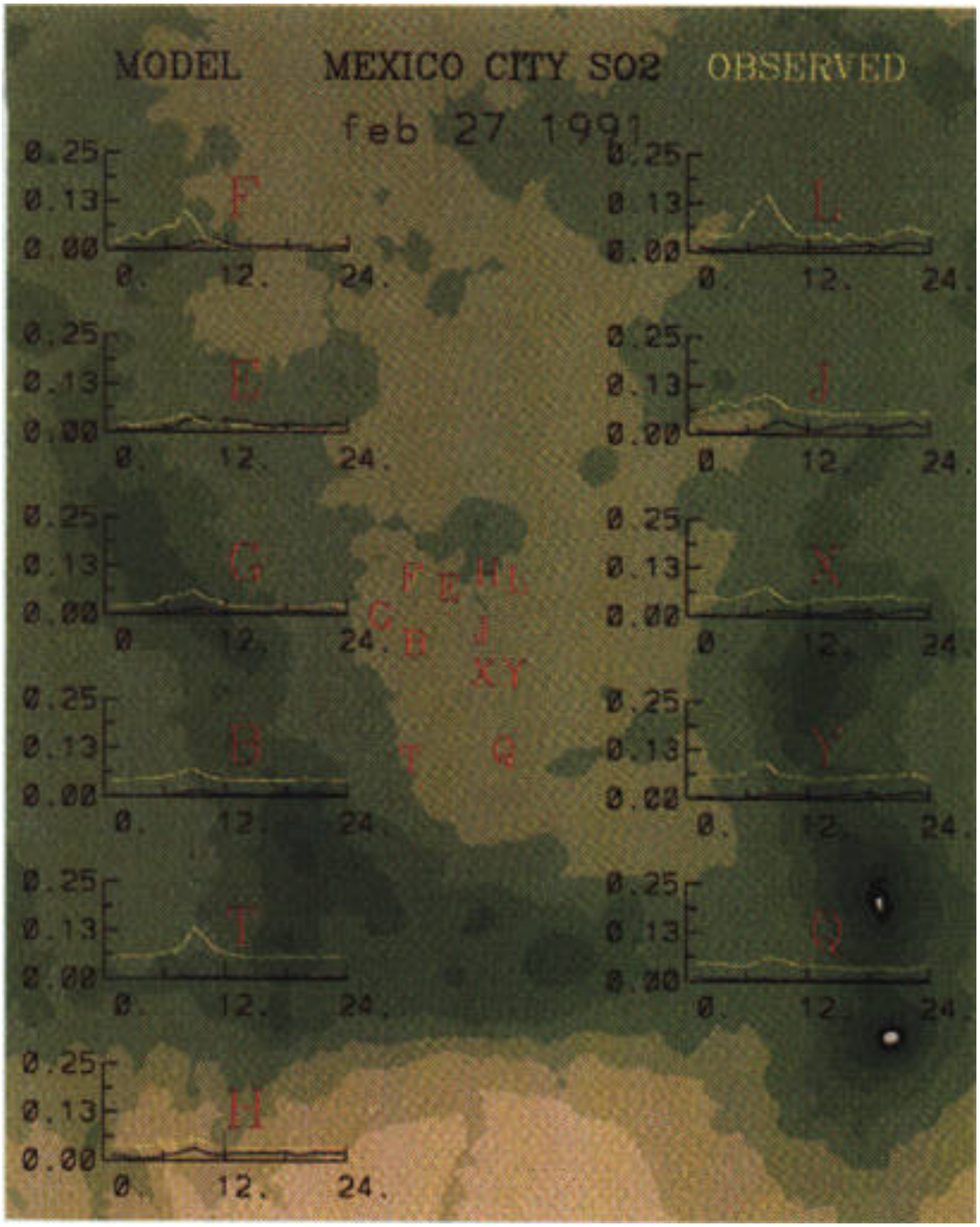

Figure C.26. Comparison of hourly measured SO_2 concentrations (yellow) from the SEDESOL surface monitoring network with modeled ones (blue) with station locations for February 27, 1991.

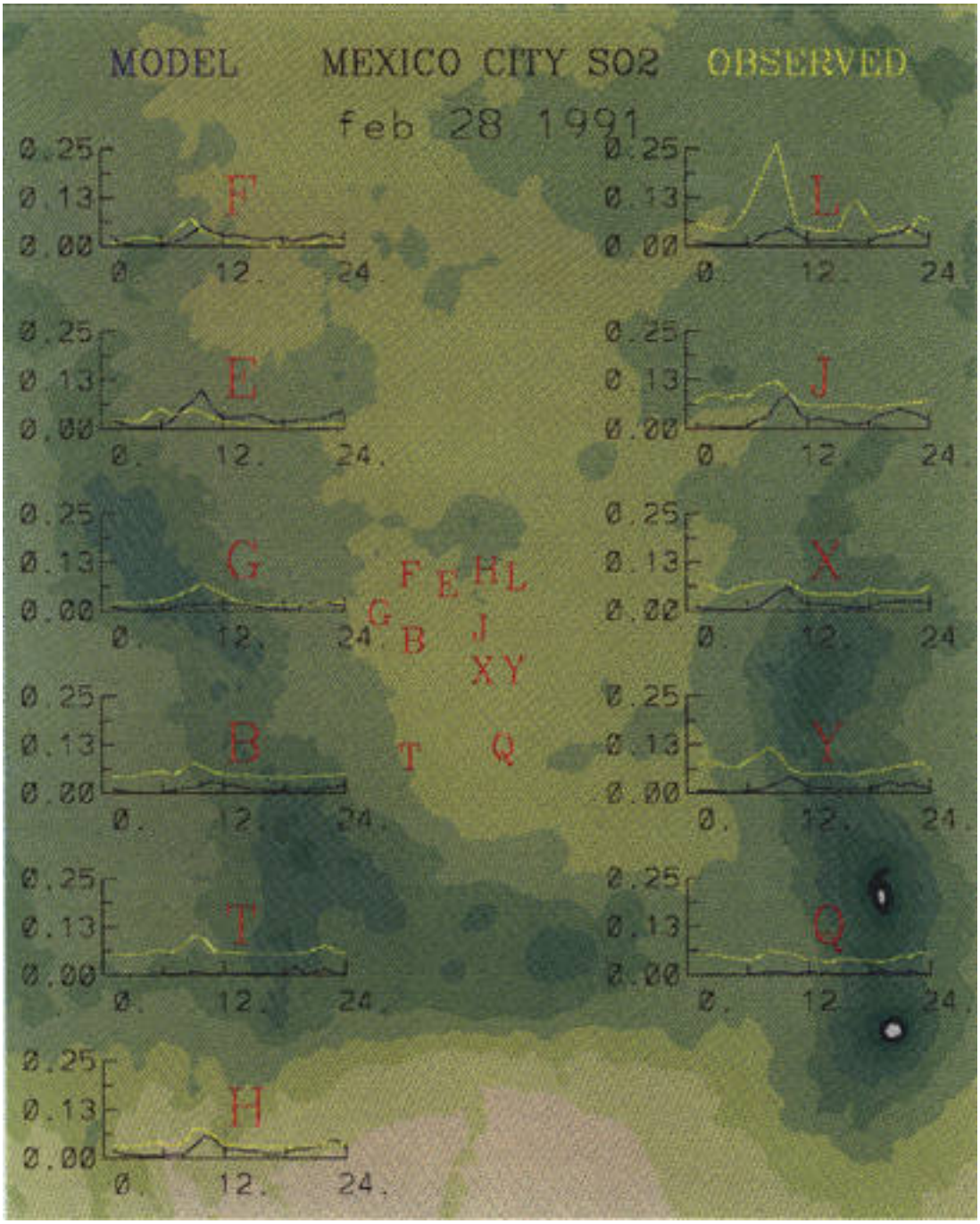

Figure C.27. Comparison of hourly measured SO_2 concentrations (yellow) from the SEDESOL surface monitoring network with modeled ones (blue) with station locations for February 28, 1991.

TABLE C.1 Comparison for Modeled and Measured CO Concentrations

Comparison for CO Concentrations	
Model mean	4.3
Observation mean	6.8
Standard deviation of predictions	4.2
Standard deviation of observations	3.6
Regression intercept	1.8
Regression coefficient	0.38
Correlation coefficient	0.33
Root mean square error	5.2
Systematic root mean square error	3.4
Unsystematic root mean square error	3.9
Index of agreement	0.55
Skill error	1.1
Skill variance	1.1
Model maximum	30.2
Observation maximum	31.5

TABLE C.2 Statistics for the Comparison of Modeled and Measured SO_2 Concentrations

Comparison for SO_2 Concentrations	
Model mean	0.017
Observation mean	0.050
Standard deviation of predictions	0.015
Standard deviation of observations	0.031
Regression intercept	0.013
Regression coefficient	0.083
Correlation coefficient	0.17
Root mean square error	0.046
Systematic root mean square error	0.044
Unsystematic root mean square error	0.015
Index of agreement	0.43
Skill error	0.48
Skill variance	0.49
Model maximum	0.098
Observation maximum	0.279

The model gives a somewhat lower mean than does the observations, although a 2.5 ppm correction would give perfect agreement. Generally, the model seems to be doing quite well given the uncertainty in both the emission and meteorological inputs. Table C.2 summarizes the statistics for the comparison between modeled and measured SO_2 concentrations.

The model underestimates the observed surface concentrations in a fashion similar to that found in comparison to the aircraft measurements. The regression and correlation coefficients are low, but it is difficult to obtain good hour-by-hour and station-by-station agreement in these circumstances.

Comparison with the aircraft measurements of CO suggests good model performance overall. For SO_2 both surface and aircraft measurements show a consistent pattern of underestimation, but there are significant discrepancies in recent SO_2 emission inventories that could explain the behavior. There is also a problem in that the effective stack height for industrial sources is not known except for the refinery and the power plants, and the one used in the simulations may be in error. However, it is clear that any particular station may not be represented perfectly at any given time. The ambient concentrations tend to support the evidence from the wind comparisons that there is stronger convergence over the city than the model is producing. The horizontal traverses do not suggest that the model is greatly overpredicting the late morning mixing height. Figure B.42 suggests that the model should have its highest overprediction of the mixing height at about 11:00 a.m., which should lead to a large underestimation of the CO concentrations aloft, but Figure C.12 shows a fairly good agreement with the measurements.

7. Model Applications

There were two major applications of the dispersion modeling: support for the strategy evaluation and studies of the Tula refinery's impact on Mexico City air quality. In the first instance, the simulations were based on the meteorology of the February 22 period. The simulations were carried out with adjustments to the emission inventory. In the case of the Tula refinery, most of the simulations were carried out with the bad day meteorology of the earlier set of simulations. The simulations were conducted to obtain an understanding of the potential consequences of expanded production at the Tula refinery to compensate for lost production at the Mexico City refinery. The bad day meteorology was used as the basis, but changes were made in the wind directions to see what might happen under unfavorable circumstances.

a. Input for Strategy Evaluation

Two sets of simulations were done for the strategic evaluation group. The first set was an attempt to reproduce the CO concentration levels in 1986 using an estimation of the 1986 emission levels and to estimate what the CO levels would have been in Mexico City in 1991 if no control measures had been implemented. The second set of simulations was to obtain the CO levels that would exist if the strategies developed by the Task III group were implemented.

The emissions data for CO in the 1986 simulation were changed by modifying the combustion sources (including vehicular traffic) by the change in fuel sales between 1991 and 1986. Noncombustion sources such as evaporative emissions were assumed to change in proportion to the population change in Mexico City between 1980 and 1990. These emission changes were applied uniformly to the spatially distributed mobile and fixed sources.

The estimate of what the CO emissions would have been in 1991 if no control measures had been implemented was obtained from estimates appearing in the World Bank Study (World Bank 1992). These estimates were for the excess emissions that would occur in 1995 if no controls were implemented. An annual rate of increase in these excess emissions was calculated from the World Bank estimates and then this rate of increase was applied to the base line 1991 data. In addition, emission reduction measures for fixed sources that had been implemented since 1989 were added back into the 1991 data. These sources were

- emissions from the refinery that was closed,
- emissions that would have occurred if petroleum storage tanks had not been covered,
- emission reduction resulting from switching power plants to natural gas,
- emission reductions that were obtained by cleaning foundries, and
- emission reductions resulting from the use of low sulfur fuel oil (gasoleo).

Increased emissions from these sources were added to the base case emissions and spatially distributed as necessary.

The total CO emission reductions (additions) for these two cases are presented in Table C.3. The results of the calculations for CO for these two cases are given in Table C.4. The predicted reduction in CO levels for the 1986 scenario can be compared with the actual CO levels shown in Figure C.28. The 26% reduction in CO levels predicted for 1986 scenario compare favorably with the actual 30% to 61% difference in the reported values of CO in 1986 and 1991.

TABLE C.3 Emission Changes for Estimates of 1986 Emissions and Estimated 1991 Emissions if No Controls Had Been Implemented

	1986 Emission Reduction Estimates			Emission Increase Estimates for 1991 without Controls		
Pollutant	Mobile Sources	Stationary Sources	Total	Mobile Sources	Stationary Sources	Total
NO_X	25%	19%	21%	(7%)	(0.1%)	(5%)
HC	24%	1.5%	13%	(12%)	(1.7%)	(7%)
SO_2	23%	19%	28%	(2%)	(24%)	(21%)
PST	26%	1.5%	1%	(0.1%)	(0%)	(0%)
CO	26%	3.5%	25%	(16%)	(0%)	(15%)

TABLE C.4 Results of Model Calculation for Estimated 1986 Emissions and Estimated 1991 Emissions if No Controls Had Been Implemented

		IMECA Values By Zone	
Sector	Base Case	1986	1991/without control
Central	103	75	126
Northeast	41	31	48
Northwest	55	41	64
Southeast	63	47	73
Southwest	68	50	79

		% Decrease in IMECA Values	
Sector	Base Case	1986	1991/without control
Central	0%	27%	–22%
Northeast	0%	26%	–16%
Northwest	0%	26%	–16%
Southeast	0%	26%	–16%
Southwest	0%	26%	–16%

Estimated CO levels were also calculated based on the implementation of three strategies, each consisting of a number of options for reducing CO emissions. The CO emission reductions were applied uniformly to the mobile and fixed sources except for the minor cases where some spatial variation could be determined. Table C.5 presents a) the spatial results of these calculations and b) the percentage reduction in CO emissions.

b. Tula Studies

The refinery at Tula is approximately 50 km north and 10 km west of the center of Mexico City. The SO_2 emissions that were modeled come

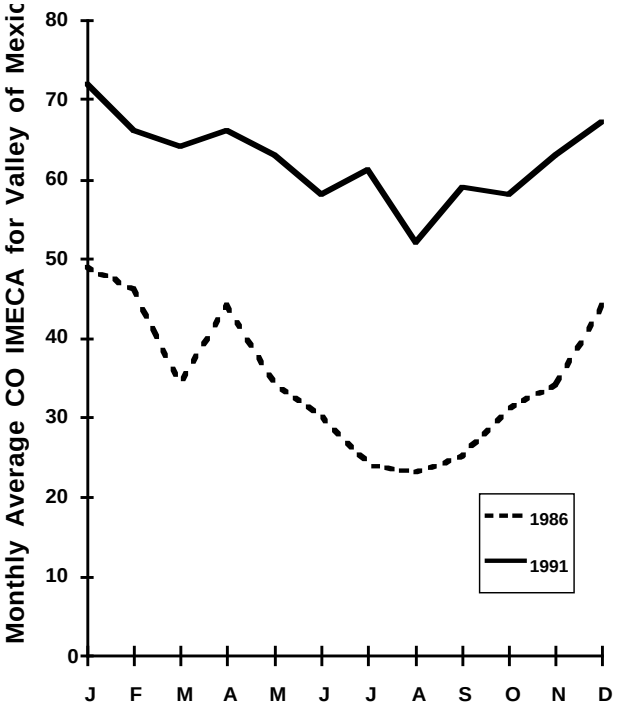

Figure C.28. CO IMECA values for Mexico City for 1986 and 1991. The values plotted are the peak daily values averaged over the month.

from the sulfur in the fuel oil. About one quarter of the total energy flow was assumed to come from fuel oil containing 4.2% sulfur. The remainder of the energy flow was assumed to come from natural gas with negligible sulfur content. The total emissions amount to about 20 tons of SO_2 per day. Four wind-direction scenarios were considered: (1) winds from 350 degrees, (2) winds from 360 degrees, (3) winds from 10 degrees, and (4) winds from 30 degrees, which is the same as the bad day scenario.

For each wind direction, three stack heights were considered: (1) 60 meters, (2) 120 meters, and (3) 200 meters. The effective stack height includes the plume rise, which varies over time during the day. At night or in the early morning the plume rise will add about 120 meters to the stack height, while in the daytime a figure of 300 meters would be more representative. The effective stack height, including both the physical stack height and the plume rise, was used in all the modeling.

Each simulation included a 30-hour release beginning at 8:00 p.m. on the evening before the bad day. Concentrations were calculated for a grid over the city and at each of the SO_2 monitoring sites. The highest one-hour concentrations were calculated for site N (San Augustin) and were associated with interaction between the plume and Pico de Tres Padres. This occurred for scenario 1 with a wind direction of 350°. Figures C.29 and C.30 show two different perspectives of the plume as it travels from Tula and interacts with the mountains. The highest value was about 500 micrograms per cubic meter in a one-hour average. The highest concentration was associated with the 60-meter stack height. Increasing the stack height to 120 meters dropped the maximum concentration to 130 micrograms per cubic meter. A further increase to of stack height to 200 meters dropped the maximum, which was found at site H (La Presa.), to 40 micrograms per cubic meter. The 24-hour average would be about 7 micrograms per cubic meter. In each case some of the plume is being trapped in the cold air draining off the mountains.

The bad-day simulations produced slightly lower concentrations of about 27 micrograms per cubic meter at stations S (Sta. Ursula) and T (Pedregal) in the southwestern part of the city. Figure C.31 shows the plume behavior during this simulation. Under these conditions, the behavior is not very sensitive to the plume height because the mountains are high enough to trap the highest plumes and allow cold air to carry them into the city.

TABLE C.5.A Predicted CO IMECA Values by Zone for the Three Strategies

		Predicted IMECA Values By Zone		
Sector	**Base Case**	**Strategy 1**	**Strategy 2**	**Strategy 3**
Central	103	56	29	29
Northeast	41	24	15	15
Northwest	55	35	19	17
Southeast	63	33	20	20
Southwest	68	39	24	22

TABLE C.5.B Predicted Percentage Decrease in IMECA Values by Zone for the Three Strategies

		% Decrease in IMECA Values By Zone		
Sector	**Base Case**	**Strategy 1**	**Strategy 2**	**Strategy 3**
Central	0%	46%	71%	71%
Northeast	0%	42%	63%	63%
Northwest	0%	36%	66%	68%
Southeast	0%	48%	69%	69%
Southwest	0%	42%	64%	67%

These simulations were particularly interesting because they pointed to the potential significance of out-of-city sources, a problem to which little attention has been paid. Further, the need for a model with capabilities as described herein is clear; simple models would not have been able to address the complexity of this situation.

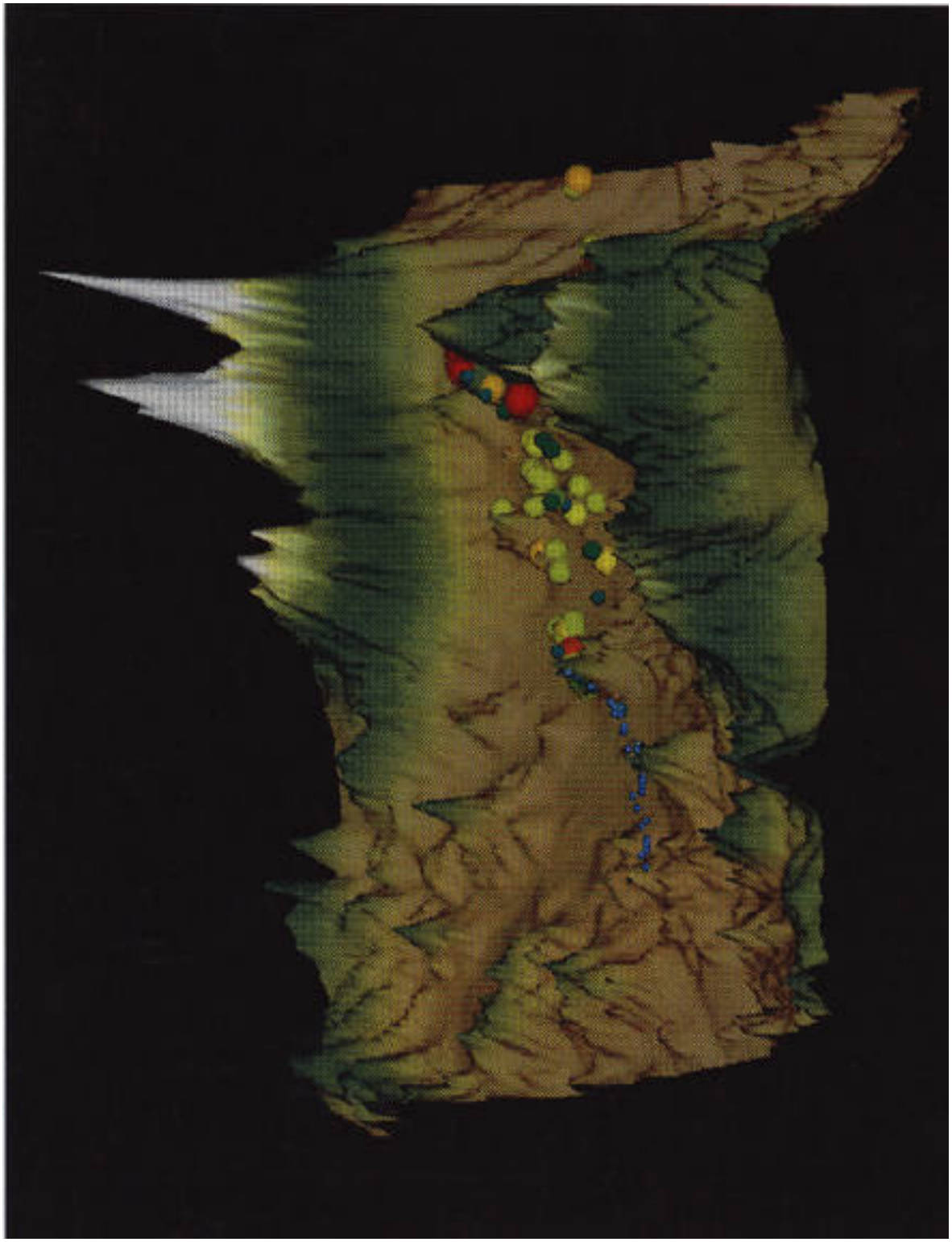

Figure C.29. Pseudoparticles interacting with Pico de Tres Padres after release from a source near Tula with winds from 350 degrees and bad-day meteorology as seen from the north.

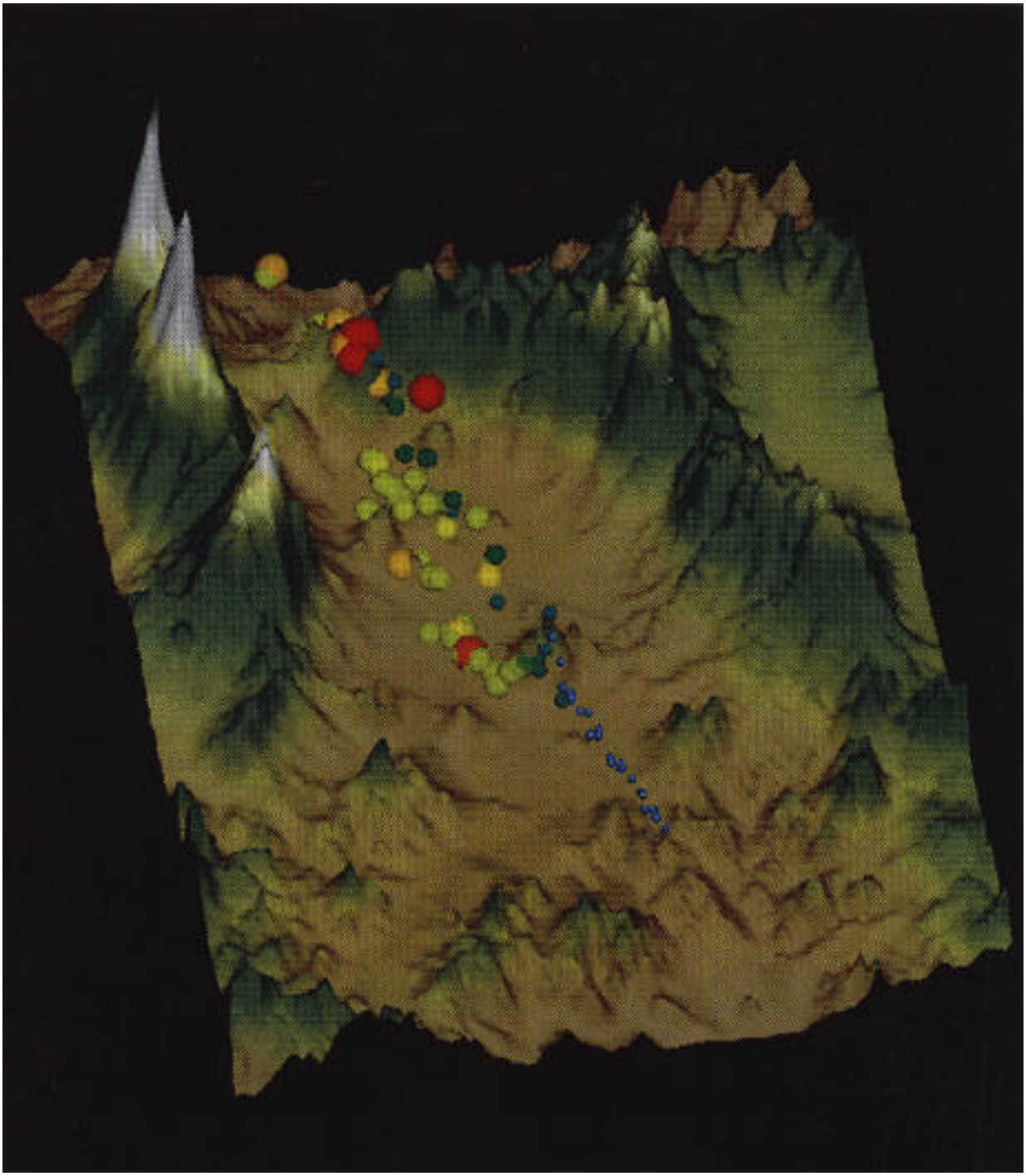

Figure C.30. Pseudoparticles interacting with Pico de Tres Padres after release from a source near Tula with winds from 350 degrees and bad-day meteorology as seen from the west/ northwest.

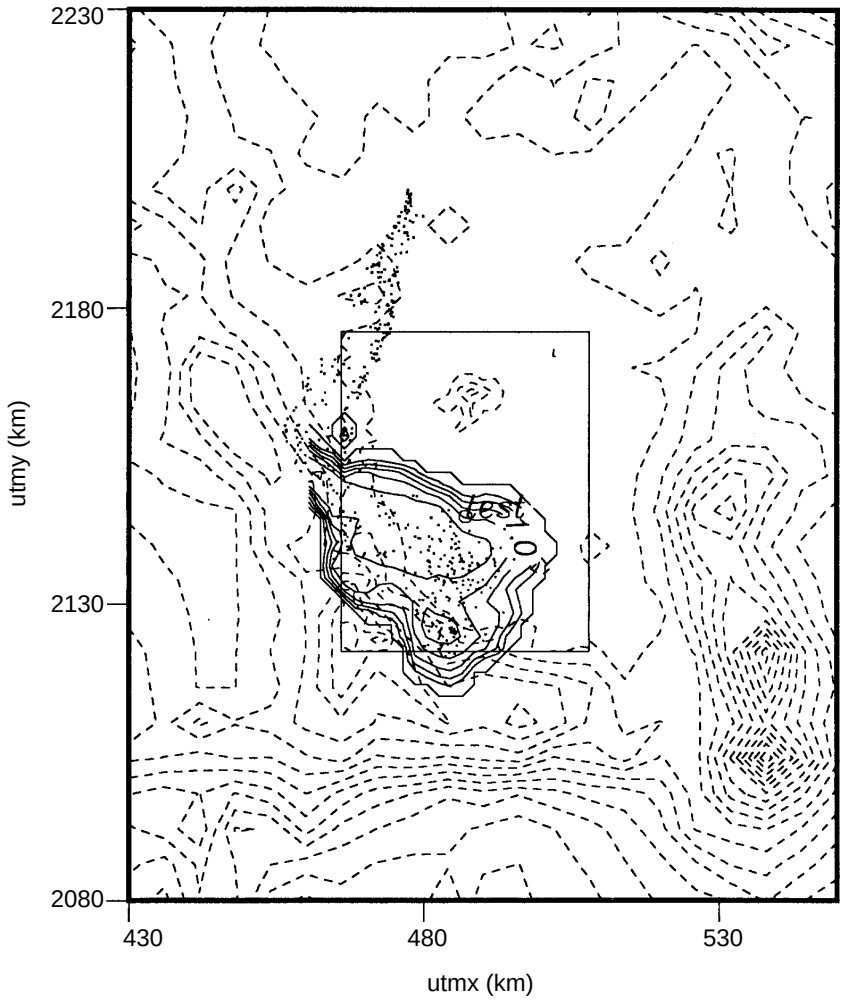

Figure C.31. Pseudoparticle positions illustrating the movement of material from Tula to the Mexico City area with wind directions associated with bad-day meteorology. Solid lines show the fine-grid area and contours of pollutant concentrations.

D. PHOTOCHEMICAL MODELING

1. Objectives

The primary objective of photochemical modeling is to predict the formation of O_3 and the diurnal evolution of O_3 concentration in an urban area or region. This prediction is dependent upon an assumption of some level of emissions of reactive gases and is most frequently applied to prescribing control of those emissions in order to affect a change in peak O_3 concentration. The core of the photochemical model is the mathematical description of a complex series of chemical reactions involving sunlight, HC, oxides of nitrogen and other atmospheric species. This chemistry module may constitute most of the model as in a nondimensional box model, or it may be only one component of a sophisticated three-dimensional model that also incorporates many details of atmospheric dynamics and physics.

As air quality research matures in a given city or region, there are usually more data available on the details of the air pollution problem such as concentrations of other minor reactive species and speciation information on emitted and ambient HC. The objective of photochemical modeling then is to improve the simulation and prognostic capabilities developed earlier by requiring more stringent validation against the behavior of minor species, such as specific HC, or another photochemically generated compounds, such as peroxyacetylnitrate. Typically then, the model is used for more sophisticated analyses of emission control or air quality improvement strategies to provide three-dimensional concentration distributions over the urban area or region. This spatially and temporally defined data can be used in assessment of population exposure and the effects of air quality management initiatives on population exposure.

2. Photochemical Modeling in Air Quality Research and Management

Air pollution, in particular smog formation represented by O_3, is an environmental problem that is both unrelenting and difficult to control. It is especially difficult to assess the actual impact of the programs devoted to the control of air pollution. As a secondary pollutant O_3 is not emitted directly into the atmosphere but is photochemically formed from the interaction of atmospheric species, with HC and NO_X being most important in an urban environment.

Because O_3 is a secondary pollutant, its control and abatement are much more difficult than that of the primary pollutants, including its precursors. The understanding and evaluation of the persistence of secondary photochemical pollution can be performed through the modeling of those processes that drive the diffusion, transport and transformation of the species in the atmosphere. While smog chambers have provided the backbone of our current understanding of air pollution photochemistry, they cannot be used to simulate many complex aspects of ambient smog formation such as the spatial and temporal variations of primary pollutant emissions; mixing heights, transport, and diffusion can not be simulated satisfactorily in smog chambers. Indeed, mathematical simulation is an attempt to circumvent these difficulties by coupling the knowledge of photochemistry gained from laboratory studies with a detailed

representation of the emissions and dispersion that occur in the real world. A photochemical air quality model is the compilation of those models that describe such processes.

Air quality models are formulated to describe the relationship between emissions and air quality under a given set of meteorological conditions and, thus, can enable us to examine the implications of controlling secondary pollutants via the control of their precursors. A wide variety of air quality models have been developed. There are simple models that linearly correlate the concentration of pollutants with their precursor concentrations or that empirically examine the influence of experimentally measured relevant variables in the pollutant concentrations. There are also complex airshed models, which attempt to incorporate into a mathematical formulation realistic descriptions of the meteorology, chemistry, origin, and fate of specific emissions, as well as pollutant sinks within an air basin.

Gaussian plume models describe the concentration of pollutants in a plume downwind from a point source. Occasionally, these models are applied to emissions from line sources (roads) or area sources (commercial districts). A schematic description of the main features of these models is given in Figure D.1.

More complex than the Gaussian plume models, however, are box models. In these models the air mass over a region is treated as a box into which pollutants are emitted and undergo chemical reactions. In Figure D.2 a representation of these models is given. Transport of species into and out of the box, as well as dilution processes from the variation of the mixed layer height throughout the day, are taken into account through the variation of meteorological parameters. Because chemical mechanisms are included in this type of model, it is possible to describe the O_3 temporal behavior, from a set of initial conditions to the corresponding maximum O_3 concentration, in good agreement with monitored values. The formulation of the model does

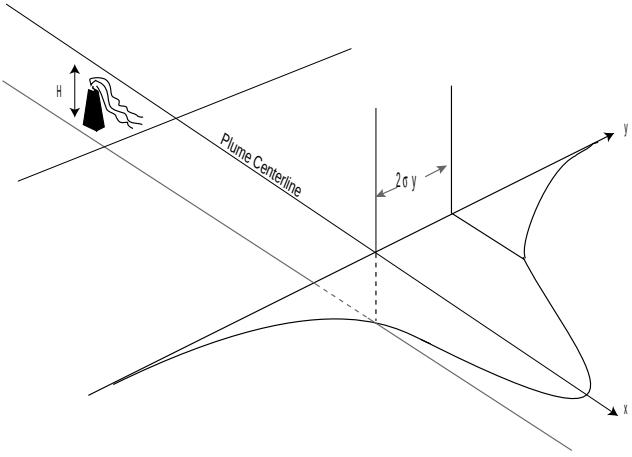

Figure D.1. A schematic description of the main features of a Gaussian plume model. For clarity, only the horizontal dispersion in the y direction, perpendicular to the wind direction, is shown.

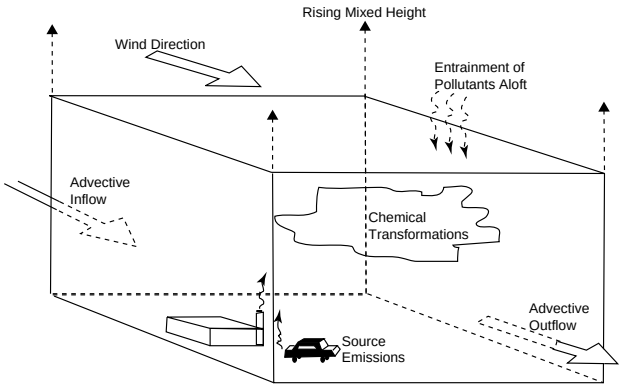

Figure D.2. A schematic representation of the box model, in which species of emissions are transported into and out of the box.

not have spatial resolution; consequently, emissions, photochemistry and pollutant impacts are homogeneous throughout the modeled region.

Given a set of initial conditions, specifically O_3 precursor concentrations, a maximum O_3 concentration may be calculated. However, since the chemical processes are not linear, it is possible to attain the same maximum O_3 concentration from different combinations of initial conditions. The common procedure, then, is to plot O_3 isopleths, or contour lines of maximum O_3 concentration, as a function of initial conditions, usually NO_X and HC concentrations. Isopleth diagrams are widely used in the U.S. to plan specific emission reduction strategies in a given geographical area. In Figure D.3 a set of isopleths for the Mexico City Metropolitan Area (MCMA) is depicted.

The trajectory models are an improvement to the box models. They consider one column of air following a trajectory predicted by the prevailing meteorology. As the air parcel containing certain initial pollutant concentrations moves, it experiences the combined influences of advection, turbulent diffusion, chemical reaction, fresh emissions, and removal processes. These models are most useful for examining the emissions, chemistry, and potential control strategies for one or a limited number of major point sources in a geographical region not highly influenced by distributed sources. This type of model may be implanted in a quasi three-dimensional mode since it is possible to define several layers in a vertical direction, as shown in Figure D.4.

Even more complex models are known as airshed models. The area to be modeled is divided into an Eulerian three-dimensional grid (Figure D.5). The equations that describe the pollutant concentration variations from initial conditions are solved within each cell of the grid, which imposes a large computational effort. The concentration of species may vary by the incorporation of new emissions, transport of chemical species in and out of each cell, dilution, and chemical reactions, all as a function of time. One advantage of this type of model is geographical resolution for control strategies and impacts. A major disadvantage is the relatively great expense required to develop the necessary model input to run these models. A more extensive description of the box, trajectory, and Eulerian models can be found in Section D.3.

The input data to air quality models include the meteorological description over the entire region of interest (i.e., wind field, mixing-height variation, temperature profiles and atmospheric stability) and temporally and spatially distributed emission inventory data (most of the models require that the data be classified according to the chemical classes considered by the mechanisms). In addition, a set of initial and boundary conditions corresponding to the particular simulation should be specified. Unfortunately, uncertainties, approximations, and assumptions in the chemical mechanism, description of physical processes, meteorology, and particularly emission databases are common to every application of airshed modeling.

The development of air quality models has been directed mainly to the understanding of O_3 formation as the most serious secondary pollutant. Thus, O_3 formation is well-described by moderate- to high-complexity models, but this is usually not the case for other secondary pollutants, to whose description, major research efforts should be made. Consequently, good agreement for all major pollutants under all conditions is rarely obtained.

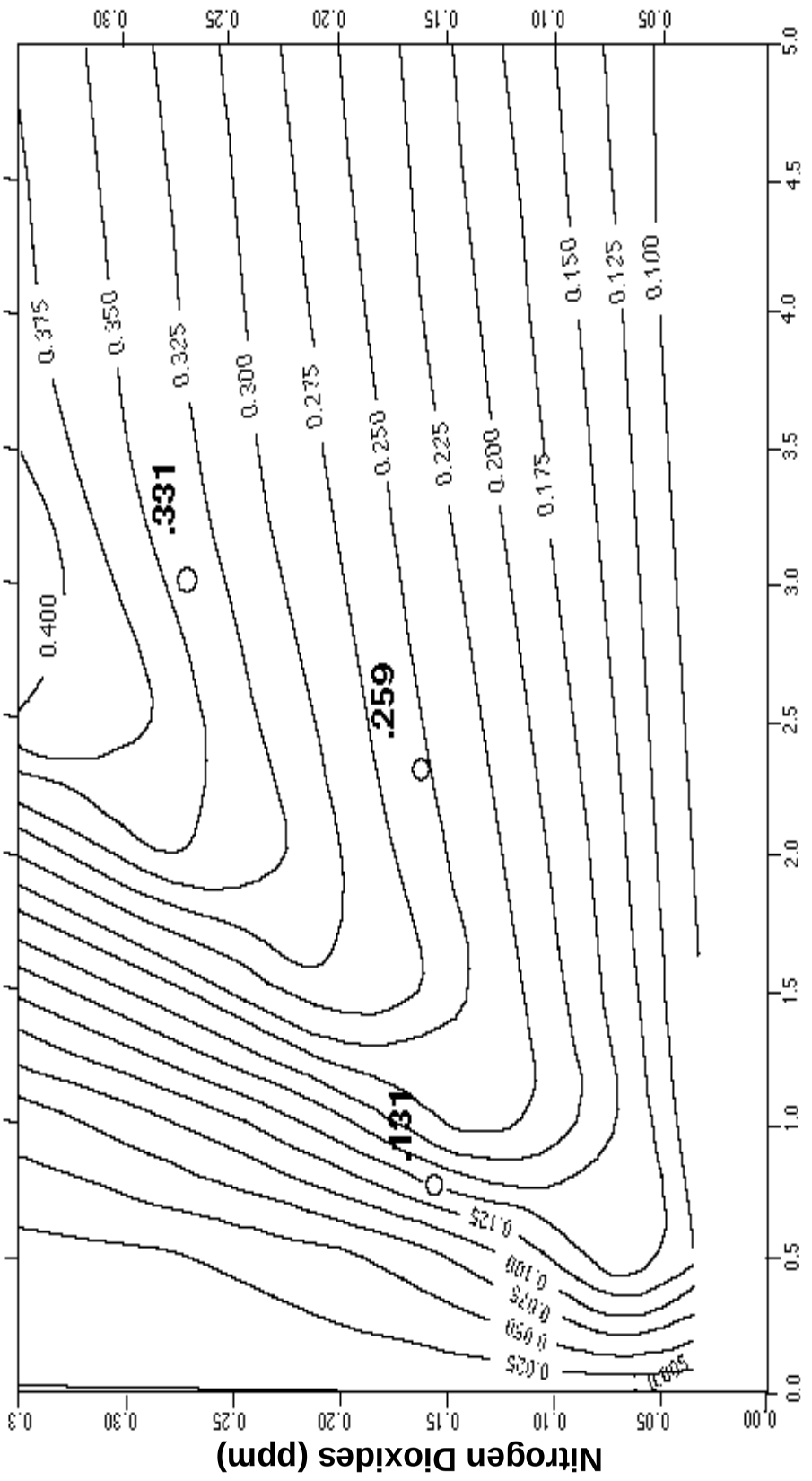

Figure D.3. A set of isopleths representing O_3 concentration for the MCMA.

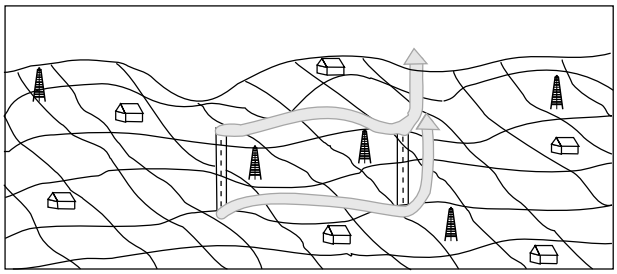

Figure D.4. A schematic diagram of the Lagrangian-type trajectory model.

The current generation of airshed models can predict with reasonable accuracy the maximum O_3 concentration downwind of an urban area as a result of meteorological conditions and source emissions. It is also possible to predict the impact produced by changes in the emissions in different areas within the modeling region. These models also determine the extent to which the emissions should be decreased to attain a noticeable change in O_3 concentration.

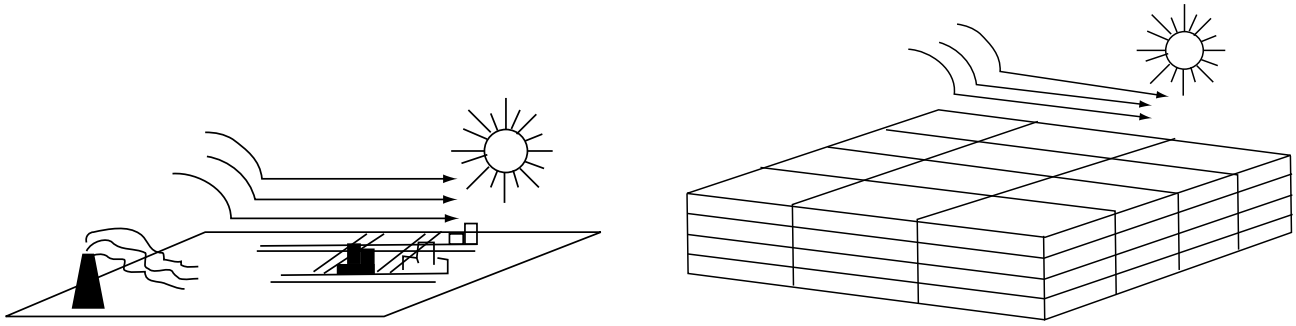

(A) Geographical Area Designated for Modeling

(B) Specification of the Grid Area

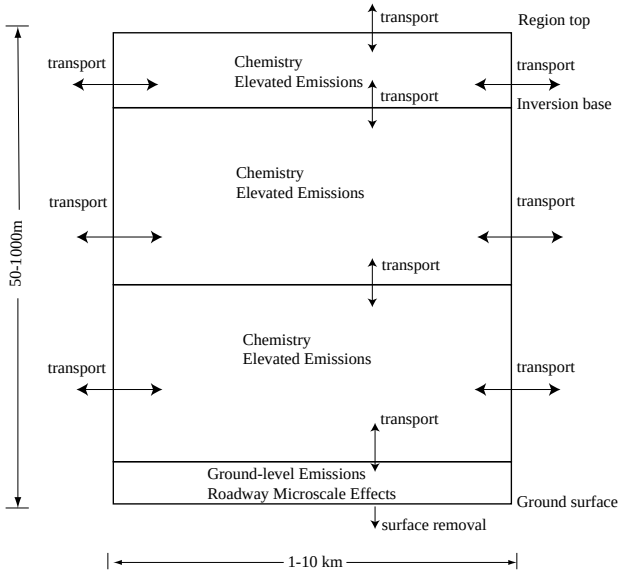

(C) Atmospheric processes treated in a column of grid cells

Figure D.5. A schematic diagram of the grid used in a Eulerian airshed model. The diagram also represents the treatment of atmospheric processes.

3. Description of Models

a. O_3 Isopleth Plotting with Optional Mechanisms, Version 4 (OZIPM-4)

The OZIPM-4 model is a U.S. EPA-supported model that uses the Empirical Kinetic Modeling Approach (EKMA) (EPA 1989). This version of the model includes a photochemical mechanism called the Carbon Bond Mechanism-IV (Gery et al. 1989) as the default mechanism, but it includes the provision for modification of the mechanism or for use of an alternate mechanism. This model has been widely applied in the U.S. for the purpose of calculating city-specific relationships between photochemical oxidants, expressed as O_3, and the photochemical oxidants' precursors, nonmethane organic compounds (NMOC) and NO_X. This relationship is usually plotted in terms of an O_3 isopleth chart, which forms the basis for emissions reductions policies designed to meet the National Ambient Air Quality Standard for O_3.

The OZIPM-4 is a chemistry-intensive, trajectory-type model designed to simulate O_3 formation in urban atmospheres. It mathematically simulates the physical and chemical processes taking place in the atmosphere within the limitations of the concept of the model. It is assumed that a column of air containing O_3 precursors is transported along a trajectory. The height of the column is the height of the mixed layer, and the fresh emissions that enter the column as it moves are instantaneously and uniformly mixed throughout the height of the column. Horizontal concentration gradients are assumed to be small so that exchange of air between the column and its surroundings is insignificant.

OZIPM-4 was applied to Mexico City in a simulation of February 22, 1991, both in modeling the episode of that day and in calculating a set of isopleths based on conditions of that day. Isopleths are generated by a series of calculations with different initial NMOC and NO_X concentrations, but over the same trajectory with the same emissions, the same diurnal change in mixing height, and the same solar (or actinic) flux. Thus, the isopleths are city-specific.

b. CIT* Photochemical Airshed Model

The CIT airshed model (McRae et al. 1982 and 1983, Russel et al. 1988) is an Eulerian photochemical air quality model that calculates the transport and chemical reactions of pollutants in the atmosphere (Figure D.5). This model solves numerically the atmospheric diffusion equation for a set of reacting chemical species:

$$\frac{\partial C_i}{\partial t} + \nabla \cdot (\mathbf{u}\, C_i) = \nabla \cdot (K \nabla C_i) + R_i + Q_i$$

where C_i is the concentration of species i, **u** is the 3-D wind velocity vector, K is the eddy diffusivity tensor (here assumed to be diagonal), R_i is the rate of generation of species i by chemical reactions, and Q_i is a source term for elevated point sources of species i. If the above equation is written repeatedly for each of the chemical species tracked by the model, a system of coupled nonlinear equations is obtained.

*CIT is derived from the California Institute of Technology and the Carnegie Institute of Technology at Carnegie Mellon University, the two institutions responsible for developing the model.

To solve the equation system, a set of initial and lateral boundary conditions should be established. The values of the different variables are set using measured pollutant concentration data. The ground-level boundary condition sets upward pollutant fluxes equal to direct emissions minus dry deposition. A vertical concentration gradient for each species is set so that it decreases to a zero value at the top boundary, ensuring that there is no vertical transport of pollutants through the top of the modeling region.

Typical photochemical reaction mechanisms that are used within regional air quality models simplify the treatment of the volatile organic compounds by aggregating the emissions of hundreds of individual species into a much smaller number of lumped species classes. The version of the CIT model used in the simulation of O_3 formation in the MCMA contains a condensed version of the Lurmann, Carter, and Coyner (LCC) mechanism. (Lurmann, Carter, and Coyner 1987)

The extended LCC mechanism includes 106 chemical reactions involving 35 different inorganic and organic species. In the mechanism the organic species are lumped by molecular classes. Compounds that have similar structure and reactivity are grouped together. The chemistry of all molecules within a single lumped class is then represented using one or more surrogate species (e.g., toluene is used to represent the chemistry of all monoalkylbenzenes). A list of the lumped organic species groups and the corresponding surrogate species is shown in Table D.1.

The chemical mechanism includes separate reactions with the hydroxyl radical for each of the lumped organic species. In addition, the mechanism includes the reactions of ethene and lumped C_3+ alkenes with O_3, the nitrate radical, and atomic oxygen. In the chemical mechanism, the photolysis reactions involving the aldehydes and ketones are also considered.

TABLE D.1 Lumped Organic Classes in the LCC Mechanism

alkanes
alkenes
ethene
toluene
di- and tri-alkyl aromatics
formaldehyde
higher aldehydes
carbon monoxide

The removal of pollutants at the ground surface by dry deposition is included in the model. Dry deposition velocities are computed using local meteorology, surface roughness, and land use data in each square cell of the simulation grid. (Russel et al. 1992) Resistance to dry deposition from turbulent transport in the atmospheric boundary layer, r_a, and the molecular diffusion through the laminar sublayer near the ground, r_b, are calculated by fluid mechanical considerations. Then a surface resistance term, r_s^i, specific to the pollutant and land-use type is included to account for pollutant-surface interactions.

The final formulation is

$$v_g^i = \frac{1}{r_a + r_b + r_s^i}$$

where v_g^i is the actual deposition velocity for species i used in the model. Surface resistance values are derived from the recommendations of Sheih, et al. (1986) and engineering judgment. Thirteen different land-use categories are specified, derived from satellite data. (Williams et al. 1992) Dry deposition velocities for the HC,

though rarely measured, are generally thought to be low because most of the HCs are neither highly reactive nor highly soluble in water, and therefore surface resistance terms for these species are large. (Wesley 1989)

4. Model Implementation

a. Photolysis Rates

Sunlight drives atmospheric chemistry as certain molecules are photodissociated into atomic and molecular free radicals, which are highly reactive. This is the case with nitrogen dioxide, which in the troposphere participates in O_3 formation, as described by the following:

$$NO_2 + h\nu \rightarrow NO + O \quad O + O_2 \rightarrow O_3 \ .$$

The geographical conditions of the MCMA, which is located in an elevated basin 2240 m above sea level at latitude 19.5° N, favor the formation of photo oxidants. The latitude of a region affects the solar altitude and the zenith angle, which are also influenced by the time of the day and the season of the year. As a consequence, the solar zenith angle and solar altitude for Mexico City are higher than those for Los Angeles, or London. In Figure D.6 the diurnal variation in solar zenith angle is given for summer and winter for 20°, 35° and 50° N latitude. These latitudes may be identified with the above-mentioned cities. A higher solar zenith angle implies higher actinic irradiance.

The calculation of the photodissociation rate coefficients of the main atmospheric species is necessary in order to appropriately model their dissociation by the influence of solar irradiation over Mexico City. This is done by calculating the integral over all wavelengths of the product of actinic flux, cross section, and quantum yield for each photoactive molecule. Of these parameters, the actinic flux is the most difficult to estimate because it requires a solution for the radiative transfer equation which contains variables as multiple scattering, absorption, surface and cloud albedos.

The photodissociation rate coefficients of NO_2, O_3 and HCHO (formaldehyde) under MCMA conditions were calculated solving the radiative transfer equation by the δ-Eddington method. (Joseph and Wiscombe 1976) A computational code was developed to estimate the actinic flux in the spectral region (280-410 nm). Data on absorption cross sections and quantum yields may be easily introduced for the species of interest. In this model the atmosphere is considered as a combination of air, nitrogen dioxide, O_3, and dry aerosols. The tropospheric aerosol above MCMA was obtained as an average of

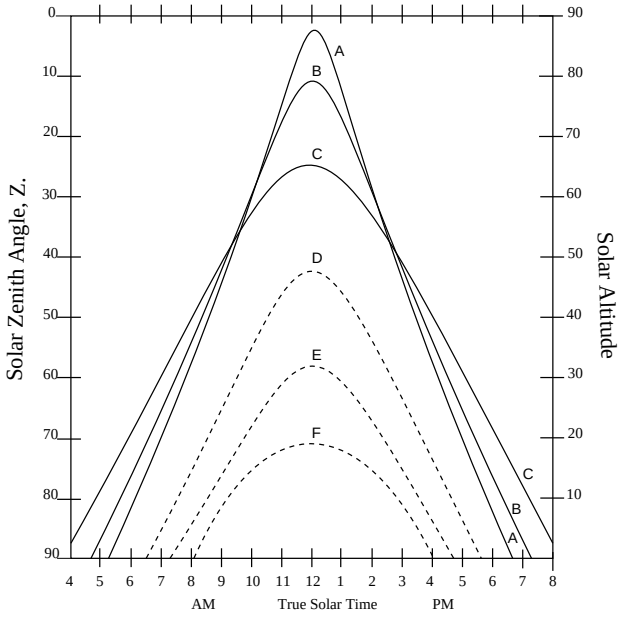

Figure D.6. Effect of latitude on solar zenith angle. A & D, 20° N latitude, summer and winter solstices; B & E 35° N latitude, summer and winter solstices.

aerosol size distributions in 360 measurements during a three-year period from 1987 to 1989.

The photolysis rates for NO_2 and O_3 obtained with the code described above (Ruiz-Suarez, J.G., et al 1993a) compare reasonably well (within less than 10%) with measurements made previously at 3 km altitude in the vicinity of Boulder, CO (Parrish et al. 1993) and in Ann Arbor, MI (Dickerson et al. 1982).

During February 1991, an extensive measurement campaign was performed in the MCMA under the Mexico City Air Quality Research Initiative (MARI). In the period from February 16 to March 1, 1991, particulate matter was collected at three different sites where other simultaneous experiments were taking place. Particulate matter in the atmosphere attenuates direct solar radiation by scattering, reflection, refraction, and diffraction, and the term "particle diffusion" refers to the combination of these effects. If the amount, nature, and size distribution of the particulate matter were known in detail, the resulting attenuation coefficient and its variation with wavelength could be calculated by the Mie theory. Particle size distribution covered a diameter range of 0.006 – 1.0 μm. With the averaged data, the Mie theory was used to calculate extinction coefficients and single scattering albedos. (Eidels-Dubovoi 1993) The calculations were done for four wavelengths 0.50 μm, 0.55 μm, 0.88 μm, and 1.06 μm, assuming a typical tropospheric aerosol refractive index of $1.65 - 0.005i$.

The associated visibility was derived using the Koschmieder formula, which simply relates visual range with the extinction coefficient. The visual range was found to be at a minimum on February 23 (5.4 km) and at a maximum on February 27 (47 km). Empirical single scattering albedos, ϖ_e, were obtained using average values of optical depths measured at two wavelengths: 0.50 μm and 0.88 μm. It was found that in this period ϖ is practically constant: 0.97 (0.50 μm) and 0.98 (0.88 μm), whereas ϖ_e varies: 0.86 – 0.92 (0.50 μm) and 0.68 – 0.76 (0.88 μm). Differences between ϖ and ϖ_e were overcome by changing the absorptive part of the refractive index used in Mie calculations.

Based on data for the period from February 16 to March 1, 1991, we can conclude that rather than absorption, scattering by atmospheric aerosols governs the attenuation of solar radiation, especially in the visible part of the spectrum.

b. Hydrocarbons and Atmospheric Reactivity

The formation of O_3 in the troposphere is the result of a complex series of reactions between volatile organic compounds (VOC) or HC in the presence of (NO_X) and sunlight, as described briefly by the following set of reactions:

$$NO_2 + h\nu \rightarrow NO + O$$
$$O + O_2 \rightarrow O_3$$
$$O_3 + NO \rightarrow NO_2$$
$$\{O_3, H_2O, h\nu\} \rightarrow H_2O_2$$
$$H_2O_2 + h\nu \rightarrow 2\ OH$$
$$RH + OH \rightarrow R + H_2O$$
$$R + O_2 \rightarrow RO_2$$
$$RO_2 + NO \rightarrow RO + NO_2$$
$$RO + O_2 \rightarrow \text{(a) } RCHO + \text{(b) } R_2 + \text{(c) } R' + \text{(d) } HO_2$$
$$RCHO + OH \rightarrow RCO$$
$$RCHO + h\nu \rightarrow R + HO_2$$
$$RCO + O_2 \rightarrow RCO_3$$
$$RCO_3 + NO \rightarrow R + CO_2 + NO_2$$
$$HO_2 + NO \rightarrow NO_2 + OH$$

(RH is a hydrocarbon in this reaction scheme.)

The oxidation of HC usually starts with the hydroxyl radical (OH above). Because these reactions are not occurring in isolation in the atmosphere, but in the presence of an enormous variety (~200 different VOCs) of other compounds that are reacting at the same time, many different intermediate and final products are formed. Among the intermediate products of reaction are aldehydes (RCHO above), secondary reactive organics (R and R_2 above), and hydroxyl and hydroperoxy radicals (HO_2 and OH above). Peroxy radicals are a direct contributor to the formation of NO_2, the direct O_3 precursor. The overall process is a complicated combination of reaction rates and product speciation.

The major sources of VOCs in the atmosphere include exhaust and evaporative emissions from motor vehicles, evaporative emissions from solvent use, and emissions from chemical and petroleum industries. Recently, the importance of biogenic emissions (emissions from vegetation) has been pointed out as a major source of VOCs. (Office of Air Quality Planning and Standards 1993) NO_X comes mainly from combustion processes from a variety of sources including industrial and residential boilers, motor vehicles, forest fires, power plants, etc. Carbon monoxide, which also influences O_3 production, comes almost solely from mobile sources.

It can be deduced from the above set of reactions that the specific structure of individual VOCs influences either the rate of O_3 formation or the maximum concentration attained. In the last decades the relationship between VOC and O_3 formation has been evaluated in an attempt to define reactivity scales, which relate the potential for O_3 formation to specific HC.

Several factors have been suggested for consideration as the base of reactivity scales. Some of the possible factors are the maximum amount of O_3 generated in irradiated mixtures of single HC, NO_X, and air for several hours; the rate of NO photo oxidation; the rate of O_3 formation from specific HC; the rate of VOC consumption, and the rate constants for the reaction of the VOCs with the hydroxyl radical. Although there are differences among the resulting reactivity scales, it is accepted that the reactivities of VOCs are in increasing order: alkanes and monoalkyl-benzenes, < 1-alkenes and dialkyl-benzenes, < trialkyl-benzenes and internal alkenes. Thus, the determination of the specific nature of individual HCs (speciation) in the atmospheric mixture emerges as an important parameter to use when assessing the reactivity of the atmosphere in a given region.

It is also clear that the speciation of VOCs is not the only factor that influences O_3 formation. Maximum concentration and time evolution of the daily O_3 peak also depend on the initial concentrations ratio of VOCs and NO_X. At high VOC / NO_X ratios (greater than 8 – 10), O_3 concentrations are relatively insensitive to VOC concentrations, and NO_X control is more effective in lowering O_3 peaks. In some polluted areas where the VOC / NO_X ratio is less than about 8, decreasing VOC concentration in the atmosphere reduces O_3 levels. With low VOC / NO_X ratios it might also happen that NO_X control actually increases O_3. In this case, the individual nature of the VOCs has a more definitive influence on O_3 formation.

Usually, as the air mass travels from a central-city location downwind to the suburban and rural fringes, a gradual change from relatively low- to high-VOC / NO_X ratios occurs. Thus, when NO_X reductions are applied in large urban areas, greater O_3 reductions are likely to be

seen several kilometers downwind of the central urban core. This occurs because NO_X availability becomes the limiting factor in further O_3 production when the VOC / NO_X ratio is high.

This generalized spatial response pattern has important implications for population exposure to pollutants. In the particular case of O_3, which may be transported long distances, the models often suggest that programs should be oriented towards NO_X control. However, certain modeling studies have suggested that NO_X control resulted in less reduction in total O_3 exposure relative to VOC control in the New York City and Los Angeles airsheds. (Rao 1987) The conclusions of such studies suggest that NO_X controls should be implemented in order to reduce O_3 downwind; however, to lower O_3 levels inside metropolitan urban areas, VOC controls should be applied.

Before 1991 very few determinations of ambient VOCs in the MCMA had been performed. (Ruiz et al 1993) In 1992 and 1993, under MARI activities, two VOC sampling campaigns took place. Three sampling sites were used for both sampling campaigns: Xalostoc (NE), Merced (downtown) and Pedregal (SW). The sites were located along the common wind trajectory in the MCMA (northeast to southwest). Primary land use for each site is substantially different; the areas are characterized mainly by their industrial, commercial, and residential activities. Samples from nominally clean areas in the boundary of the MCMA were also obtained.

Experimental determination of the atmospheric VOCs in the MCMA was performed by collecting air samples in stainless steel canisters. The samples were then analyzed in the laboratory by gas chromatography (GC). U.S. EPA "TO-14" methodology was followed for all sampling. This methodology consists of collecting ambient VOCs for a three-hour period (6:00 a.m. to 9:00 a.m.). These samples are considered to be representative of the O_3 precursors.

The two campaigns (1992 and 1993) were carried out in the same month (March). The samples collected in canisters were analyzed by GC with flame ionization detection in a collaboration with the Atmospheric Research and Exposure Assessment Laboratory of the U.S. EPA. The concentrations of total VOC, speciated VOC, methane and CO were determined for each sample. The results for VOCs during the 1992 campaign (Seila et al. 1993) showed a very high mean total HC concentration of about 3.5 ppmC (parts per million for carbon).

The information gathered experimentally was processed in order to define the HC partition to be used within the CIT simulations. The VOC data also served to improve the spatial distribution of the VOC emission inventory and to substantiate a significant increase of the total VOC inventory beyond that obtained in the independently derived emission inventory.

c. Air Quality and Meteorological Inputs

High-quality inputs for airshed simulations are critical for deriving credible model conclusions. In the most general sense, the input consists of data from three groups: meteorological conditions; boundary, initial, and air quality parameters; and the emissions inventory. The main concern about input data is always related to uncertainties contained in the emissions inventory.

The major meteorological inputs are three-dimensional, time-dependent winds; mixing heights; surface humidity and temperatures; and solar radiation. Initial conditions, i.e. initial concentrations of a number of important species, are needed throughout the modeling domain. Boundary conditions must be specified at ground level at the top and on the sides of the modeling domain. The surface removal of species is determined by the dry deposition velocity, surface roughness definition, and land-use categories.

The emissions inventory should be supplied as hourly emissions geographically distributed and should include both surface and elevated sources. The emissions inventory should be speciated in accord with the chemical species considered by the LCC mechanism (shown in Table D.1).

1. Modeling Domain.

The Mexico City Metropolitan Area (MCMA) contains two federal entities: the Distrito Federal (DF), which is the home of the federal government, and the suburbs that belong to the State of Mexico (EdoMex). The urban area, shadowed in Figure D.7 has an extension of about 2396 sq. km. It covers sections in both the DF and the EdoMex.

One of the major difficulties in simulating air pollution is the specification of boundary conditions. Typically, a large domain is chosen so that boundary concentrations, which may be quite uncertain, do not significantly affect results. Further complications emerge from the fact that the topography of the MCMA basin is very complex, and its irregularities may influence meteorology. Consequently, a large external area was considered for the wind-field simulation. This area was 120 km (east-west) by 150 km (north-south). The total area, 18,000 sq. km, contains all the surrounding mountains. The CIT model was applied in a smaller region of 70 km (east-west) by 80 km (north-south) within the meterological domain. Both regions are depicted in Figure B.1.

The CIT model uses a terrain-following coordinate system with a fixed height above the surface. In the numerical solution of the CIT model a computational grid of squares is required. Commonly, the modeling area is subdivided into 5 km $\times$ 5 km cells (for the MCMA 14×16 cells in the horizontal plane). In the z direction, 7 vertical layers are considered for a total of 1568 cells. The origin of the grid is located in the southwest corner at 460 east-west and 2110 north-south UTM coordinates.

The maximum computational height was taken as the highest mixing height plus approximately 200 meters. The first set of simulations were for February 21st and 22nd, 1991. In this instance, the maximum mixing height was 2500 meters, and the vertical depth of the cells was 2400 meters. The modeled mixing height for February 22 is shown in Figure B.41.

2. Base Case Selection.

In February 1991, an intensive and extensive experimental campaign headed by the Instituto Mexicano del Petróleo and the Los Alamos National Laboratory took place in the MCMA. This experimental campaign, in which about 15 institutions and more than 100 people participated, lasted for more than three weeks. The campaign consisted of 14 different experiments grouped by surface, airborne, and remote

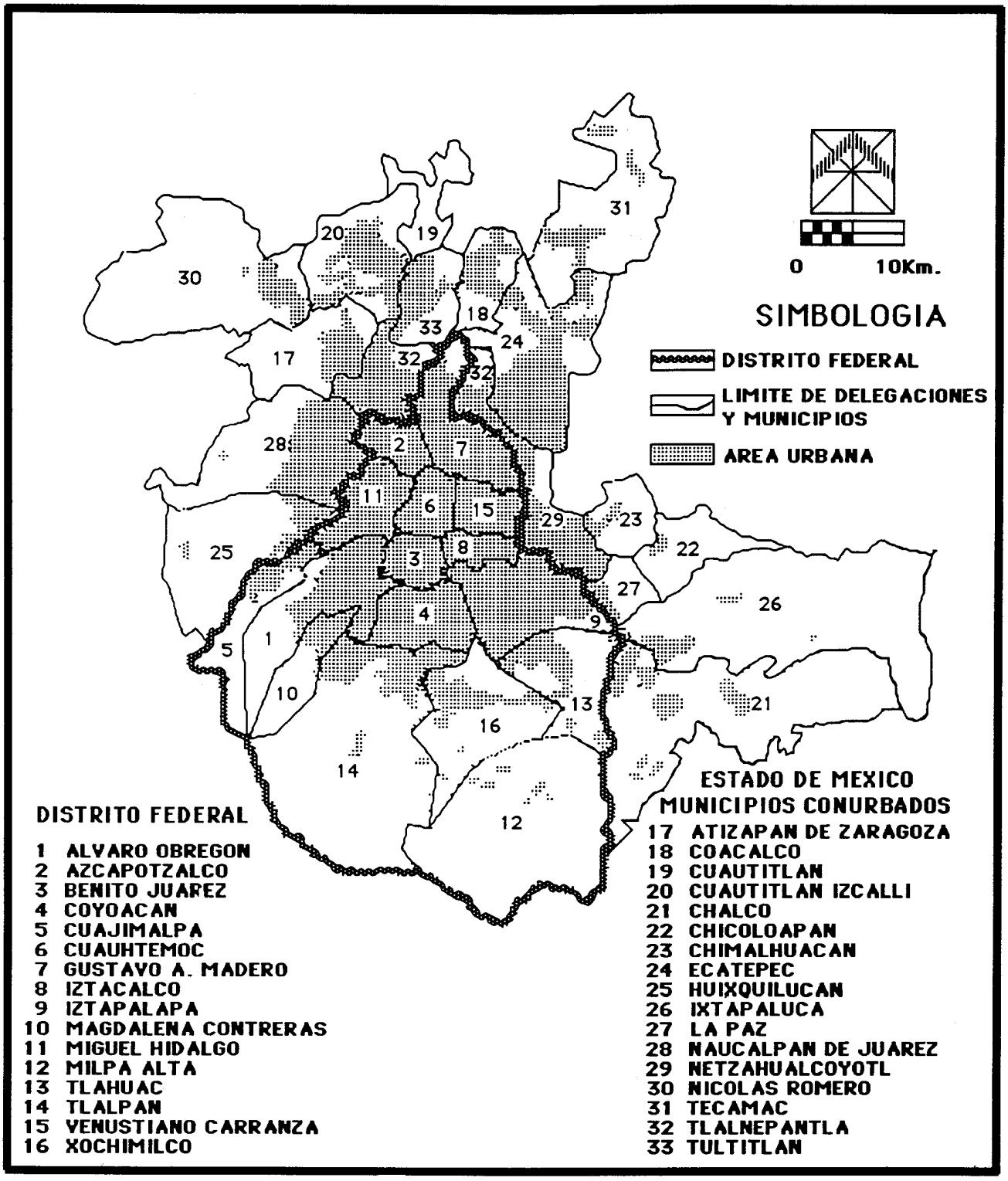

Figure D.7. The MCMA showing the urban area (shaded), the delegaciones of the DF, and the municipalities of the EM.

sensing measurements. The remote sensing measurements included the use of three different lidars. At the surface level, another novel remote sensing technique applied was FEAT (Fuel Efficiency Automotive Test). Through the use of FEAT it was possible to record CO, CO_2, and HC in the vehicular exhaust emissions. At the same time a TV camera recorded a freeze-frame of the license plate, so a correlation between emissions and model and manufacture of the car could be found. During two weeks the records from 32,000 cars were obtained.

In another experiment, the NCAR instrumented research aircraft flew over the MCMA in 14 flights totaling about 40 hours. Vertical profiles of meteorological parameters and pollutant concentrations were also obtained during airplane ascent and descent. The airplane flew an E-shaped route over the MCMA, gathering data at two or more altitudes on each flight. Vertical meteorological soundings were carried out using a tethersonde, and rawinsondes were launched seven times a day. The tethersonde was equipped with an O_3 probe in order to obtain vertical profiles of O_3 concentration. One of the most relevant surface measurements consisted of the recording of solar radiation by solar ultraviolet radiometers and total suspended particle collection to determine the aerosol size distribution. These experiments were performed at the same sites where the vertical soundings were done.

A screening of the experimental data, including the air quality parameters, showed that a typical O_3 episode occurred on February 22, 1991, with an O_3 maximum concentration of 0.331 ppm in the SW station. In Figure D.8 the daily values of the maximum O_3 concentration during February are plotted for several monitoring stations. A full suite of experimental measurements were carried out on February 22nd. In fact, more data were recorded on that day than any other day in the campaign. Thus, it was selected as the base case to be simulated by the models. A second choice was the period from February 26 to 28, also plotted in Figure D.8, in which the maximum O_3 concentration showed an increasing trend. This episode is useful to study the multi-day episodes and the overnight buildup of reactive species. It should be pointed out that during this episode the highest O_3 concentrations were registered at monitoring stations in the western part of the MCMA.

3. Data Development.

The meteorological wind fields for February 21-22, 1991, were derived from the prognostic model HOTMAC. The vertical extent of the modeling region was 2400 m, subdivided in seven different layers 24 mm, 96 mm, 456 mm, 456 mm, 456 mm, 456 mm, and 456 m thick. The temperature, humidity, and solar radiation fields were prepared by spatial interpolation of the available observations.

The boundary condition values shown in Table D.2 are taken from the aircraft data collection, except for NMHC, which is the average concentration at sites in the MCMA boundary. (Ruiz et al. 1993)

For VOC speciation, GC analyses of ambient air samples were used since there is no official speciated VOC emission inventory available. The relative weight of the different lumped molecules is given in Table D.3. Aldehydes concentration and speciation were determined from adsorption cartridge measurements of carbonyl compounds. (Guillermo et al. 1993)

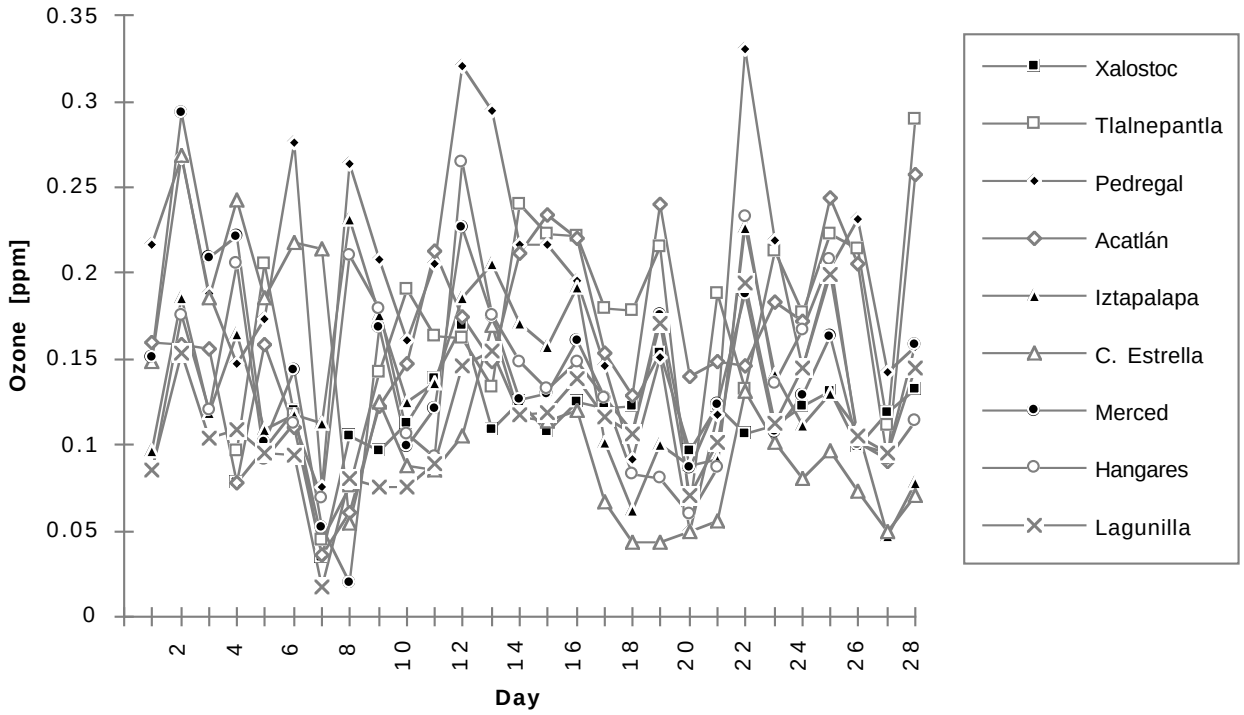

Figure D.8. The values of the maximum daily O_3 concentration during February for several monitoring stations.

TABLE D.2 Upwind Boundary Condition Values (ppm)

Species	CO	NO_2	NO	SO_2	HCHO	RCHO	NMHC*	O_3
boundary conditions	0.200	0.001	0.001	0.001	0.002	0.005	0.100	0.060

* nonmethane HC, ppm for carbon

TABLE D.3 Speciated VOCs for the LCC Mechanism

Species	Average Relative Weight
alkanes	0.5662
alkenes	0.0984
ethene	0.0595
toluene	0.0787
aromatics	0.1188
formaldehyde	0.0143
higher aldehydes	0.0357

With the emissions inventory for the MCMA provided by the official authorities in Mexico (Section D.4.d) a gridded emissions inventory for the whole modeling area was developed. The official emissions values reported in Table D.5 were distributed into the grid cells considering the specific land use and activities within the cells. The reported values correspond to emissions within the urban area. For the remaining cells outside the urban area but inside the modeling region, it was necessary to estimate emissions. The total emissions estimated for the CIT

domain are given in Table D.4. Mobile source emissions were obtained from emission factors derived from MOBILE-MCMA, which is a version of the EPA automotive emissions model MOBILE4, adapted to the conditions of the MCMA. For this model, an average speed of 26 km/h was used. The emissions from tall stacks of the Pemex 18 de Marzo Refinery (still in operation in February 1991) and the two MCMA thermoelectric power plants (Jorge Luque and Valle de México) were explicitly included. Emissions from the other stationary sources were included as surface emissions within the appropriate cells.

As mentioned, February 26-28 was a period within the intensive monitoring campaign that qualified as a multiday episode. Model setup for this episode utilized appropriate experimental data from the intensive campaign; however, much of the input, such as the emissions inventory, is the same as for the base case. Diffusivity coefficients calculated by HOTMAC were used in place of the default CIT formulation. This substitution leads to significantly better simulation results.

TABLE D.4 Categories in the CIT Model Emissions Inventory (metric tons/year) for the Valley of Mexico

Sources	CO	VOC	NO_X	PST	SO_2
Stationary					
Minor Combustion	770.0	158.4	25 973.2	2 890.8	79 081.2
Residential Combustion	878.4	331.2	5 472.0	806.4	3 542.4
Waste Burning	8 622.3	4 434.2	616.1	1 642.2	102.8
Unplanned Fires	117 751.2	20 193.6	3 343.2	14 296.8	0
Solvent Use	0	80 358.4	0	0	0
Industrial Processes	64 202.3	4 506.9	21 981.8	45 426.3	90 989.9
Miscellaneous Processes	0	73 344.0	0	290 880.0	0
New Biogenic Emissions	0	124 789.5	0	0	0
Total Stationary	192 224.2	308 116.2	57 386.3	355 942.5	173 716.3
Mobile					
Private Cars	1 436 715.0	151 959.8	46 115.0	4 709.3	3 640.8
Taxis	325 683.8	34 462.9	10 456.4	1 067.5	825.4
DF Collective Vehicles	287 404.6	28 670.2	7 254.7	794.1	439.7
EdoMex Collective Vehicles	78 719.1	7 863.6	1 982.8	217.3	123.7
DF Light Duty Gas Veh.	8 348.8	1 586.2	110.1	77.9	
EdoMex Light Duty Gas Vehicles	8 951.5	1 197.3	220.5	15.0	228.2
DF Busses	6 791.1	2 621.1	8 855.1	256.2	5 352.2
EdoMex Busses	14 238.2	5 695.4	20 061.1	642.6	13 375.9
Transport Trucks	843 383.0	73 099.4	18 665.9	1 269.5	2 824.9
Heavy-Duty Diesel Trucks	17 905.2	7 863.6	28 696.0	988.1	976.9
Other	150.1	38.8	205.3	27.7	18.8
Other Aircraft	5 248.0	1 779.8	2 747.2	123.8	238.5
Total Mobile	3 033 538.4	316 838.1	145 370.1	10 189.0	28 045.0
Grand Total	3 225 762.0	624 954.3	202 756.4	366 131.5	201 761.3

TABLE D.5 PICCA Emissions Inventory (metric tons/year)

Sources	CO	VOC	NO_X	PST	SO_2
Stationary					
PEMEX	52 645	31 730	3 233	1 154	14 781
Power Plants	560	113	6 613	3 545	58 247
Industry	15 816	39 981	28 883	10 242	65 732
Commercial	466	121	3 988	2 469	22 060
Total Stationary	69 487	71 945	42 717	17 410	160 820
Mobile					
Private Cars	1 328 133	141 059	41 976	4 398	3 557
Taxis	301 162	31 986	9 518	997	806
Collectives & Minibuses	404 471	42 748	10 059	1 062	856
DDF Buses (R-100)	6 260	2 439	8 058	240	5 224
EdoMex	12 612	5 298	18 262	601	13 062
Gasoline Trucks	779 585	67 864	16 994	1 186	955
Diesel Trucks	16 515	7 293	26 126	923	20 063
Other (trains, airplanes, etc.)	5 040	1 693	2 698	142	251
Total Mobile	2 853 778	300 380	133 691	9 549	44 774
Ecological					
Eroded Areas	419 439				
Fires & Other Processes	27 362	199 776	931	4 201	131
Total Ecological	27 362	199 776	931	423 640	131
Grand Total	2 950 627	572 101	177 339	450 599	205 725

4. Base Case Evolution.

The implementation and performance test of the model for O_3 behavior simulation in the MCMA was a progressive task in which the input data were improved and, in a proportional response, a better agreement of predicted results with monitored values at several stations was obtained. Results are presented, in Figures D.9 to D.15 for seven stations at different locations in the MCMA: Xalostoc in the NE, Tlalnepantla in the NW, Lagunilla and La Merced in the Downtown area, Iztapalapa y Cerro de la Estrella in the SE and Pedregal in the SW. Three cases are reported in the figures, each labeled by the date when the calculation was carried out. The major difference from one simulation to the next is the detail of the emissions inventory.

In the first base case simulation (done in March, 1992) differences in the spatial and temporal distribution pattern of emissions from mobile and stationary sources were considered. This was done without speciation in the emissions categories. In the second iteration of the base case, performed in October 1992, categorization and speciation of VOC emissions from stationary sources were introduced. In addition, OZIP calculations and ambient measurements provided strong evidence that the VOC emissions inventory was severely underestimated.

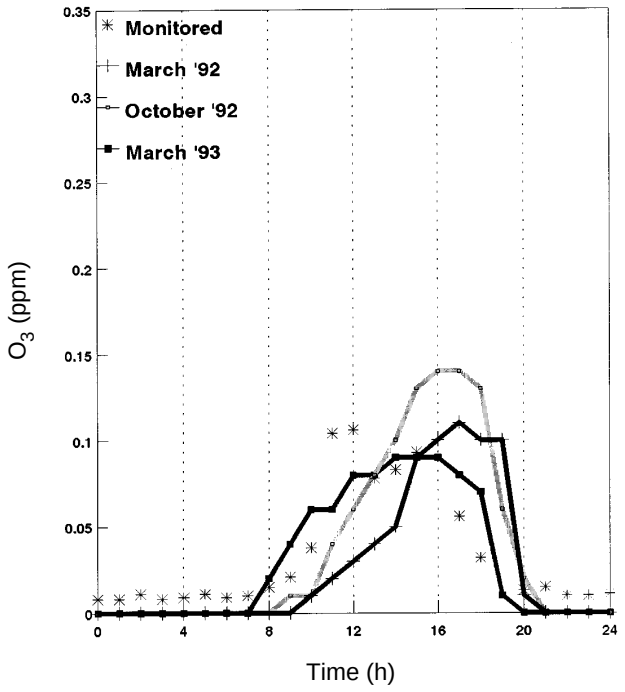

Figure D.9. Successive base case simulations compared to measured O_3 at the Xalostoc monitoring station in the northeast.

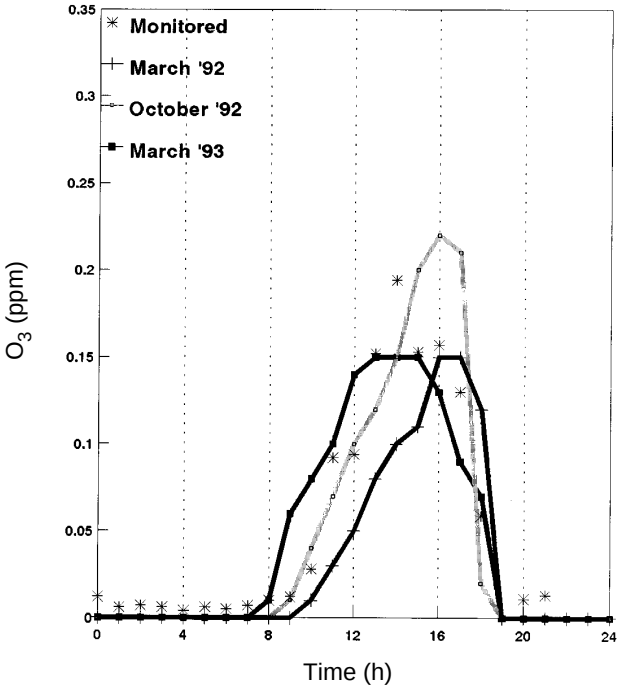

Figure D.11. Successive base case simulations compared to measured O_3 at the Lagunilla monitoring station in the downtown area.

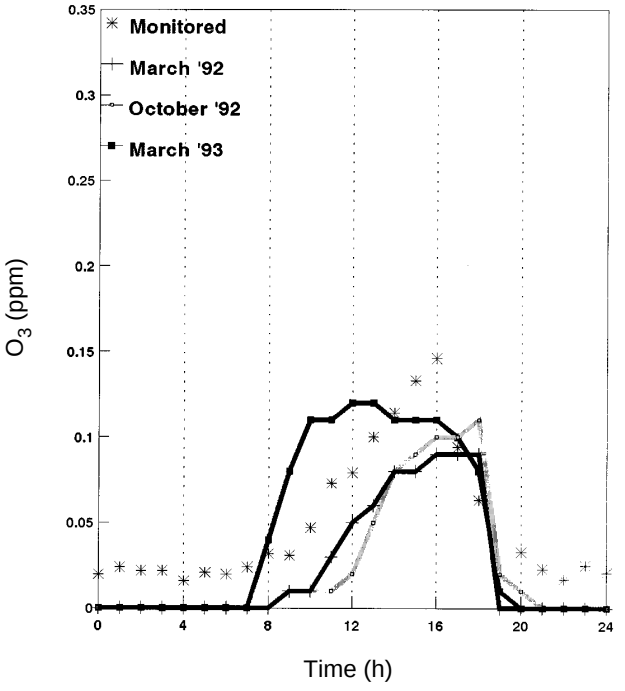

Figure D.10. Successive base case simulations compared to measured O_3 at the Tlalnepantla station in the northwest.

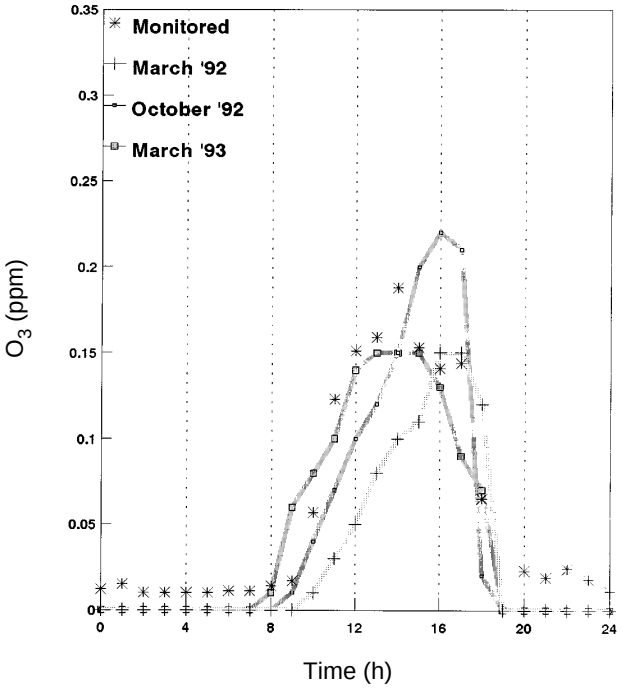

Figure D.12. Successive base case simulations compared to measured O_3 at the Merced monitoring station in the downtown area.

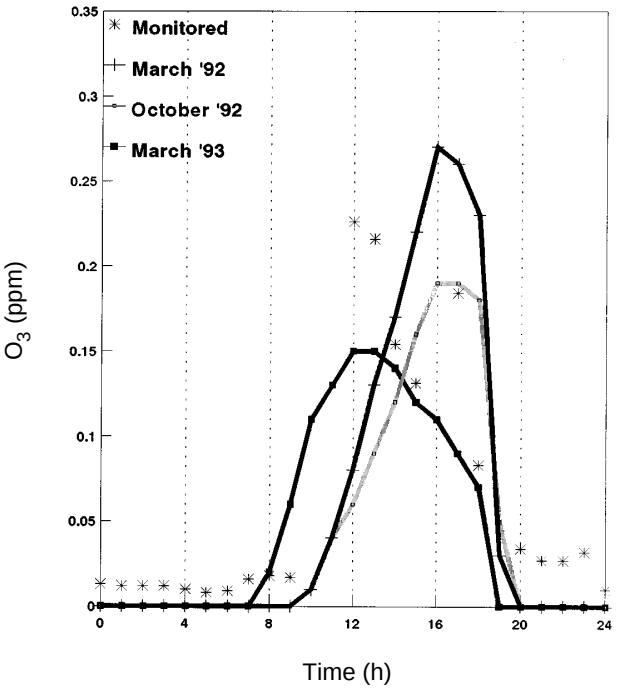

Figure D.13. Successive base case simulations compared to measured O_3 at the Iztapalapa monitoring station in the southeast.

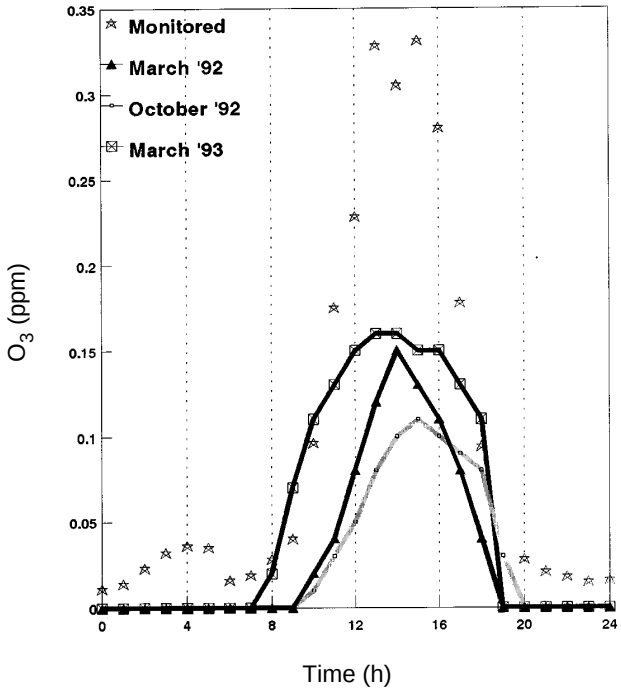

Figure D.15. Successive base case simulations compared to measured O_3 at the Pedregal monitoring station in the southwest.

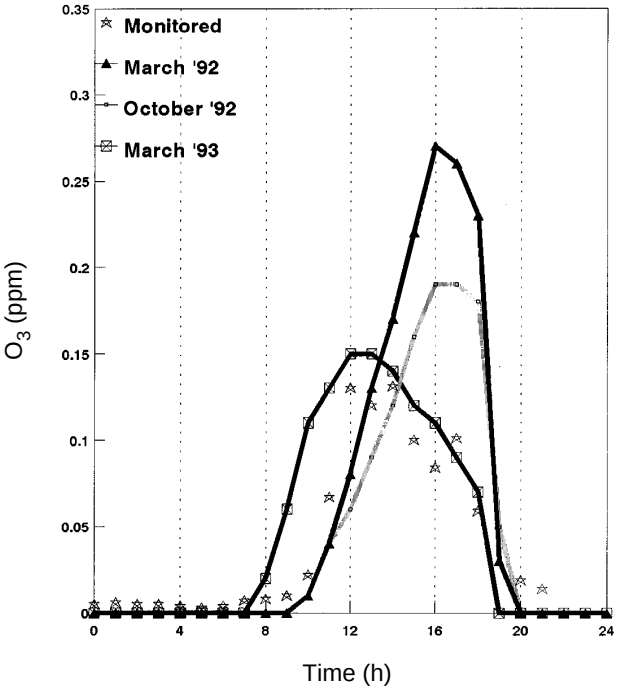

Figure D.14. Successive base case simulations compared to measured O_3 at the Cerro de las Estrella monitoring station in the southeast.

A multiplication factor of four applied to all VOC emissions brought substantial improvement to the results. In the last base case (done in March 1993), spatially and temporally distributed biogenic emissions were introduced. Categorization and speciation of emissions from mobile sources were also introduced. Moreover, data on the evaporative emissions from gasoline storage tanks and gas stations were available and specifically included. The base case simulations show that the model is ready to analyze pollutant behavior and control strategies.

d. Emissions Inventory

An emissions inventory is a database that ideally contains the temporal, spatial and detailed chemical composition of emissions from anthropogenic and biogenic sources. The

emissions need to be classed as point (industry, power plants), line (major traffic arteries) and area or distributed (residential, commercial, other traffic). A further breakdown by type of industry, commerce or vehicle is needed to explore emissions control options.

The emissions inventory is a *sine qua non* for airshed modeling; obviously there can be no description of the behavior and fate of air pollution if there are no pollution sources. The emissions inventory, coupled with simulation, also forms the starting point for most air quality improvement strategies; it is almost universal to forecast a certain improvement in air quality if emissions are reduced a certain percentage. The translation of that percentage to tons of emission reduction required is, of necessity, based on the emissions inventory.

Therein lies the rub. The greatest uncertainty in input to air quality simulations is always the emissions inventory, particularly for HC, a critical precursor to O_3 formation. There is a growing body of evidence that the HC emissions inventories are severely underestimated in urban areas around the world. Before this was understood, less than satisfactory simulation results, whether from the EKMA or the airshed approach, were often used for air quality management planning. This led to frustration in achieving air quality improvement because a certain number of tons reduction of HC emissions is actually a much smaller percentage reduction than expected when compared to the realistic emissions inventory. Consequently, a much smaller percentage improvement in air quality (referring to O_3) is achieved than was anticipated.

To conclude this brief discussion, the development of a good emissions inventory is a difficult project, usually entailing many refinements and iterations from the starting point. In process, the emissions of the study area are always changing; new emissions controls have gone into effect, population and concomitant traffic have grown, industries have grown or departed, etc. Because air quality management studies look at "what-if" scenarios starting from some base case, it is necessary to fix the emissions inventory for some specific year and develop the base case for that year. Only occasionally should an updated emissions inventory be adopted because it necessitates a new cycle of base case development and scenario simulation.

Base case simulations for this project were set to several dates in February 1991. Thus, a 1991 emissions inventory was needed. In February 1991 the PEMEX (Petróleos Mexicanos) 18 de Marzo refinery was still operating (it was closed by Presidential decree the following month) so the emissions inventory used and presented here includes the refinery.

The emissions inventory developed for modeling purposes in this project was adapted and derived from several sources, none of which meet the ideal criteria set forth at the beginning of this section. However, the Departamento Distrito Federal (DDF—Federal District Department) well recognizes the importance of a good emissions inventory and has supported and continues to support projects designed to improve the inventory for the MCMA.

The first effort to produce an emissions inventory for the MCMA was a collaborative effort between the DDF and the Japan International Cooperation Agency (JICA) begun in 1986

with the report issued in 1988 (JICA, 1988). This inventory, for NO_X, SO_2 and CO, was established for a 1 km^2 grid covering the MCMA. Traffic volume surveys coupled with dynamometer testing of a selection of used vehicles were used to calculate mobile emissions. A voluntary survey taken of 361 factories requesting information on types of activities and processes, fuel usage, chimneys and flue gas volume and temperature, and installed pollution control equipment was used in conjunction with U.S. EPA emission factors to calculate emissions for these large sources. Spot-check measurements were made on a small number of stacks. Business license data from the DDF for 4739 commercial and service establishments were used to obtain business type and fuel use. U.S. EPA emission factors were again used to calculate emissions.

The second emissions inventory for the MCMA is for 1989 and is presented in the Programa Integral Contra la Contaminación Atmosférica de la Zona Metropolitana de la Ciudad de México, universally referred to as PICCA, (Comprehensive Program Against Air Pollution of the MCMA) published by the Secretariado Técnico Intergubernamental in 1990. (PICCA, 1990) We do not know many details of the development of this inventory, presented in Table D.5, except that a version of MOBILE4, adapted to the MCMA was used and U.S. EPA emission factors were used for industry and commerce. However this inventory bears the imprimatur of numerous federal secretariats, the DDF, PEMEX, the EdoMex, and the Federal Electricity Commission so it served as the primary base to develop the inventory used in this project.

A brief look at the data of Table D.5 shows that mobile sources contribute 97% of the CO, 53% of the HC, 75% of the NO_X and 22% of the SO_2. Stationary sources contribute only 2.4% of the CO, 13% of the HC, 25% of the NO_X, but a significant 78% of the SO_2.

The third major source of data for the emissions inventory for this project was the pilot study undertaken in 1990 and 1991 by a collaboration between the German consulting firm, TÜV-Rheinland, and the DDF. (TÜV, 1991) For this study an area of roughly 5 km by 20 km was defined across the northern part of the MCMA. This area included parts of the EdoMex municipalities of Naucalpan de Juárez and Tlalnepantla and the DDF delegaciones* Azcapotzalco and Gustavo A. Madera. Two data sets were used for stationary emissions: data on industrial plants from SEDESOL and data on fuel usage at combustion sites from TecnoConsult. Mobile source emissions were derived from traffic surveys and MOBILE-MCMA. The report acknowledges several shortcomings to this inventory, particularly in stationary sources, but since this is the most recent information available, we applied the ratio of emissions from this study compared to JICA as a general scale-up ratio for the remainder of the MCMA.

Final preparation of the emissions inventory for the CIT simulations required a combination of distributing / grouping the data from the studies discussed above into a 5 km^2 grid. Temporal distribution of mobile emissions was derived

*A delegación is a large political subdivision of the DDF.

from a composite of traffic surveys and for stationary emissions from an electric power hourly demand chart. See Figure D.16. On occasion when the emissions inventories presented seemingly unreconcilable data, judgments had to be made. The procedures and assumptions that went into preparation of the emissions inventory for this project were presented to the technical staff of the DDF, and they granted approval.

The PICCA and TÜV inventories show ratios of the emissions of HCs to the emissions of NO_X to be slightly higher than 3:1. Assuming early morning emissions obey the same ratio, it is easy to see that this HC / NO_X ratio is far too low. As discussed in Volume IV, HC measurements in Mexico City showed very high ambient concentrations. With NO_X levels measured at the same time, the HC / NO_X ratio is calculated to be in the range of 15:1 or higher. Modeling results, discussed further in section 5 of this volume, showed that the onset, slope, and peak of O_3 production could in no way be simulated with the base emissions inventory. Further, HC concentrations in the simulation using the base emissions inventory were far lower than measured ambient values. An arbitrary, but reasoned, multiplicative factor of four applied to all HC emissions led to significant improvement in model performance for O_3 prediction and HC concentration tracking. Consequently, the HC emissions inventory used in this project for airshed modeling was also adjusted by a factor of four. It is recognized that this is a gross factor, but it serves to highlight the severe underestimation of HC emissions in the MCMA. Refinement is still needed in identifying the underestimated sources and the temporal and spatial distribution needed for a reliable emissions inventory remains to be done.

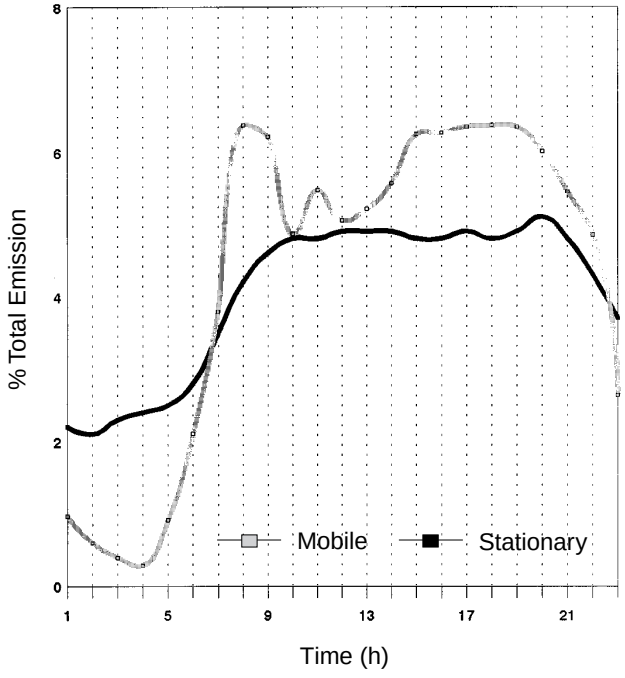

Figure D.16. Temporal distribution of mobile emissions derived from a composite of traffic surveys and for stationary emissions from an electric power hourly demand chart.

e. Linking Meteorology and Airshed Models

Special computational codes were written to take the HOTMAC output, transform the coordinate system to the CIT grid and compute average hourly winds in the CIT system. Mass consistency was forced in the CIT system although some divergence was produced when the fields were written into the CIT input files because of the limited precision in the format. The basic HOTMAC output is mass-consistent, but the grid system is different from that of the CIT model, which implies that the local slopes are different for each model, and the rotation of coordinate systems permits small errors to occur that can affect mass balance.

5. Model Applications and Results

a. OZIP

1. Episode simulation of February 22, 1991.

On February 22, 1991, the recorded peak for O_3 in Mexico City occurred at the Pedregal monitoring station at 3:00 p.m. This one-hour average peak was 0.331 ppm, but in actuality a broad peak above .3 ppm was observed: the 1:00 p.m. reading was 0.328 ppm and the 2:00 p.m. reading was 0.305 ppm.

For the simulation, a trajectory was established beginning in the vicinity of Xalostoc in the northeast of the city and moving to Pedregal in the southwest of the city. The simulation was started at 7:10 a.m. (sunrise was at 7:06 a.m.) with the air parcel arriving at Pedregal at 2:00 p.m., moving past Pedregal for two hours and then returning with the late-afternoon wind shift. The trajectory was consistent with a back trajectory derived from a HOTMAC-RAPTAD simulation. The diurnal change in mixing height was obtained from the HOTMAC simulation for that day. Emissions were taken from the appropriate grid cell of the emissions inventory, which was set up for the CIT simulation with a resolution of 5 km by 5 km. The fresh emissions entering the air column were calculated specifically for the time of day at which the trajectory passed over a grid cell. Temperature and humidity were taken from the nearest monitoring station at each hour or (for some hours) as an average of two nearby stations.

Photolysis rates were calculated by standard techniques using an actinic flux calculation specific to the latitude and altitude of Mexico City. The actinic flux was calculated using the integral equation for radiation transfer with multiple scattering (Anderson and Meier 1979), a method that has previously been demonstrated to give good results for Los Angeles (an urban application) and Niwot Ridge, Colorado (a high altitude application) (Streit 1985). It was necessary to make a calculation specific to Mexico City because there is a much lower overhead stratospheric O_3 column at that latitude and month than is ever experienced over major U.S. urban areas. The default photolysis rates in the model are for a generic U.S. urban area similar to Los Angeles. The low overhead O_3 column (a natural phenomenon) allows greater penetration of the ultraviolet part of the solar spectrum into the troposphere and enhances photolysis rates for species that absorb in that region of the spectrum. This includes O_3 itself and, most notably, the aldehydes. As a consequence, the photochemistry in Mexico City appears to be somewhat accelerated when compared to that in U.S. cities.

Initial concentrations of CO and NO_X were set equal to the concentrations measured at the Xalostoc monitoring station that day, 7 ppm and 0.2 ppm respectively. The average 6:00 a.m. to 9:00 a.m. NMOC concentration measured at Xalostoc in March 1992 was 4.5 ppmC. Since the mixing height does not change during this period, it was assumed that the ambient NMOC concentration actually increases as urban activity, especially traffic, increases in the morning. So the 7:00 a.m. concentration for NMOC was chosen to be 3.0 ppmC. This gives an initial NMOC / NO_X ratio of 15.

The episode simulation with initial conditions and assumptions as described above could be termed to be a dramatic flop. The O_3 peak showed a very slow and steady increase to a

one-hour peak average of 0.186 ppm centered at 5:25 p.m. However, it was a flop only in terms of reproducing the February 22, 1991, Mexico City episode. A closer look at the results produced some interesting observations:

- the calculated peak was much lower than the actual peak,
- the onset or rise to the calculated peak was much slower than actual, and
- despite initiating the calculation with a quite high 3.0 ppmC of NMOC, the calculated concentration of NMOC dropped in the initial hours of the calculation and thus did not come close to reproducing the observed 6:00 a.m. to 9:00 a.m. average of 4.5 ppmC.

These observations, along with the knowledge that it is now thought that the NMOC emissions inventory for the Los Angeles area was underestimated by a factor of three, provide very strong support to the assumption that the Mexico City NMOC emissions inventory is severely underestimated. A series of calculations were done with the same initial conditions and certain multiplicative factors applied to the NMOC emissions. This factor was applied to all NMOC emissions without regard to time, location, or type of source. Though the initial NMOC / NO_X ratio remained the same, the NMOC / NO_X ratio during the calculation increased as NMOC emissions were increased. The onset of the O_3 peak became steeper, and the peak height also increased. When the multiplicative factor was four, the best fit to the actual peak (considering both slope and concentration) was obtained. The calculated 6:00 a.m. to 9:00 a.m. average NMOC rose to nearly 4 ppmC, still lower than the observed average, but a significant improvement over the calculation with the original emissions inventory.

This factor of four was carried over to the CIT airshed calculations as well and brought about significant model performance improvement. While the factor of four works well in gross application to the emissions inventory, it is clear that much refining work needs to be done. The time, location, and source type for the increased emissions need to be determined. Obviously, automobiles are the prime suspect, and it could be that their emissions are underestimated by more than a factor of four while stationary source emissions are not so severely underestimated. It could also be that some sources are not even included. However, it is not conceivable that there are any missing sources that would remove the primary burden from the automotive source.

2. Ozone Isopleths and Control Strategies.

Given the now increased NMOC emissions inventory and the same initial conditions discussed above, a set of O_3 isopleths was calculated for Mexico City. This set of isopleths is shown in Figure D.3. These are labeled as plausible isopleths for Mexico City because while it is certain that Mexico City is very HC-rich, there are obvious uncertainties in the amount and reactivity of HC emissions. These isopleths illustrate a condition that is so HC-rich that initial reductions in HC emission will result in an increase in O_3. This is chemically possible but not frequently observed because it is unusual (based on U.S. experience) to have such high HC levels. The chemistry that prevents O_3 from accumulating under these conditions can include O_3 reaction with olefins, NO_2 reaction with organic

free radicals or radical-radical termination reactions. Thus, a lowering of HC could lead to increased O_3. Much more commonly observed in U.S. experience is the situation in which reduction of NO_X leads initially to increased O_3.

The point to be made though, whether the isopleths are curved as shown or flat as is more commonly expected, is that reduction of HC will have to proceed to a very great extent before significant reductions in O_3 are seen. An NO_X control strategy might yield faster progress, but it cannot be recommended because there are other strong factors that mandate that HC be reduced. These include concerns dealing with toxic organics and the fact that HCs are also a precursor in secondary aerosol, or haze, production. It must be understood by the populace and the policy makers that emissions control options that account for only a few percent of emissions will not, of themselves, accomplish much, but the cumulative effect of many such options must be pursued. When the time comes in Mexico City that significant reductions in emissions have been achieved and the emissions database has been updated and improved, new modeling efforts will be needed to guide the evolution of air quality policy at that time.

3. Analysis of Emissions Control Options.

The OZIPM-4 model was also used to provide screening-level predictions of the relationship between emissions reductions and peak O_3 concentrations for the linear programming effort in the Strategic Evaluation Task of this project. A series of simulations were carried out with emissions reductions ranging from 1% to 70% for NO_X and/or HC. Because small reductions in HC only were predicted to lead to increased O_3, the cumulative effect of summing the emissions reductions for all the options in a strategy had to be determined. Then each individual option was assigned a proportionate amount of the cumulative benefit so that all options had a positive benefit for the linear programming analysis.

b. CIT

1. Daylight Savings Time (DST).

The DST program is designed to take advantage of natural solar light. It is associated with an appreciable savings in the afternoon electric demand. It also favors commercial and tourist sectors in the country. However, the shift in the legal time implies that emissions from vehicular morning traffic peak (6:00 a.m. to 9:00 a.m.) may remain concentrated longer, leading to higher rates of photochemical smog production. This is due to the inversion breakup being postponed for one hour.

In order to analyze the effect of the proposed DST program in O_3 behavior, calculations were carried out using the box version of the CIT model and the base case conditions and inputs for February 22nd, 1991. The expected changes in the emission inventories were simulated by shifting the emission temporal pattern one hour.

Three cases were calculated: the base case, the shift in the emission temporal pattern one hour in advance, and the shift one hour delayed. The results are shown in Figure D.17. A 48-hour time period is depicted because two successive days were simulated in order to account for nighttime carryover of emissions. This effect is noticeable in the results for the second day.

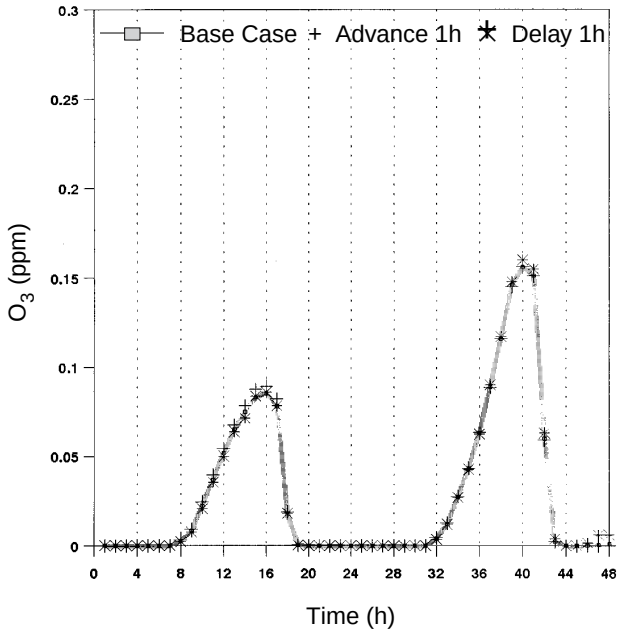

Figure D.17. Results for the daylight savings time program simulation. Three cases were calculated: the base case, a one-hour in advance in the emissions pattern, and a one-hour delay in the emissions pattern.

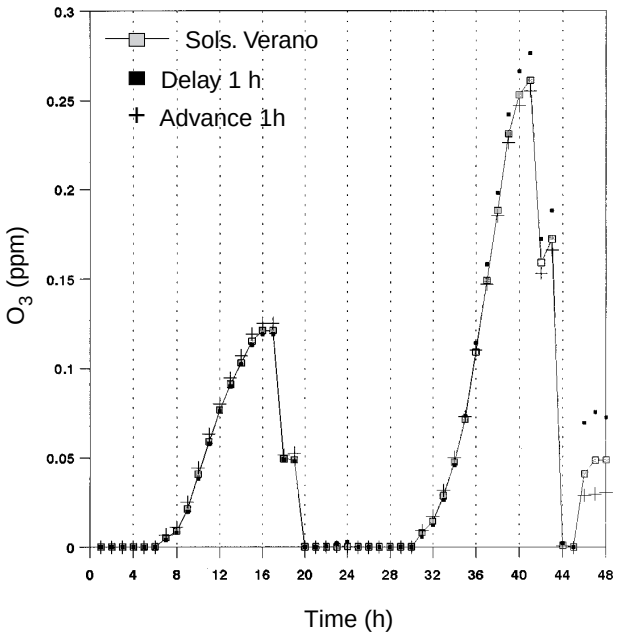

Figure D.18. Daylight savings time simulation results for the summer (June 22nd).

In addition to the base case scenario, which can be considered as an episode in wintertime (February 22), an occurrence in the summer (June 22nd) was also examined. Results for this latter scenario are depicted in Figure D.18. In the comparison of the figures, the difference in the O_3 maxima concentration is clearly seen. This can be easily explained considering that irradiation during summertime lasts longer and is more intense, thus promoting photochemical reactions in the atmosphere.

Even though there are appreciable changes in the predicted O_3 maxima concentration because of the shift in the emission pattern, changes are about 10% in relation to the base case values and within the uncertainty of the model and emissions inventory.

Further calculations, varying the initial VOC/NO_X ratio, were performed with the airshed model. Overall results for the different areas in the city improve with a higher VOC/NO_X ratio. In Figures D.19 and D.20 it is shown that, in the results for the Pedregal station, the VOC/NO_X ratio has more influence than the shift in the temporal emission pattern does.

2. Impact of Refinery Shutdown.

The main feature in the development of input for the airshed simulation of the "18 de Marzo" refinery shutdown was the incorporation of emissions from the main tall stack into an elevated layer isolated from the surface. A total of 14 stacks of 20 m height or greater were used for description of the plants and the petroleum refinery.

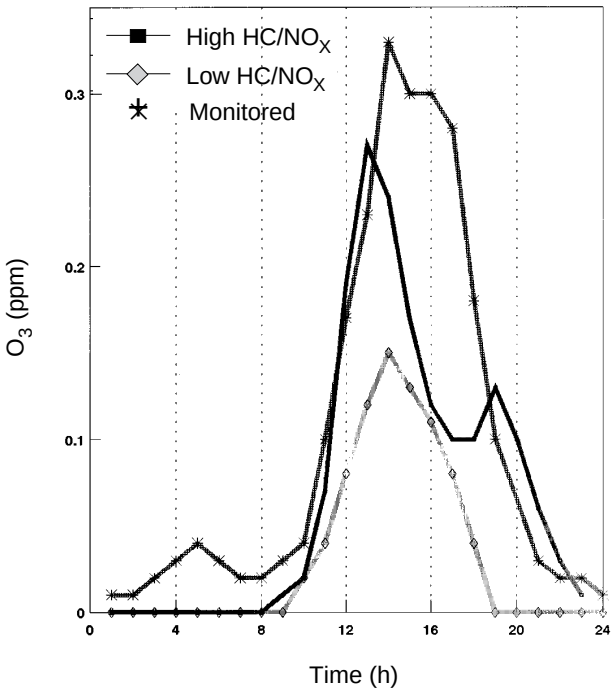

Figure D.19. Simulation results with different VOC/NO_X ratios. Values are for the Pedregal station in the southwest area of the city.

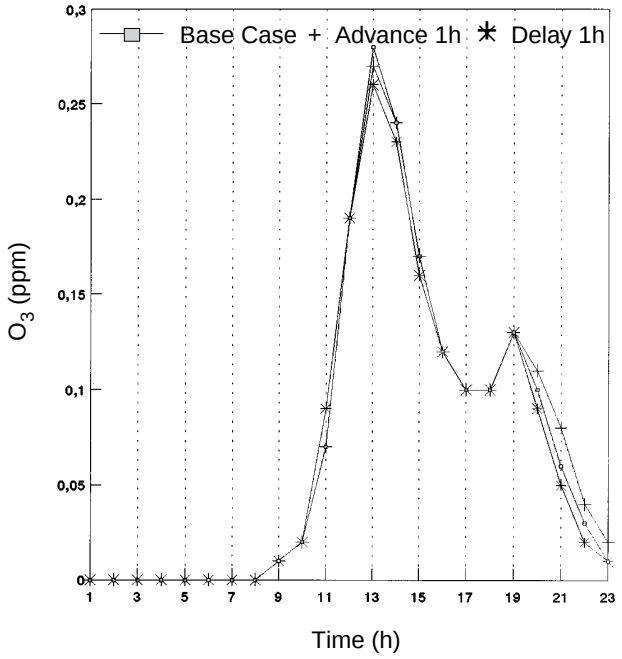

Figure D.20. Emission time-shift results for the Pedregal station in the southwest area of the city. The VOC/NO_X ratio has more influence than the shift in the temporal emission pattern.

The simulation results indicate, as expected, a different impact for different zones of the MCMA. For the northeast and center of the MCMA, no impact in the O_3 behavior was predicted. For the near-refinery region of the northwest (Acatlán and Tlalnepantla stations) a major impact is predicted: a decrease of about 20% in the O_3 maxima concentrations. For the southwest zone (Pedregal) of the MCMA a decrease of only 5% in the maximum is predicted. In the simulations, the conditions and inputs for the base case (February 22nd, 1991) were used.

3. Strategies Evaluation.

A linear programming model was applied to analyze a set of 37 options drawn from the PICCA report and other sources for listing emission control options. The list of options is given in Table D.6.

Given an objective, for instance a specific percentage reduction in the ambient concentration of a pollutant, linear programming analysis selects a list of options to meet that objective. This list is selected on the basis of the highest benefit-to-cost ratio. The set of options that satisfy the initial objective are defined to be a strategy.

The linear programming model predicts pollutant reduction to be the sum of the reductions associated with individual options. However, it is known that the benefit in the improvement of the air quality is not equally distributed over the city because local activities are very different. Thus, air quality simulations are needed to predict the actual impact in the different areas. Three strategies were designed and their impact on O_3 formation and other pollutant concentrations was determined through a series of simulations.

TABLE D.6 Air Quality Improvement Options

OPTIONS

1. Produce gasoline conforming to international standards
2. Produce low-sulfur diesel fuel
3. Produce low-sulfur fuel oil and gasoleo (combination of fuel oil and diesel)
4. Expand Ruta 100
5. Authorize expanded bus routes
6. Expand the verification program for gasoline and diesel vehicles
7. Convert public vehicles and delivery trucks to liquefied petroleum gas (LPG) and install catalytic converters
8. Retrofit catalytic converters on minibuses
9. Require taxis to be newer than '84 and combi's to be newer than '80. (Combis are minivans and other vehicles that are not marked like taxis but are nonetheless licensed to carry passengers)
10. Substitute natural gas for fuel oil in industry
11. Clean and / or relocate the foundries in the Valley of Mexico
12. Improve combustion and install control equipment on small boilers.
13. Implement a program to reforest Mexico City and the Valley of Mexico
14. Remove very obviously polluting cars and prevent them from entering city
15. Use natural gas in the MCMA thermoelectric power plants
16. Prohibit all open burning
17. Limit use of paints and finishes in industries that don't control vapors
18. Limit operation of closed trash burners to optimum time of day
19. Install vapor recovery systems in filling stations (both storage and delivery)
20. Reduce circulation of official vehicles by 30%
21. Coordinate traffic lights to speed flow of traffic
22. Implement information system on traffic conditions
23. Construct and police parking lots next to public transportation stations
24. Improve taxi efficiencies by use of taxi stands
25. Create toll streets and roads for single passenger vehicles
26. Control and increase fees on parking lots
27. Construct Line 8 of the Metro
28. Improve electric transport (trolleys)
29. Better organize traffic and parking in the Central Historical District
30. Reduce emissions from metal cleaning and degreasing
31. Reduce emissions from dry cleaning
32. Continue to require catalytic converters on automobiles
33. Convert gasoline trucks to compressed natural gas (CNG)
34. Require gasoline trucks to conform to 1993 standards
35. Replace gasoline trucks not suitable for conversion to CNG or LPG
36. Pave roads
37. Purchase highly polluting old cars

The objective for Strategy 1 was to reduce the O_3 peak by 33%. This objective could be accomplished with a high cost effectiveness by not requiring that private vehicles be equipped with catalytic converters. The list of options selected for this first strategy is shown in Table D.7.

The objective for Strategy 2 was to reduce the O_3 peak by 43% in the most cost-effective manner. This represents a moderately aggressive program; the associated control options are listed in Table D.8.

TABLE D.7 Options Comprising Strategy 1

OPTIONS

1. Produce gasoline conforming to international standards
2. Authorize expanded bus routes
3. Expand the verification program for gasoline and diesel vehicles
4. Convert public vehicles and delivery trucks to LPG and install catalytic converters
5. Retrofit catalytic converters on minibuses
6. Improve combustion and install control equipment on small boilers
7. Implement a program to reforest Mexico City and the Valley of Mexico
8. Remove very obviously polluting cars and prevent them from entering city
9. Prohibit all open burning
10. Install vapor recovery systems in filling stations (both storage and delivery)
11. Construct and police parking lots next to public transportation stations
12. Improve taxi efficiencies by use of taxi stands
13. Create toll streets and roads for single passenger vehicles
14. Improve electric transport (trolleys)
15. Reduce emissions from metal cleaning and degreasing
16. Reduce emissions from dry cleaning
17. Convert gasoline trucks to CNG
18. Require gasoline trucks to conform to 1993 standards

TABLE D.8 Options Comprising Strategy 2

OPTIONS

1. Expand the verification program for gasoline and diesel vehicles
2. Convert public vehicles and delivery trucks to LPG and install catalytic converters
3. Retrofit catalytic converters on minibuses
4. Improve combustion and install control equipment on small boilers
5. Implement a program to reforest Mexico City and the Valley of Mexico
6. Remove very obviously polluting cars and prevent them from entering city
7. Prohibit all open burning
8. Install vapor recovery systems in filling stations (both storage and delivery)
9. Improve taxi efficiencies by use of taxi stands
10. Improve electric transport (trolleys)
11. Reduce emissions from metal cleaning and degreasing
12. Reduce emissions from dry cleaning
13. Continue to require catalytic converters on automobiles
14. Convert gasoline trucks to CNG
15. Require gasoline trucks to conform to 1993 standards

The objective for Strategy 3 was also to reduce the O_3 peak by 43%, but by preferentially controlling emissions from industrial sources. The list of options selected is given in Table D.9.

Not surprisingly, the linear programming, OZIP, and airshed models predict different reductions in maximum O_3 and CO concentrations as reported in Table D.10. In this table, the values for the airshed (3-D) simulations are reported as average values over the whole modeling area. It is worthwhile to note that airshed modeling is able to predict different impacts at different locations. The linear programming estimates are high because the method does not account for the fact that emissions reductions for some options are not independently additive.

c. Comparison with Measurements

1. Surface O_3 and NO_X Distribution.

Box, trajectory and airshed simulations of O_3 formation in the MCMA were performed. In this section, predictions from trajectory and airshed simulations are compared with monitored values for surface O_3 and NO_X.

TABLE D.9 Options Comprising Strategy 3

OPTIONS

1. Expand the verification program for gasoline and diesel vehicles
2. Retrofit catalytic converters on minibuses
3. Improve combustion and install control equipment on small boilers
4. Implement a program to reforest Mexico City and the Valley of Mexico
5. Remove very obviously polluting cars and prevent them from entering city
6. Prohibit all open burning
7. Limit use of paints and finishes in industries that don't control vapors
8. Install vapor recovery systems in filling stations (both storage and delivery)
9. Improve taxi efficiencies by use of taxi stands
10. Improve electric transport (trolleys)
11. Reduce emissions from metal cleaning and degreasing
12. Reduce emissions from dry cleaning
13. Continue to require catalytic converters on automobiles
14. Convert gasoline trucks to CNG
15. Require gasoline trucks to conform to 1993 standards

TABLE D.10 Percentages of Reductions for O_3 and CO as a Result of Implementation of Strategies

Pollutant	O_3			CO	
Method	Linear Program	OZIP	Airshed	Linear Program	Airshed
Strategy 1	33	16	24	62	42
Strategy 2	43	30	32	78	67
Strategy 3	43	30	32	74	69

Taking into account the time and place of the O_3 peak, a trajectory for the air mass was established by tracking HOTMAC wind fields backwards. The resulting trajectory indicates the displacement of the air mass from the northeast to the southwest in the MCMA. The emissions of the corresponding cells in the trajectory are incorporated into the simulation. The meteorological parameters registered at the corresponding monitoring stations are incorporated as well. Table D.11 is a list of the time and the corresponding monitoring station whose parameters were used to simulate the air mass trajectory for February 22, 1992, from 7:00 a.m. to 2:00 p.m.

For the trajectory calculations, the VOC emission inventory was multiplied by a factor of 4 and the NO_X by 1.5. A comparison between the results for O_3 and NO_X and those registered at the monitoring stations, at the same locations in the trajectory, is given in Figures D.21 and D.22. Good agreement is observed for both species; however, the agreement for O_3 is better.

The O_3 evolution for the base case airshed simulations compared with the monitored values is given in Figures D.23 to D.29. The agreement is much better for those stations in the north and east of the MCMA than for those in the south and west. For the southwest, the model considerably underpredicts the peak O_3 concentration.

2. Ozone Vertical Profiles.

With the CIT model it is possible to depict the O_3 vertical profile since seven vertical layers are taken into account in the simulations. In Figure D.30 two vertical profiles of O_3 concentration are shown, both corresponding to the base case. They are the result of trajectory simulations. In the figure it can be seen that at noon the O_3 concentration decreases above 1 000 m, but during the night ground-level O_3 concentration is very low (less than 0.07 ppm). However, above 200 m at night the concentration increases to values as high as 0.350 ppm. This last result is consistent with experimental findings that suggest that the atmosphere is stratified in layers. In each layer, the chemical species and meteorological parameters are significantly different, indicating the isolation of layers from each other and from the ground. This is shown in Figures D.31 and D.32.

The analysis of data from a morning aircraft flight (10:27 a.m. to 11:05 a.m.) has shown that the atmosphere is in fact stratified. (Diaz-Frances et al., submitted) A concentration of 0.204 ppm of O_3 was measured at 300 m height, whereas at the same hour, in a similar location, the O_3 concentration at ground level was only 0.06 ppm.

TABLE D.11 Time and Related Location of Air Mass Parcel for a Trajectory Simulation

Time	Monitoring Station	Time	Monitoring Station
07:00	Xalostoc	11:00	Merced
08:00	Xalostoc	12:00	Merced Plateros
09:00	Xalostoc Merced	13:00	Plateros
10:00	Merced	14:00	Pedregal

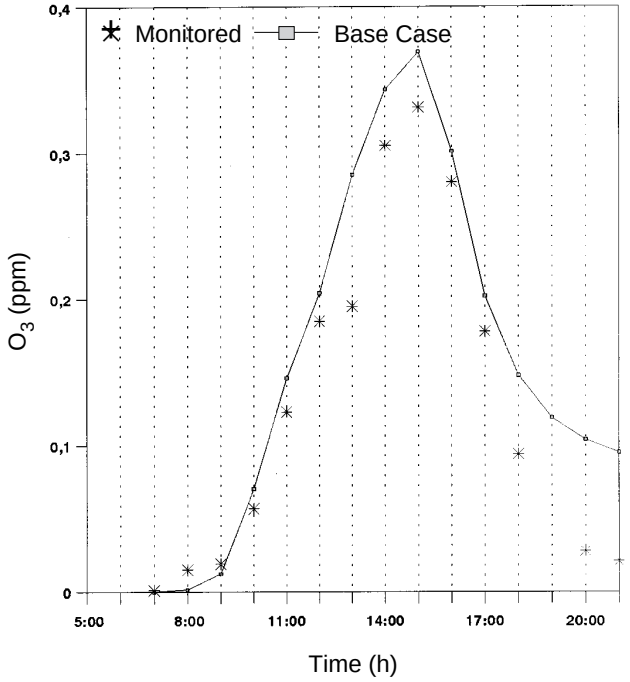

Figure D.21. Trajectory calculation results for O_3 compared to values measured at a corresponding time and place.

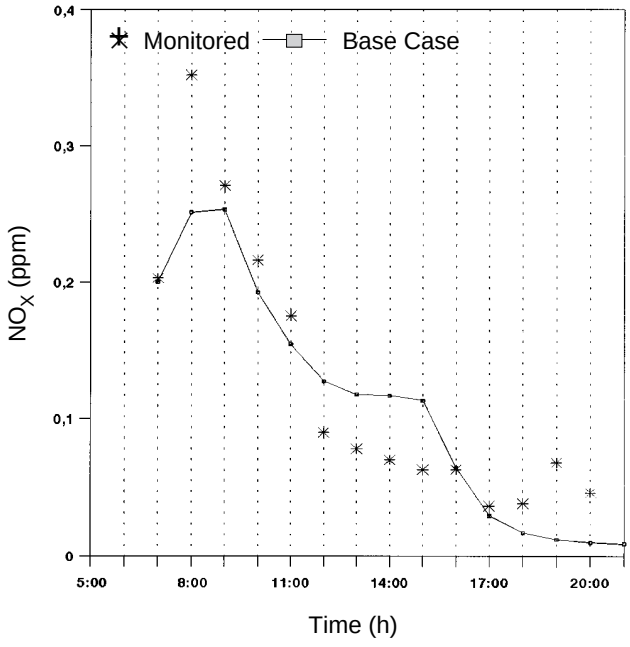

Figure D.22. Trajectory calculation results for NO_X compared to values measured at a corresponding time and place.

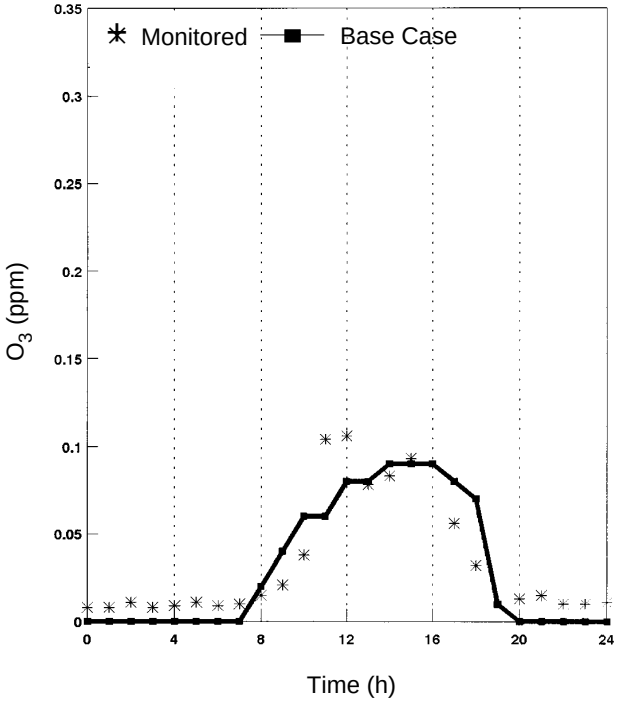

Figure D.23. O_3 behavior from the base case airshed simulations compared to the monitored values at Xalostoc.

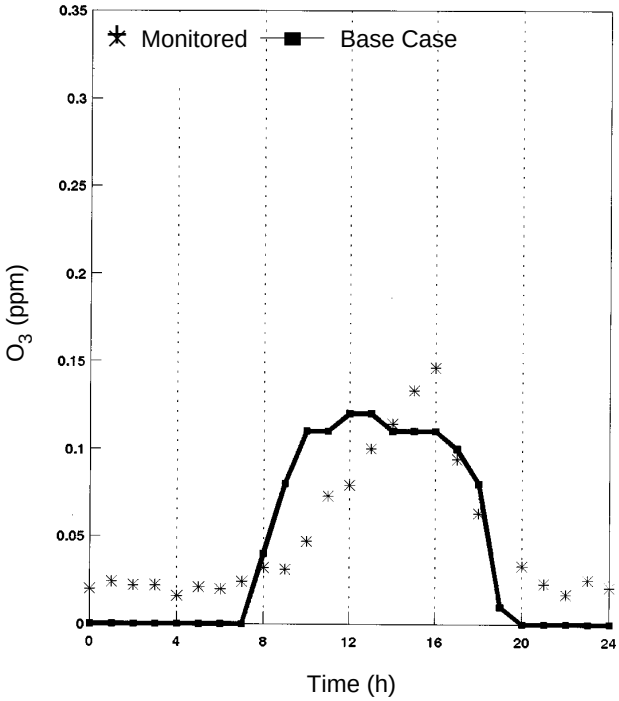

Figure D.24. O_3 behavior from the base case airshed simulations compared to the monitored values at Tlalnepantla.

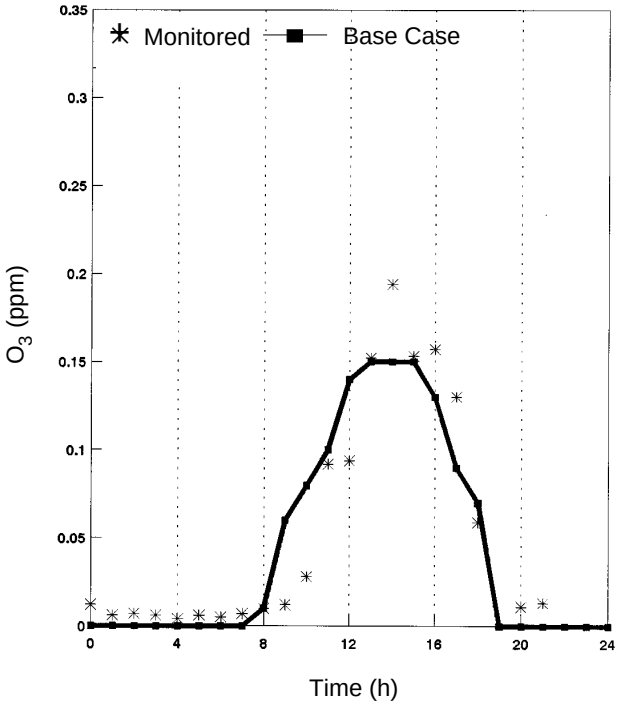

Figure D.25. O_3 behavior from the base case airshed simulations compared to the monitored values at Lagunilla.

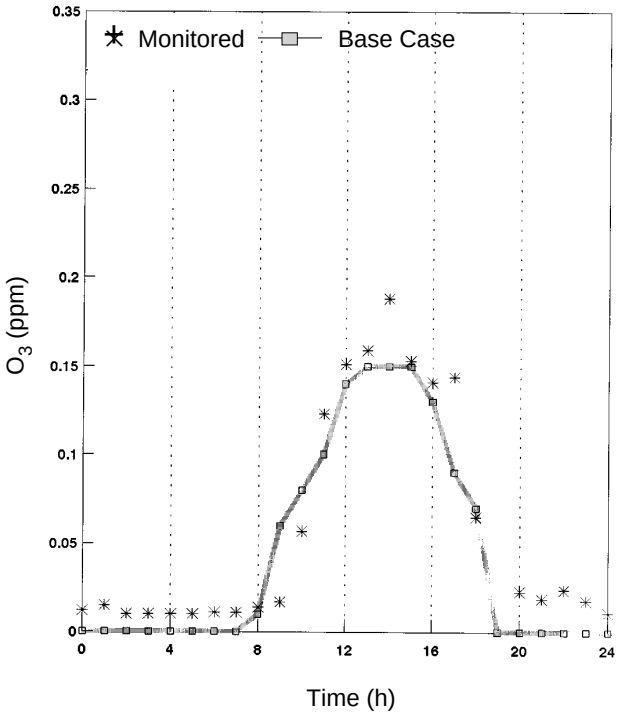

Figure D.26. O_3 behavior from the base case airshed simulations compared to the monitored values at Merced.

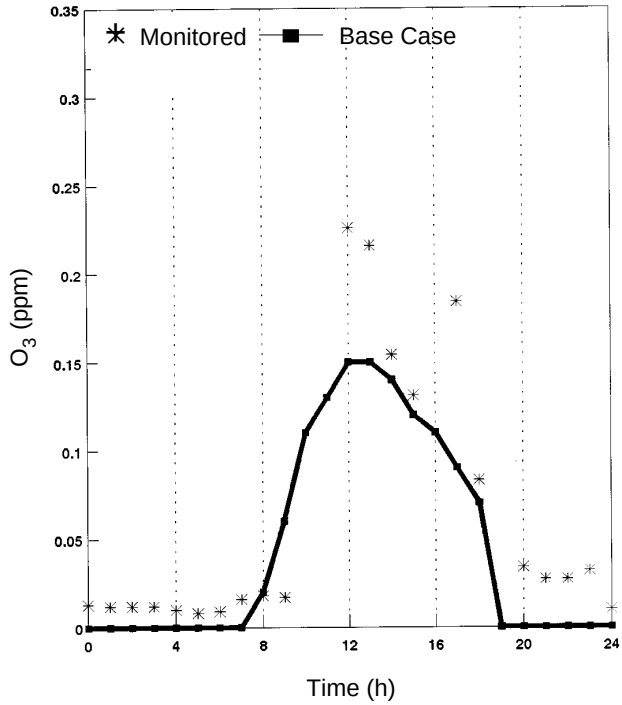

Figure D.27. O_3 behavior from the base case airshed simulations compared to the monitored values at Iztapalapa.

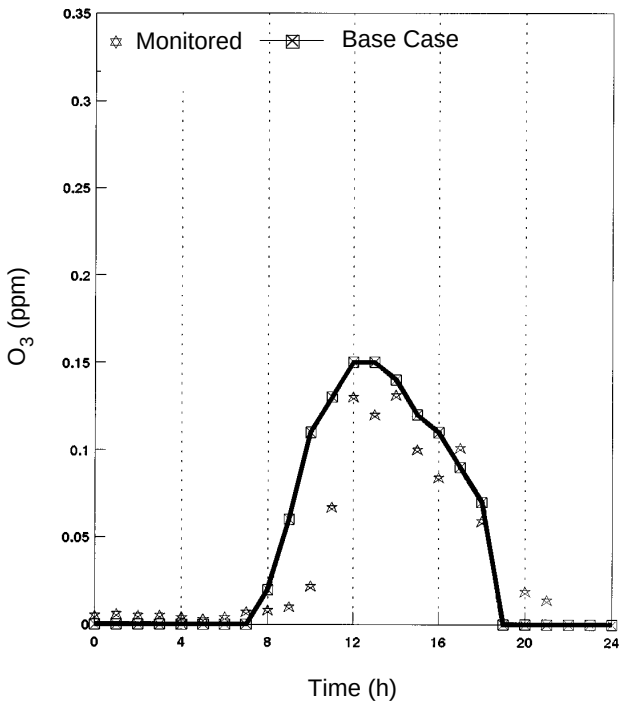

Figure D.28. O_3 behavior from the base case airshed simulations compared to the monitored values at Cerro de la Estrella.

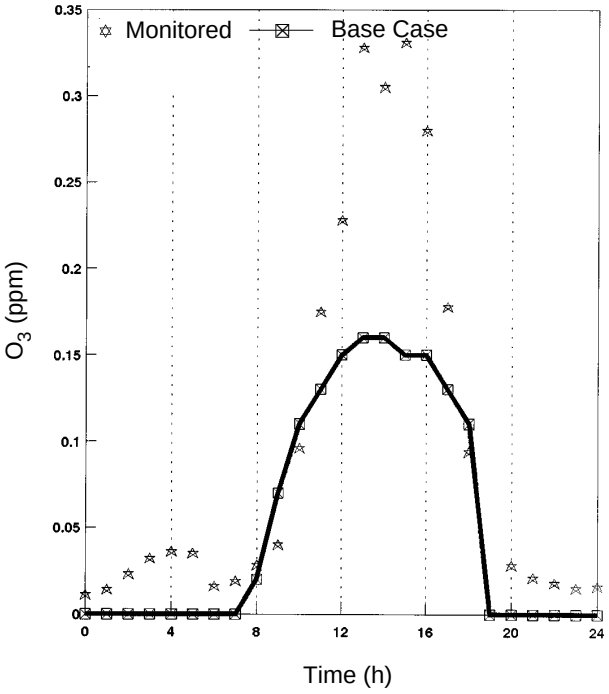

Figure D.29. O_3 behavior from the base case airshed simulations compared to the monitored values at Pedregal.

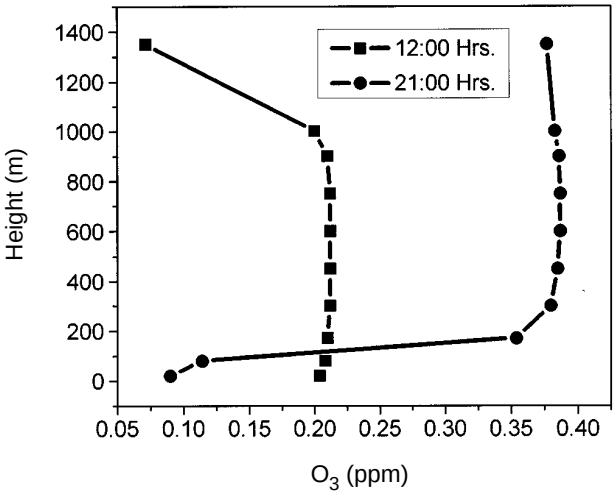

Figure D.30. Simulation of vertical profiles of O_3 concentration, both corresponding to the base case.

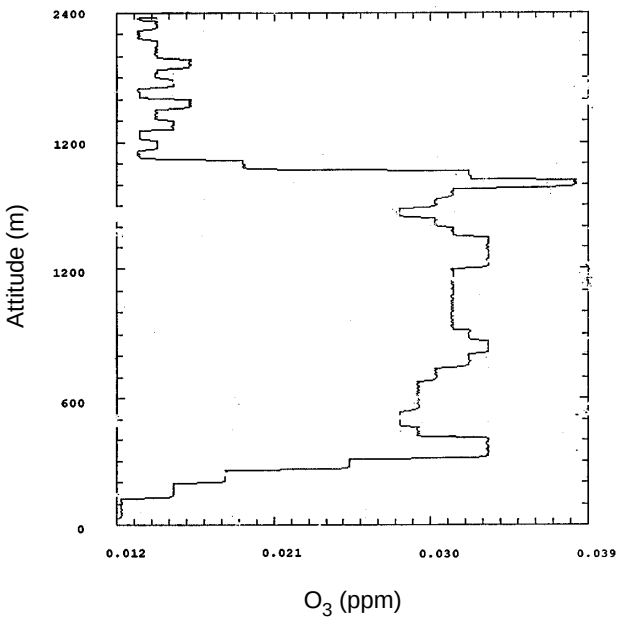

Figure D.31. O_3 vertical profile obtained by aircraft for February 13, 1991. The profile is taken in the morning and shows atmospheric stratification.

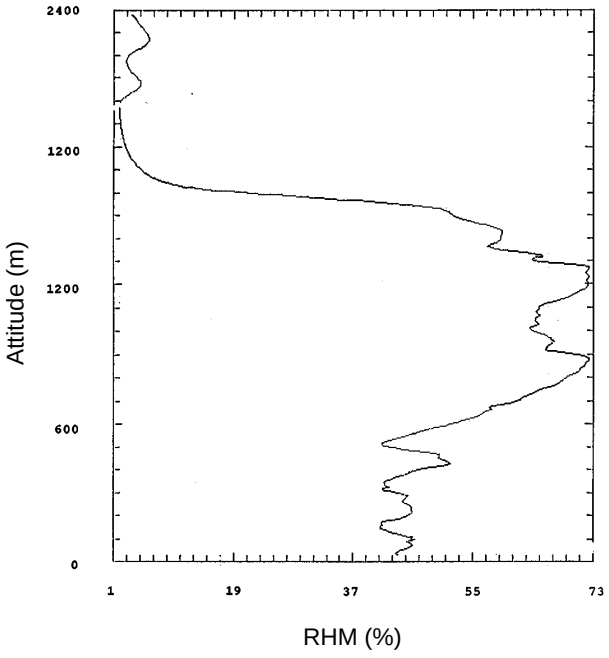

Figure D.32. Relative humidity vertical profile taken by aircraft on the morning of February 13, 1991. The profile demonstrates atmospheric stratification.

6. Performance Summary

The comparison of airshed simulated concentrations at several parts of the MCMA with the corresponding monitored values showed that the CIT simulations underpredicted O_3 concentrations for the southwest of the MCMA. The simulations did, however, show adequate behavior for the northern and eastern parts. Model performance tests for the other three pollutants, CO, NO_2, and SO_2, displayed a fairly similar behavior. These results show that the model can follow the diurnal variations and transport of these four species.

The simulation of the period from February 26 to 28 reproduces the increase in the O_3 concentration from one day to the next quite well. In Figures D.33 and D.34 the simulation results for the February 22nd and the February 27th-to-28th periods are compared with monitored values for several stations in the MCMA. In general, the agreement is quite good; however, it is better for the stations in the northeast, southeast and downtown areas than for those in the west of the MCMA.

If one looks at the results for February 22 over the entire simulation area, one sees that there are locations near the boundary of the modeling region at which O_3 concentration remains high even at night. This is shown in Figure D.35, which represents O_3 concentration in the CIT domain at 10:00 p.m. Unfortunately, there are no monitoring stations in these locations, so there is no possibility to check if these predictions are correct. The remaining O_3 may be explained by one of two possibilities: either it is a consequence of low evening NO_X emissions

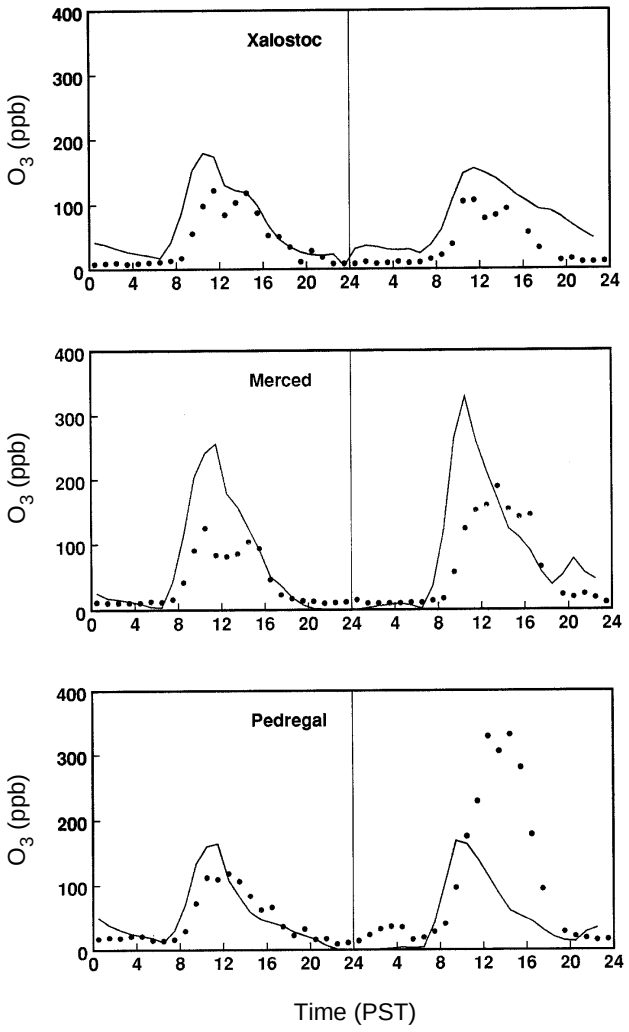

Figure D.33. CIT model simulation results for O_3 concentration. The simulation results are for the February 22nd period.

(which react with O_3) because those locations are sparsely populated or, it is an aberration caused by boundary conditions in the model.

A more stringent test of the model and the input data would be to model an O_3 episode from another season. However, at this time the data is not readily available to perform such a test.

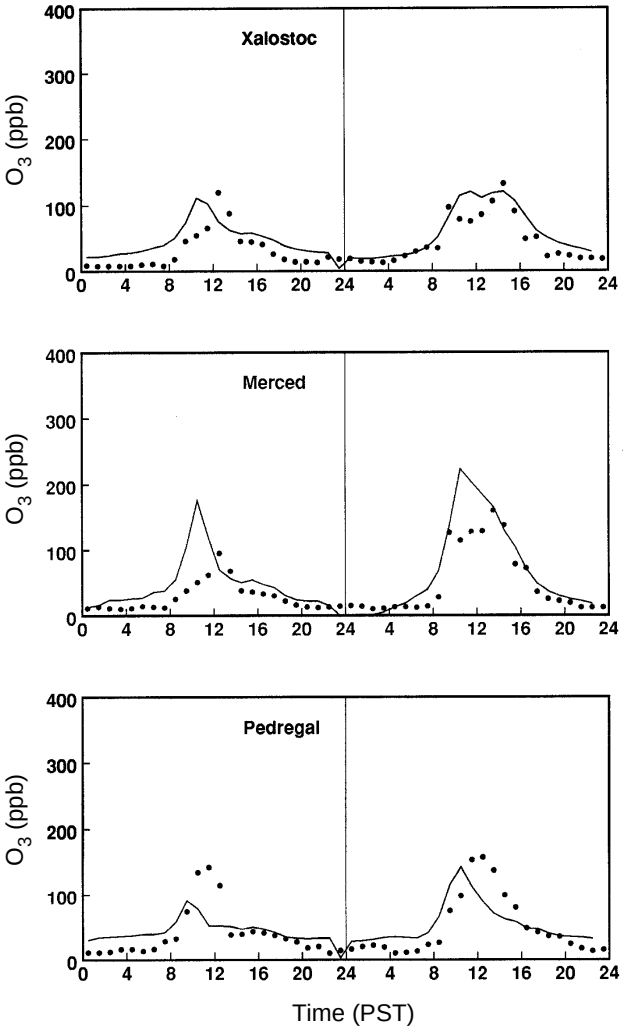

Figure D.34. CIT model simulation results for O_3 concentration. The simulation results are for the February 26 to 28th period.

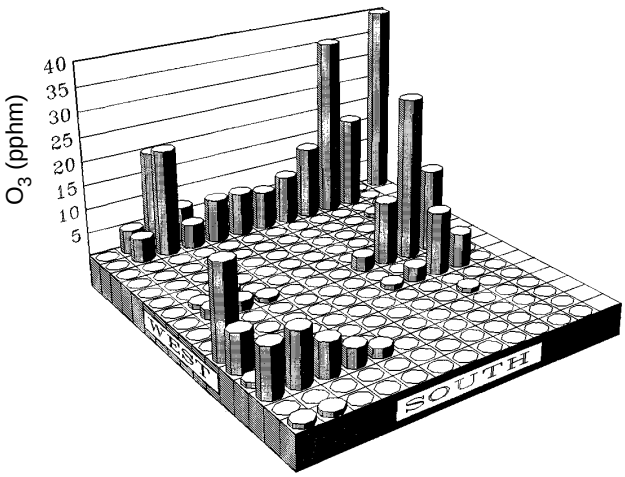

Figure D.35. CIT simulation showing residual O_3 in parts per hundred million on the boundaries of the domain at 10:00 p.m.

7. Improvements and Future Applications

a. Simulation using a larger domain (February 22, 2628).

A set of calculations was performed with a larger domain in order to determine whether background pollutant concentrations, as reflected in boundary conditions, could have inordinately influenced the smaller domain calculations. The effect on the MCMA of sources outside the immediate urban area can also be examined when they are included in the simulation via expanding the domain.

A comparison of the domains can be found in Figure D.36. Use of the larger domain had quite an effect on the results as can be seen in Figures D.37 and D.38. An examination of these results for February 22nd shows a sharp peak in O_3 concentration at 10:00 a.m. However, for the large-domain calculations the 10:00 a.m. peak is less sharp and, in general, the predicted values are closer to the observations than those from the smaller-domain calculation. The temporal profile of the O_3 peak is broadened in the large-domain calculation. It appears that the use of the larger domain improves model performance, particularly in the central and southern areas.

The predicted CO concentrations for the larger domain are higher than observations, as is also the case in the smaller domain calculation. Nevertheless, the model performs well in the southeastern areas and not as well in the northwestern areas. Model performance for NO_2 was similar for both simulations, even though

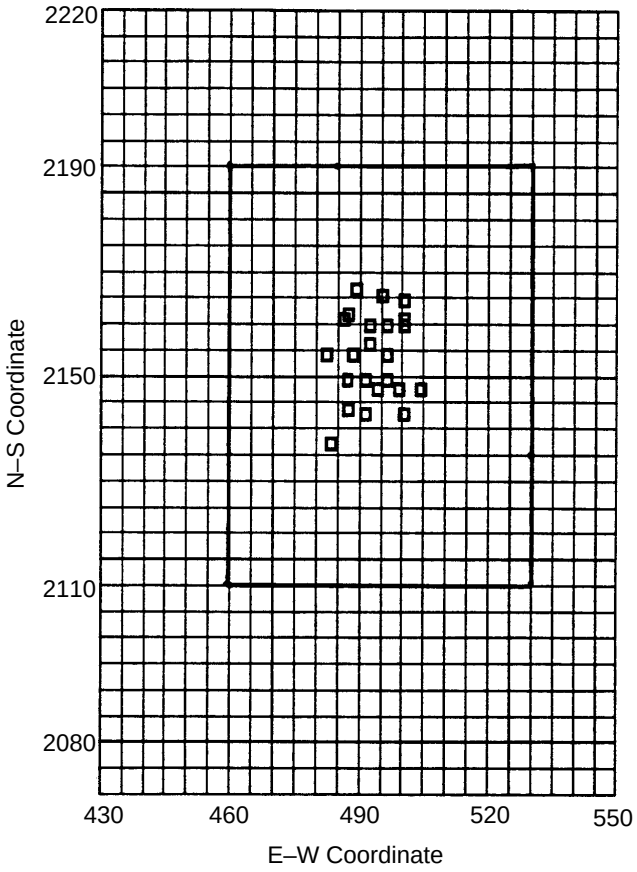

Figure D.36. A comparison of the CIT model domains with monitoring station locations indicated. The small grid squares are 5 km on a side. The heavy line defines the small domain, and the scattered boxes represent monitoring stations.

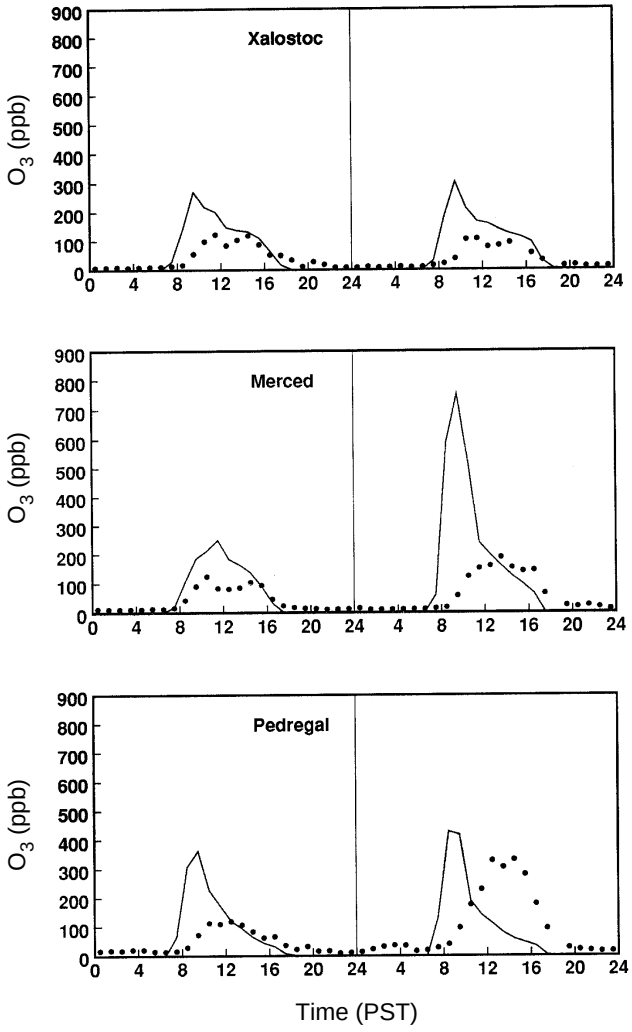

Figure D.37. Small-domain calculation for the February 22nd period.

the stations with large overpredictions were different. Although SO_2 concentrations are still very high at night with the use of the larger domain, the performance is good from noon to 4:00. Model performance improved in the south with use of the larger domain.

Comparison of predictions for the 22nd and the 26th (both for the large domain) show that the predictions for the 26th did not have the sharp early peaks seen in the simulation of February 22nd. The behavior of CO, NO_2, and SO_2 in the large-domain simulations for the 22nd and 26th tracked daytime observations quite well. All of these pollutants show early to midmorning peaks.

Figure D.38 illustrates the large domain simulation for February 22nd using the default diffusivity coefficient. Figure D.39 illustrates a simulation using the enhanced, or HOTMAC, diffusivity coefficient. With the enhanced coefficient, the O_3 peak is less sharp, but still appears a little early compared to observation. The morning and evening peaks for CO, NO_2, and SO_2 are all lowered with a tendency toward

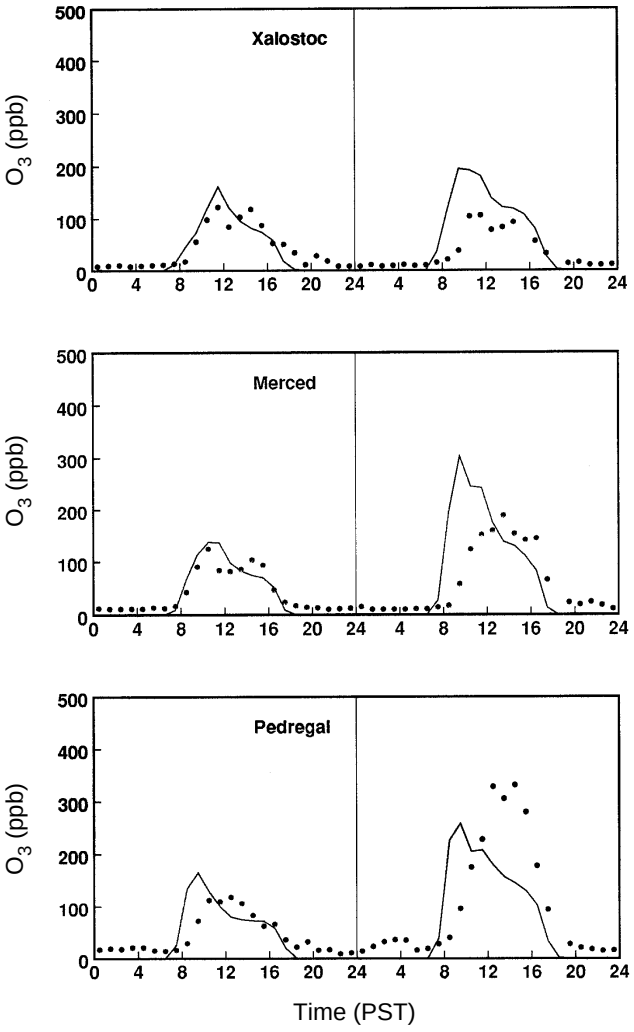

Figure D.38. Large-domain calculation for the February 22nd period with default diffusivity coefficient.

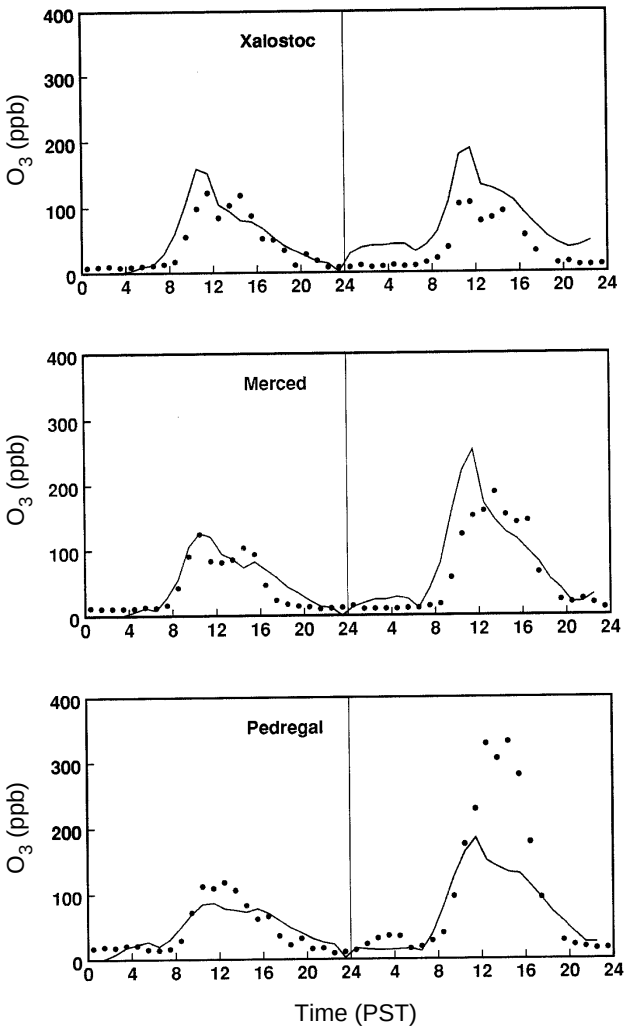

Figure D.39. Large-domain calculation for the February 22nd period using the enhanced, or HOTMAC, diffusivity coefficient.

underprediction, but the daytime variation is tracked fairly well. Figures D.40 and D.41 show a similar comparison for the February 26-28 simulation period.

Another possible improvement would involve drawing a domain that included the gulf coast. This domain would better represent the effects of the linked sea breeze. This would be done by surrounding the existing coarse grid with another grid with 18 km cell size. It would allow a better representation of moisture and temperature changes which occur over the coarse of the simulation. Some of the anomalous winds as represented by Station B might be associated with an eddy produced by the effects of the sea breeze. In the current simulations the effects of the sea breeze were captured by the tethersonde or rawinsonde driving winds. An additional grid would cost very little in computational time because the large grid cells would give much longer time steps than those used for the inner grids.

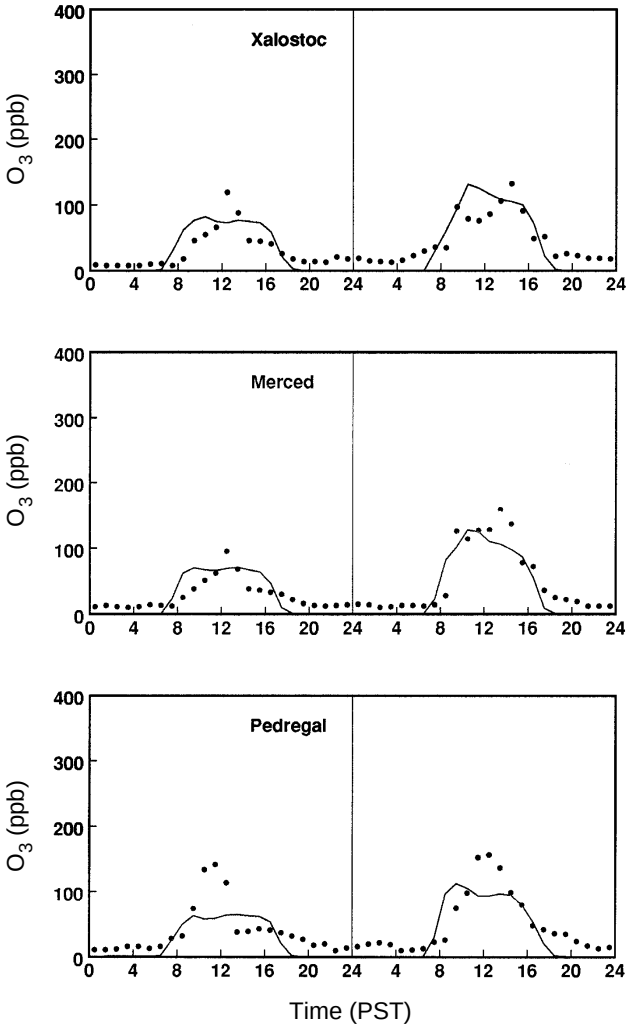

Figure D.40. Large-domain calculation for the February 27th-28th period with default diffusivity coefficient.

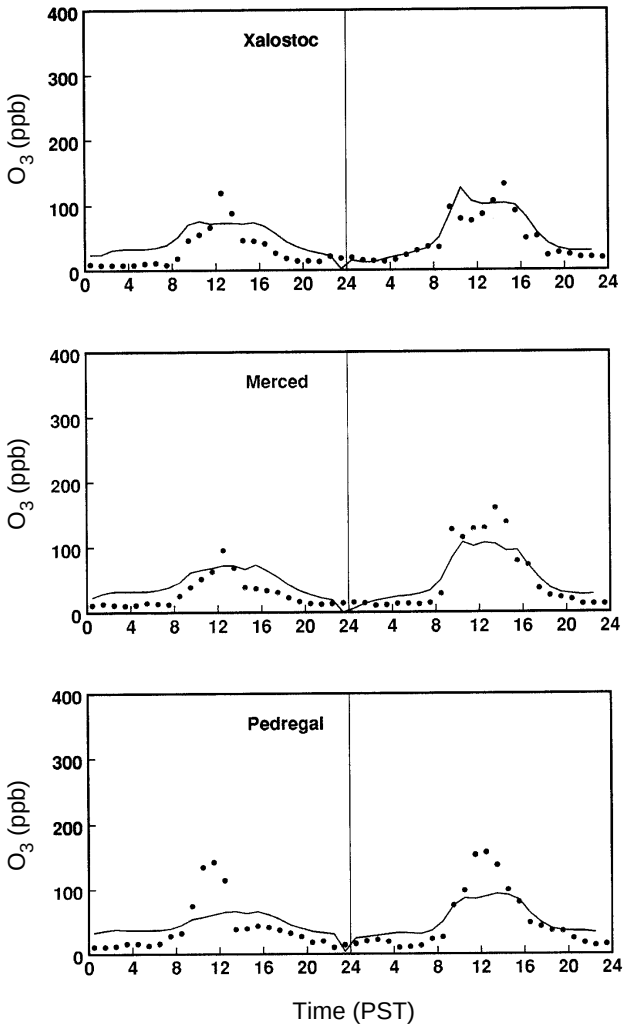

Figure D.41. Large-domain calculation for the February 27th-28th period using the enhanced, or HOTMAC, diffusivity coefficient.

Using hourly averaged wind speeds and directions at different heights from the large sodar (sound detection and ranging instrument) now operating in downtown Mexico City would also improve the results. The wind measurements would provide a better representation of the averaged wind descriptions that the model uses. This step would require very little or no changes in the model itself.

There are four areas in which model or model input changes might be helpful. One area would be to consider the effects of spiraling winds and make appropriate adjustments so that wind speeds are not underestimated because of the changes of direction with height. A second area would be to improve the properties of the surface coverages used in the model. We are currently using bulk properties, which ignore the effects of differences in materials. For example, a small layer of dead vegetation can act as an effective insulator, which can produce a much different energy balance. The surface parameters used for various surface coverages represent, at best, preliminary estimates that could probably be significantly improved.

Another area in which the model could probably be improved is in the treatment of long-wave radiation. The treatment depends upon a simple representation of how moisture and CO_2 absorb and reradiate energy as a function of temperature throughout the atmosphere. One study has measured long-wave radiation about 10% lower than that calculated by the model. Such changes could have a significant effect on the energy balance and may explain why the modeled temperature in the early morning is higher than the measured temperature. A reexamination of the coefficients might produce better agreement with measurements.

A major area that might improve model performance would be the use of an improved treatment of the short-wave and long-wave radiation effects of clouds. An improved treatment of short-wave radiation has been tested in a one-dimensional version of the code, but it has not been implemented in the three-dimensional version. The long-wave radiation effects have been used in other applications, but they were not used in this study.

E. EVALUATION OF INTEGRATED AIR QUALITY MODELING SYSTEM

1. Description

In recent years, the desire and priority given to decreasing the atmospheric pollutant concentrations in the MCMA has grown significantly. In fact, much has been accomplished. The application of air quality modeling to analyze pollution abatement measures and to provide support for policy making is one of a large number of programs designed to decrease emissions or to manage improvement in air quality.

The first step towards using these models to analyze control strategies is the simulation of base case scenarios of specific episodes. Initial simulations lead to model refinement by identifying weaknesses in input data and, consequently, areas for further investigation. These simulations can also point to weaknesses in the model formulation when applied to a particular location.

It was found that predicted pollutant concentrations from the base case simulation with the most recent emissions inventory and meteorological inputs did not match observations as well as was expected. Two possible weaknesses were identified and tested. One was the limitation of the model for determining vertical diffusivities. The model used for the calculation of the vertical diffusivity is believed to underestimate diffusivities when there is significant turbulence resulting from shear. This is an important phenomena in the MCMA. The second weakness was the major influence of boundary conditions with the small domain simulations.

As a consequence, a second series of simulations were performed with vertical diffusivities derived from the HOTMAC prognostic model and with increased domain size. With these modifications model performance, as indicated by O_3 concentration predictions, improved substantially.

2. Sensitivity Analysis

The degree of success in the application of an air quality model, which is a very complex system, to an airshed region depends both on the limitations of the model itself and on the uncertainties in the suite of input data. While improvement in the description of the atmospheric physicochemical process (the model itself) is a matter of basic research, considerable insight into the correct application of the model can be gained from studying the effect of variation on the parameters that characterize the region. This sensitivity analysis provides a direct means for evaluating how the predictions can vary as a result of changes in either input variable or structural parameters.

An analysis that considers simultaneous variation in all parameters over their full range of uncertainties is called a global method. Conversely, local analyses attempt to infer the shape or value of the response at a particular point. Conceptually, the simplest approach is to solve the system repeatedly, varying one parameter at a time.

A series of input parameters: initial conditions, the emissions inventory temporal pattern, photolysis rates, the initial VOC / NO_X ratio, HC speciation, and boundary conditions have all been identified by local sensitivity analysis as having significant influence on the performance of the air quality models applied to the MCMA.

Independent analysis of photochemical oxidation mechanisms (Ruiz-Suárez L.G et al. 1993) under the MCMA conditions (i.e., irradiation, pressure, temperature, and humidity) shows that the LCC mechanism can be used to confidently predict the O_3 formation.

3. Conclusions

The integration of the series of models—HOTMAC, RAPTAD, and CIT—has been successfully accomplished. Application of this set of models to the MCMA as a part of a larger tool for integral evaluation of pollutant control options has gained the attention of decision makers and the scientific community in Mexico.

The models were applied to the MCMA in two scenarios of interest during an intensive monitoring period (February 1991). It was found that the base case simulation with improved emissions inventory and meteorological input, did not perform as well as expected in regard to O_3 predictions. Two weaknesses were identified and tested. The first was a limitation of the photochemical module in the calculation of vertical diffusivities. The second weakness was the undue influence of boundary conditions because of the small domain originally used. New calculations with modified vertical diffusivities derived from the HOTMAC prognostic model and with a larger domain greatly improved the performance as measured by predicted O_3 behavior.

A variety of evidence, including trajectory and airshed simulations, suggests that the official emission inventory is underestimated regarding VOC emissions in particular. As anticipated, the assessment of control options shows that the potential air quality improvement will not be equal across the geographic extent of the MCMA. Hence, the use of air quality models before a control strategy is adopted is essential in order to predict the geographic variation of the expected air quality improvement. It was also shown that the improvement in the air quality to be expected by the simultaneous implementation of a group of options is not a linear response of the emission reductions.

4. Future Developments

The set of models discussed here, as adapted for application to the MCMA, are ready to be used for the evaluation of air quality management policy options at the interest of Mexican authorities or other sponsors. An evaluation of the expected benefits of reducing sulfur in diesel oil and of gasoline reformulation has been requested by PEMEX and the Metropolitan Commission.

It has also been proposed that the modeling tools developed in this project be applied and extended in a comprehensive study of the sources and fates of suspended particles in Mexico City. Suspended particulates constitute the second worst air quality problem in Mexico City. As in the present project, the integrated models will support the evaluation of options for reducing suspended particles both from a technical point of view and with consideration of socioeconomic factors.

Secondary aerosol formation, that is atmospheric *in situ* formation of aerosols from gaseous precursors, is a complex scientific problem, highly interesting and challenging. The goal is to select and combine appropriate models into a relatively seamless tool that is able to provide source-receptor impact analysis and the coupling of aerosol physics and chemistry to airshed models. Particular emphasis will be placed on the analysis of the relationship between aerosols and visibility.

F. DESCRIPTION OF DATA SOURCES

There are several kinds of data sources required to drive the models. These include

- meteorology,
- emissions,
- ambient measurements, and
- geographical inputs.

1. Meteorological Data

The primary source of measurements to drive the meteorological model was the airport balloon soundings and the tethersonde measurements. The airport balloon launches gave the vertical temperature, humidity, and wind profiles, while the tethersonde winds were used for the lowest 750 meters when available. During the intensive study period the airport balloon launches occurred about seven times a day as opposed to the normal frequency of two launches per day. More detail on the limitations of these data sets can be found in sections B.5.b and B.5.c where the model-measurement comparisons are described.

2. Emissions

The development of an emissions inventory for MCMA is relatively recent, with several efforts having been made, but only since 1986. For the present project, the development of an inventory was based on available information, which is described as follows.

In 1986 JICA, in collaboration with the DDF, performed a study to estimate emissions from both mobile and stationary sources in the MCMA. For mobile source emissions, the vehicular traffic volumes were determined in the 16 delegations of the DF and in several municipalities of the bordering EdoMex. For stationary source emissions estimates, 361 factories in the DF were surveyed. Data from these studies were used to define an emissions inventory for MCMA. This inventory reported emissions in a grid of 1 km^2 cells, and only reported emissions of NO_X, SO_2 and CO. The final report of the JICA-DDF study was released in 1988. (JICA 1988)

Starting with the JICA-DDF inventory, the DDF in 1989 and 1990 constructed an emissions inventory for PICCA. The inventory included emissions of HC, NO_X, SO_2, CO, total suspended particles, and some estimates for lead. (PICCA 1990)

In 1991, the Air Quality Management Program for the MCMA (AQMP 1991) was published with the PICCA inventory. Newer efforts which were made to refine and improve the inventory were discussed, but the results were not integrated into a new inventory.

The Mexico Transport Air Quality Management in the Mexico City Metropolitan Area: Sector Study (World Bank 1992), published at the beginning of 1992, also reported an emissions inventory. This emissions inventory was a modification, primarily for mobile source emissions, of the PICCA inventory. In this new inventory, emissions for HC, NO_X, SO_2, CO, total suspended particles, and lead were reported.

The JICA performed another study for the Mexican government and released the final report at the end of 1991. (JICA 1991) This study reported emissions for stationary sources based on an on-site survey of 97 industrial sites in the MCMA and on measurements carried out in 25 of those sites. Another report used by MARI to account for stationary sources was released in 1992. (PICCA 1992)

At this time, the German TÜV team, in collaboration with the DDF, is developing a new emissions inventory for mobile sources. (TÜV ARGE MEX 1992) Vehicular emissions are being estimated from vehicle surveys and traffic counts across the MCMA, combined with calculations from MOBILE-MCMA. Data from all the above mentioned emission inventories were used in MARI to obtain an emissions inventory for modeling purposes and strategic analyses.

3. Ambient Measurements

In addition to the experimental campaigns that are described in Volume IV of this report, air quality measurements are done at the surface level at 25 automated monitoring stations whose locations are shown in Figure F.1. The individual stations record some subset of pollutant concentrations (CO, SO_2, NO_X, H_2S, O_3) and meteorological parameters (wind speed and direction, relative humidity, temperature). Only five stations are instrumented for the full range of measurements. Total suspended particles are collected in a manual monitoring network consisting of 24 stations. In five of them, data for PM-10 are also collected.

Twice a day (6:00 a.m. and 6:00 p.m.) rawindsondes are released from the international airport. These provide a vertical profile of wind speed and direction, relative humidity, temperature, and dew point temperature.

4. Geographical Data

There were two kinds of geographical data used in the modeling activities: topographical and land coverage.

a. Topographical Data

A U.S. agency provided the project with 1-km resolution data, which covered the entire domain surrounding Mexico City. HOTMAC requires resolution equal to half the grid size, so the inner grid used 1-km resolution data, and the outer grid used 3-km resolution data.

b. Land Coverage Data

Land coverage data were developed by the University of Utah Engineering and Research Institute which used the LANDSAT satellite data to classify the fine grid area. Ultimately, they provided a 2-km mesh that was 1 km offset from the fine grid with fractional land coverage in each of 13 categories. The categories used were: (1)vegetation, (2) mostly bare soil, (3) dark soil, (4) shadow / volcanic / urban, (5) urban / lower income, (6) city and foothill vegetation, (7) water, (8) dark urban material, (9) urban material mixture, (10) urban / mostly downtown, (11) vegetation mixture, (12) mountain vegetation, and (13) rock and mountain vegetation mixture. Figure F.2 displays the cells classified in this manner. In addition to the fractional land coverage data, they also provided data on the typical values of radiation in each band associated with the various subcategories that made up each classification. These data were used to help estimate surface albedos and water above different land use classes.

The satellite data were developed from a LANDSAT image taken during the late morning on February 17, 1991.

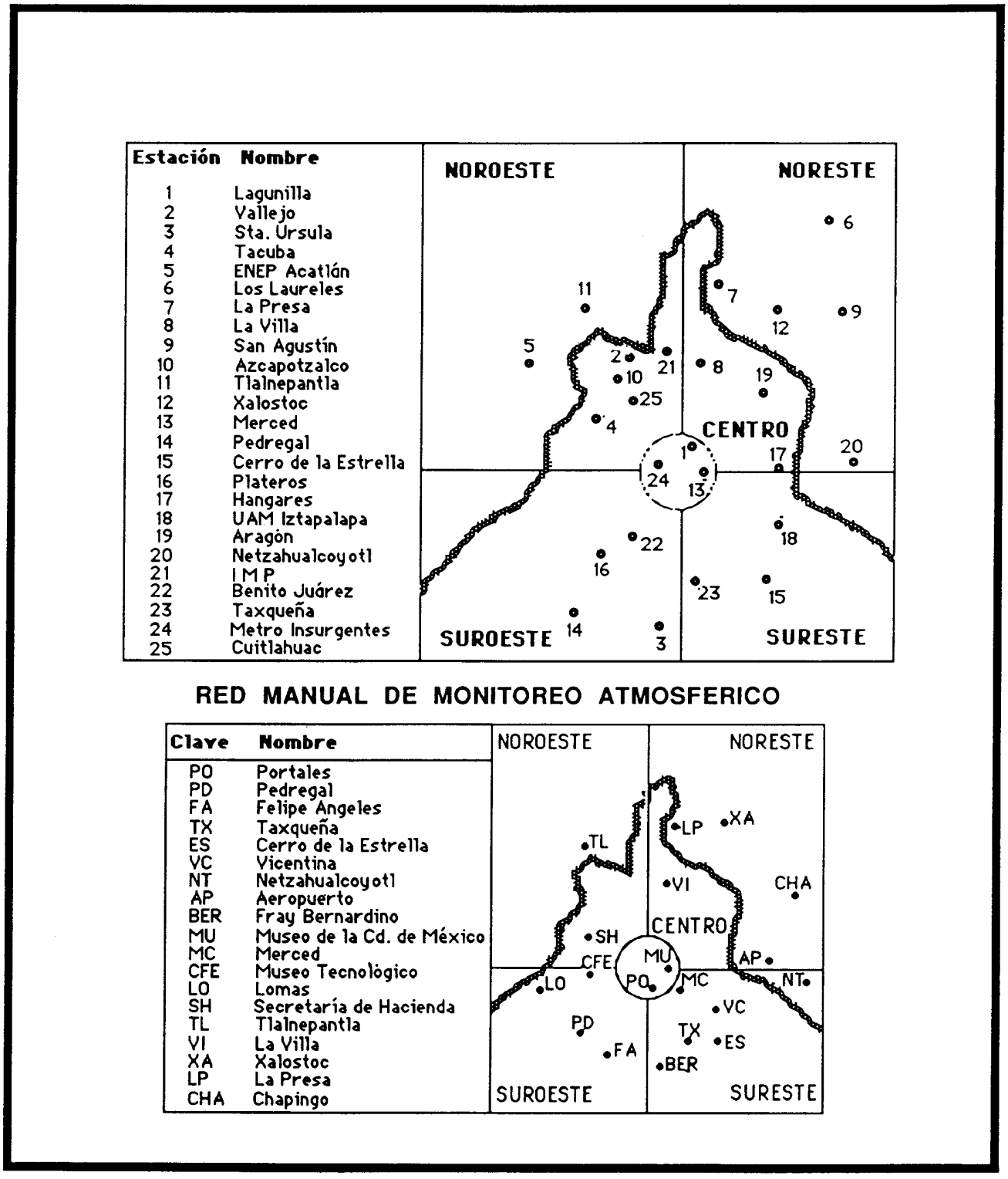

Figure F.1. Locations for the twenty-five monitoring stations in the MCMA where air quality measurements are done at surface level.

Value	Class Name	Value	Class Name
1	Vegetation	8	Dark Urban Material
2	Mostly Bare Soil	9	Urban Material Mix
3	Dark Soil	10	Urban / Mostly Downtown
4	Shadow / Volcanic / Urban	11	Vegetation Mix
5	Urban / Lower Income	12	Mountain Vegetation
6	Vegetation / Foothills & City	13	Vegetation & Rock Mixture Mountain
7	Water		

Figure F.2. A display of the land coverage grid area, which has thirteen categories.

REFERENCES

(Anderson and Meier 1979)
Anderson, Jr., D. E. and R. R. Meier, "Effects of Anisotropic Multiple Scattering on Solar Radiation and the Troposphere and Stratosphere," *Applied Optics* **18**, 1955 (1979).

(AQMP 1991)
"Air Quality Management Program for the MCMA: Short-Term Program," Vol. 1 & 2, Departamento Distrito Federal, Mexico City, Mexico, 1991.

(Bowne 1981)
Bowne, N. E. "Preliminary Results From the EPRI Plume Model Validation Project: Plains Site," EPRI EA-1788-SY, Electric Power Research Institute, Palo Alto, CA 1981.

(Briggs 1984)
Briggs, G. A., "Plume Rise and Bouyancy Effects," in Atmospheric Science and Power Production (ed. by D. Randerson) DOE / TIC-27601. U.S. Department of Energy, 1984, pp. 327-366.

(Comisión 1992)
"Programa para el Control de Emisiones Contaminantes al Aire Provenientes de la Industria en la Zona Metropolitana de la Ciudad de México," Comisión Metropolitana para la Prevención y Control de la Contaminación Ambiental en el Valle de México, Mexico City, 1992.

(Diaz-Frances et al. submitted)
Diaz-Frances E., M. E. Ruiz, G. Sosa, "Spatial Stratification and Multivariate Analyses of Mexico City Air Pollution Data," *Atmos. Environ.* (submitted).

(Dickerson et al. 1982)
Dickerson R. R., D. H. Stedman, and A. C. Delany, "Direct Measurement of Ozone and Nitrogen Dioxide Photolysis Rates in the Troposphere," *J. Geophys. Res.* **87**, 4933-4946 (1982).

(Eidels-Dubovoi 1993)
Eidels-Dubovoi S., "Solar Radiation Attenuation by Atmospheric Aerosol Particles at Different Sites in the Mexico City Valley." Proceedings of International Symposium on Heat and Mass Transfer in Energy Systems and Environmental Effects, Cancún, Mexico, August 1993.

(EPA 1989)
"User's Manual for OZIPM-4 (Ozone Isopleth Plotting with Optional Mechanisms)," U.S. Environmental Protection Agency report EPA-450 / 4-89-009a (July 1989).

(Gertler and Pierson 1991)
Gertler A. W. and W. R. Pierson, "Motor Vehicle Modeling Issues," paper 91-88.8 in Proceedings Volume 7, Air Modeling Papers from the 84th Annual Meeting, published by the Air & Waste Management Association, Pittsburgh, Pennsylvania (1991).

(Gery et al. 1989)
Gery, M. W., G. Z. Whitten, J. P. Killus and M. C. Dodge, "A Photochemical Kinetics Mechanism for Urban and Regional Scale Computer Modeling," *J. Geophys. Res*. **94**, 12,925-12,956 (1989).

(Guillermo et al. 1993)
Guillermo R., P. Coddeville, C. Bugajny, "Compte Rendu Et Premiers Resultats de la Campagne de Measures Effectuee a Mexico en Mars 1993." Ecole des Mines de Douai, Douai (France), June 1993.

(Joseph and Wiscombe 1976)
Joseph J. H. and W. J. Wiscombe *J. Atmos. Sci*. **33**, 2452-2459 (1976).

(JICA 1988)
JICA, Japan International Cooperation Agency, "The Study on Air Pollution Control Plan in the Federal District, Final Report," for Departamento Distrito Federal, Mexico City, October 1988.

(JICA 1991)
JICA, Japan International Cooperation Agency, "The Study on the Air Pollution Control Plan of Stationary Sources in the Metropolitan Area of the City of Mexico, Final Report," for Departamento Distrito Federal, Mexico City, September 1991.

(Joseph, J. H. and Wiscombe 1976),
Joseph J. H., and W. J., Wiscombe *J. Atmos. Sci*., **33**, 2452-2459 (1976).

(Lee and Stone 1982)
Lee J. T. and G. L. Stone, "The Use of Eulerian Initial Conditions in a Lagrangian Model of Turbulent Diffusion,'' Los Alamos National Laboratory report LA-UR-82-3034 (1982).

(Lurmann et.al. 1987)
Lurmann F. W., W. P. L. Carter, and L. A. Coyner, "A Surrogate Species Chemical Reaction Mechanism for Urban-Scale Air Quality Simulation Models," Volumes I and II. Report to the U.S. Environmental Protection Agency under contract 68-01-3104. ERT Inc., Newbury Park, CA, and Statewide Air Pollution Research Center, University of California, Riverside, CA, (1987).

(Mardia 1972)
Mardia K. V., *Statistics of Directional Data*, (Academic Press Inc., Orlando, Florida, 1972) pp. 127-128.

(McRae et.al. 1982)
McRae G. J., W. R. Goodin and J. H. Seinfeld. *Atmos. Environ*. **16**, 679-696 (1982).

(McRae et.al. 1983)
McRae G. J.; W. R. Goodin, J. H. Seinfeld, *Atmos. Environ*. **17**, 501-522 (1983).

(Mellor and Yamada 1982)
Mellor G. I. and T. Yamada, "Development of a Turbulence Closure Model for Geophysical Fluid Problems,'' *Rev. Geophys. Space Phys*., **20**, 851-875 (1982).

(Office of Air Quality Planning and Standards 1993)
Office of Air Quality Planning and Standards. "The Role of Ozone Precursors in Tropospheric Ozone Formation and Control," A Report to Congress, U.S. Environmental Protection Agency, Research Triangle Park, NC, EPA-454/R-93-024 (1993).

(Oliver et.al. 1993)
Oliver W. R., R. J. Dickson, and L. Bruckman, "Development of the SCAQS High-Resolution Emissions Inventory: Assessment of Inventory Uncertainties," in Proceedings of an International Specialty Conference, Southern California Air Quality Study, Data Analysis, VIP-26 published by the Air & Waste Management Association, Pittsburgh, Pennsylvania, pp. 62-73 (1993).

(Parrish et.al. 1983)
Parrish D. D., P. C. Murphy, D. L. Albritton and F. C. Fehsenfeld, "The Measurement of the Photodissociation Rate of NO_2 in the Atmosphere," *Atmos. Environ.* **17**, 1365-1379 (1983).

(PICCA 1990)
"Programa Integral Contra la Contaminación Atmosférica de la Zona Metropolitana de la Ciudad de México," Secretariado Técnico Intergubernamental, Mexico City, October, 1990.

(Rao 1987)
Rao S. T., "Application of the Urban Airshed Model to the New York Metropolitan Area," U.S. Environmental Protection Agency, Research Triangle Park, NC, EPA-450/4-87/011 (1987).

(Ruiz et.al. 1993)
Ruiz M. E., K. Gerner, M. Y. Barbiaux, "First Results of the HC-Speciation in Mexico City," Proceedings of AWMA 86th Annual Meeting and Exhibition, Denver, CO, 1993.

(Ruiz-Suárez et.al. 1993)
Ruiz-Suárez L. G., T. Castro, B. Mar, M. E. Ruiz-Santoyo, X. Cruz, *Atmos. Environ.* **27A**(3), 405-425 (1993).

(Ruiz-Suárez et.al. 1993)
Ruiz-Suárez J. C., L. G. Ruiz-Suárez, C. Gay, T. Castro, M. Montero, Eidels-S. Dubovoi and A. Muhlia, "Photolytic Rates for NO_2, O_3 and HCHO in the Atmosphere of Mexico City," *Atmos. Environ.* **27A**(3), 427-430 (1993).

(Russell et.al. 1988)
Russell A. G., K. F. McCue, G. R. Cass, *Environ. Sci. Technol.* **22**, 263-271 (1988).

(Russell et.al. 1992)
Russell A. G., D. A. Winner, K. F. McCue, G. R. Cass, "Mathematical Modeling and Control of the Dry Deposition Flux of Nitrogen-Containing Air Pollutants," EQL Report 29, Environmental Quality Laboratory, California Institute of Technology, Pasadena, CA, Report to the California Air Resources Board under Contract A6-188-32 (1992).

(Seila et.al. 1993)
Seila R. L., W. A. Lonneman, M. E. Ruiz, J. Tejeda, "VOCs in Mexico City Ambient Air," Proceedings of International Symposium on Measurement of Toxic and Related Air Pollutants, Durham, North Carolina, 1993.

(Sheih et.al. 1986)
Sheih C. M., M. L. Wesely, C. J. Walcek, "A Dry Deposition Module for Regional Acid Deposition," Atmospheric Sciences Laboratory, U.S. Environmental Protection Agency, Research Triangle Park, NC, EPA-600/3-86-037 (1986).

(Streit 1985)
Streit, G. E., "Actinic Flux and Photodissociation Rates in the High Altitude West," Twenty-Seventh Rocky Mountain Conference; Denver, CO, July 14-18, 1985, Los Alamos National Laboratory document LA-UR-85-701.

(Tesche et.al. 1990)
Tesche T. W., P. Georgopoulus, J. H. Seinfeld, G. Cass, F. L. Lurmann, P.M. Roth, "Improvement of Procedures for Evaluating Photochemical Models," final report contract No. A832-103, prepared for the California Air Resources Board, Radian Corporation, DCN:90-264-069-05-02 (1990).

(TÜV 1991)
(TÜV, 1991) "Feasibility Study: Detailed Emission Inventory in Mexico City Metropolitan Area," TÜV ARGE MEX, TÜV Rheinland, Köln, 1991, prepared for DDF.

(TÜV ARGE MEX 1992)
TÜV ARGE MEX, TÜV Rheinland Cologne, "Air Pollution Control in the Mexico City Metropolitan Area, Emissions Inventory for Mobile sources, Results of a Pilot Study in MCMA", DRAFT, TÜV ARGE MEX, TÜV Rheinland, Köln, February 1992.

(Weil and Brower 1982) Weil, J. C. and R. P. Brower "The Maryland PPSP Dispersion Model for Tall Stacks," PPSP-MP-36, Martin Marietta Corporation, Baltimore, Maryland, 1982.

(Wesely 1989)
Wesely M. L. *Atmos. Environ*. **23**, 1293-1304 (1989).

(Williams et.al. 1992)
Williams M. D., G. Sosa, G. E. Streit, X. Cruz, M. E. Ruiz, A. G. Russel, L. A. McNair, "Development and Testing of an Air Quality Model for Mexico City," Los Alamos National Laboratory report LA-UR-92-808, March 1992.

(Wesely, 1989)
Wesley M. L. *Atmos. Environ*. **23**, 1293-1304, 1989.

(World Bank 1992)
Mumme C. H., Cargajo J., Eskeland G., Margulis S., Wijetilleke K., Cornwell P., Cracknell J., Glaessner P., Weaver C. and Yamada T., "Mexico: Transport Air Quality Management in the Mexico City Metropolitan Area: Sector Study," Latin America and the Caribbean Regional Office, World Bank Report, Rept. No. 10045-ME, February 1992.

(Yamada 1981)
Yamada T., "A Numerical Simulation of Nocturnal Drainage Flow,'' *J. Meteor. Soc., Japan*, **59**,108-122 (1981).

(Yamada 1985)
Yamada T., "Numerical Simulation of the Night 2 Data of the 1980 ASCOT Experiments in the California Geysers Area,'' Archives for Meteorology, Geophysics, and Bioclimatology, Ser. A34, pp. 223-247 (1985).

(Yamada and Bunker 1988)
Yamada T. and S. Bunker, "Development of a Nested Grid, Second Moment Turbulence Closure Model and Application to the1982 ASCOT Brush Creek Data Simulation,'' *J. Appl. Meteor*. **27**, 562-578 (1988).

Los Alamos
NATIONAL LABORATORY
Los Alamos, New Mexico 87545